SAPIENZA
UNIVERSITÀ DI ROMA

Guidance and control for defense systems against ballistic threats

Scuola di Ingegneria Aerospaziale - Sapienza Università di Roma

Dottorato di Ricerca in Ingegneria Aerospaziale – XXV Ciclo

Candidate

Simone Battistini

ID number 802035

Thesis Advisor

Prof. Paolo Teofilatto

A thesis submitted in partial fulfillment of the requirements
for the degree of Doctor of Philosophy in Aerospace Engineering

2013

Thesis defended on July 18^{th}, 2013
in front of a Board of Examiners composed by:

Prof. Paolo Gasbarri (chairman)

Prof.ssa Michelle Lavagna

Prof.ssa Nicole Viola

Simone Battistini. *Guidance and control for defense systems against ballistic threats.*
Ph.D. thesis. Sapienza – University of Rome

VERSION: June 26^{th}, 2013

EMAIL: simone.battistini@uniroma1.it

Abstract

Un sistema di difesa da minacce balistiche è un sistema molto complesso dal punto di vista ingegneristico. Esso racchiude, infatti, sottosistemi di diversa natura e, allo stesso tempo, presenta dei requisiti molto stringenti. L'evoluzione delle tecnologie impiegate porta, inoltre, alla necessità di aggiornare costantemente le capacità del sistema. Uno dei campi che presentano maggiori possibilità di sviluppo è quello della guida e del controllo.

Questa tesi affronta le problematiche di guida e controllo coinvolte in un sistema di difesa da minacce balistiche. Per intraprendere questo studio, è stata analizzata anzitutto la missione di un missile balistico intercontinentale. La ricostruzione della traiettoria a partire da misure radar e satellitari è stata effettuata con un algoritmo di stima per sistemi non lineari. La conoscenza della traiettoria è il prerequisito per l'intercetto del missile balistico con un missile tattico.

L'intercetto avviene da parte di un missile dedicato. Lo studio della guida e del controllo di questo veicolo è stato oggetto di questa tesi. Particolare attenzione è stata posta sul problema della stima delle variabili dell'ingaggio all'interno del cosiddetto homing loop. I missili intercettori sono solitamente dotati di un seeker che fornisce l'angolo sotto il quale l'intercettore vede il target. Quest'unica misura risulta insufficiente a garantire l'osservabilità di tutte le variabili necessarie ad attuare leggi di guida avanzate come APN, OGL o quelle basate su giochi differenziali. In questo senso, una nuova strategia di guida concepita per ovviare ai problemi di cattiva osservabilità ha consentito di ottenere risultati soddisfacenti in termini di performance dell'ingaggio.

Il lavoro si conclude con uno studio della configurazione aerodinamica più adatta ad implementare la nuova strategia di guida e con il disegno dell'autopilota. L'autopilota consente di attuare i comandi di accelerazione laterale elaborati dal sistema di guida. Il progetto dell'autopilota è stato portato avanti con tecniche di controllo lineari, tenendo conto dei requisiti in tempo di risposta, massimo sforzo richiesto agli attuatori e risposta a un comando di tipo bang-bang derivanti dal sistema di guida.

L'analisi della bontà delle soluzioni scelte è stata compiuta sui risultati di simulazioni numeriche, sviluppate specificatamente per ogni caso di studio.

Abstract

A defense system against ballistic threat is a very complex system from the engineering point of view. It involves different kinds of subsystems and, at the same time, it presents very strict requirements. Technology evolution drives the need of constantly upgrading system's capabilities. The guidance and control fields are two of the areas with the best progress possibilities.

This thesis deals with the guidance and control problems involved in a defense system against ballistic threats. This study was undertaken by analyzing the mission of an intercontinental ballistic missile. Trajectory reconstruction from radar and satellite measurements was carried out with an estimation algorithm for nonlinear systems. Knowing the trajectory is a prerequisite for intercepting the ballistic missile.

Interception takes place thanks to a dedicated tactical missile. The guidance and control of this missile were also studied in this work. Particular attention was paid on the estimation of engagement's variables inside the homing loop. Interceptor missiles are usually equipped with a seeker that provides the angle under which the interceptor sees its target. This single measurement does not guarantee the observability of the variables required by advanced guidance laws such as APN, OGL, or differential games-based laws. A new guidance strategy was proposed, that solves the bad observability problems and returns satisfactory engagement performances.

The thesis is concluded by a study of the interceptor most suitable aerodynamic configuration in order to implement the proposed strategy, and by the relative autopilot design. The autopilot implements the lateral acceleration commands from the guidance system. The design was carried out with linear control techniques, considering requirements on the rising time, actuators maximum effort, and response to a bang-bang guidance command.

The analysis of the proposed solutions was carried on by means of numerical simulations, developed for each single case-study.

Contents

List of Figures

List of Tables

List of acronyms

AAD	Advanced Air Defence
ABM	Anti-Ballistic Missile
APN	Augmented Proportional Navigation
BTT	Bank-to-turn
CC	Collision Course
DSP	Defense Support Program
ECIF	Earth Centered Inertial Frame
EKF	Extended Kalman Filter
ERIS	Exoatmospheric Reentry Intercept System
GEM	General Energy Management
GEO	Geosynchronous Earth Orbit
GPS	Global Positioning System
HOE	Homing Overlay Experiment
ICBM	Intercontinental Ballistic Missile
IR	Infrared
IMU	Inertial Measurement Unit
KF	Kalman Filter
LOS	Line of Sight
MEL	Minimum Effort (Guidance) Law

NMD National Missile Defense

OGL Optimal Guidance Laws

PAD Prithvi Air Defence

PN Proportional Navigation

PP Pure Pursuit

STT Skid-to-turn

THAAD Terminal High-Altitude Area Defense

TVC Thrust Vector Control

UKF Unscented Kalman Filter

ZEM Zero Effort Miss

"It is good to renew one's wonder," said the philosopher.
"Space travel has again made children of us all."

Ray Bradbury - 'THE MARTIAN CHRONICLES'

Beaucoup d'observation et peu de raisonnement conduisent à la vérité:
beaucoup de raisonnement et peu d'observation conduisent à l'erreur

Alexis Carrel - 'RÉFLEXIONS SUR LA CONDUITE DE LA VIE'

Ma che poss'io, Signor, s'a me non vieni
coll'usata ineffabil cortesia?

Michelangelo Buonarroti - 'RIME'

Capitolo 1

Introduction

Most of the systems employed in defense against ballistic missiles strongly relies on guidance and control algorithms to achieve their tasks. The design of such systems requires a large effort, involving many engineers with expertise in the areas of aerodynamics, flight controls, structures, and propulsion, among others. In terms of high accuracy and low cost, an efficient system is the result of a collective design and work. Even if guidance and control are only a part of the whole system, their design largely impacts the performances of the system, because their activities involve all the subsystems.
This work analyzes the aspects of guidance and control involved in ballistic missile defense. The intent is to present solutions for all the phases of the mission. They can result in mathematical tools and formulations or in technical solutions.
In this introduction, the concepts related to ballistic missile defense will be presented along with some historical details. The defense system in a general sense will be firstly described. A review of ballistic missiles will follow and, eventually, the phases of the missile defense mission will be described.

1.1 The defense system

To own defense capability against ballistic missiles is a task for many countries. This involves the development of a complex system, able to nullify possible missile threats. The complexity lies in the different nature of the interested subsystems, in the demanding constraints, and in the constant need for updates. Basically, a defense system is composed of

- a network of sensors, with the task to localize incoming ballistic threats
- a series of appropriate weapons for destructing enemy missiles, generally indicated as tactical missiles

- a center that plans the defense and coordinates the actions

The interest of global powers in effective missile defenses against a range of long and short range ballistic missile threats has been ongoing since the end of World War II. Since the 1950s, USA and USSR began numerous programs, but only a very few saw completion to deployment. USSR and USA signed the Anti-Ballistic Missile (ABM) Treaty in 1972, which limited the number of ABM sites to two for each country. The 1991 Gulf War was the first test of a ballistic missile defense in actual combat [42]. In 2002 President G. W. Bush withdrew US from the ABM treaty, allowing for deployment of interceptor missiles in more sites. US National Missile Defense (NMD) is actually based on several components, such as ground-based interceptors, ship-based radars and interceptors (the AEGIS program), airborne systems and high-altitude interceptors (the Terminal High-Altitude Area Defense (THAAD) program). Missile defense in Russia is currently operational only in the area of Москва and it is based on the *A-135* anti-ballistic missile system.
Other countries than US and USSR have developed defense systems against ballistic missiles. France, UK and Italy use the *Aster* missile family. India relies on two interceptors, Prithvi Air Defence (PAD) and Advanced Air Defence (AAD), respectively for high altitude and low altitude interception. Israel has a system against medium-range missiles that employs the *Arrow* missile; moreover, the *Iron Dome* system is designed against short-range missiles.
Most defense systems are designed to attack their targets after their boosters have burned-out. This leaves sufficient time for defense countermeasures. Defense during the boost-phase of the ballistic missiles raises technical criticalities due to the short times available. Nevertheless, it is an attractive option, because boosting rockets are easy to detect and, in this phase, countermeasures are less effective [65]. Furthermore, a boosting missile trajectory is limited by dynamical constraints and this makes the missile more vulnerable. A good compromise is to detect the incoming missile before its burn-out, leaving its destruction to later phases.

1.2 Review of ballistic missiles

Long-range ballistic missiles are often referred to as strategic missiles or Intercontinental Ballistic Missile (ICBM). They are typically designed to carry nuclear warheads. The launch can be performed from several platforms: silos, submarines, trucks or other mobile launchers. These vehicles have been developed since 1940s as attacking weapons and also as deterrent to possible enemies attacks.
After World War II both United States and Soviet Union started rocket research programs. The first successfully launched ICBM was the soviet *R-7*, tested on August 1957. The

first US ICBM flight took place almost one year later, on June 1958, with the *Atlas* rocket. Beside the cold war arms race, these military projects paved the way to the development of the first vehicles for space exploration in the 1960s.
In 1991, the United States and the Soviet Union agreed in the START I treaty to reduce their deployed ICBMs and attributed warheads to a number of delivery vehicles to 1600 each, with no more than 6000 warheads. In some cases, the vehicles in excess were adapted to become launch vehicles and to carry a space payload instead of a warhead. This is the case of the *Dnepr* commercial launcher, formerly known as the soviet *SS-18* missile [2].
Nowadays there are only four countries known to possess land-based ICBM: China, India, Russia and United States. The latter relies only on the *Minutemen III*, a missile with a range of 13000 *km*. Russia has five models of ICBMs, each one with different range capabilities and different launch features. China has developed several ICBM models, from the class of medium to long range vehicles, all belonging to the *Dong Feng* family. India has a series of ballistic missiles called *Agni*, the latest developed with a range of 8000 *km*. Some countries (US, Russia, France, United Kingdom and China) have submarine-launched missiles. Other countries such as Iran and North Korea are reported to have ongoing ICBM projects [4].
With regards to the propellant used, most modern ICBMs employ solid-propellant boosters. Liquid-propellant boosters were developed at the beginning of the ICBMs era, since it is an easier technology to master. Nowadays, this is still an option for the countries that are trying to build their own vehicles.

1.3 Phases of the interception

The interception of an incoming ballistic missile is a mission composed of several phases. Each phase has a different task and different means to achieve it. Once the ICBM has been launched, the first action to be performed is detection. Early warning systems of ballistic missiles launches have been operated since 1970s. The Defense Support Program (DSP), for example, is a space-based system from the US army: missile detection is provided by a constellation of satellites, equipped with proper sensors that will be described in chapter 3. A dedicated sensor must cover the area where the missile is flying. A constellation of satellites can give a potentially total coverage of the Earth, while radar platforms have limited coverage. Furthermore, it might be not possible to install them near enemy launch sites.
Tracking the ICBM trajectory is the second task of the defense system. Evaluating the trajectory allows to properly plan defense countermeasures. This involves obtaining precise measurements of ICBM state variables, such as position and velocity. Again, a radar platform is able to provide the defense system with these information. Radar measurements will be described in chapter 3. Radar measurements can be also conveniently processed to

obtain a precise reconstruction of the trajectory through state estimation algorithms. The prerequisite for employing such techniques is to know the ICBM motion and its peculiarities.

When the ICBM has been acquired, it is time for the defense system to set up active countermeasures. An interceptor is hence launched against the ICBM. This is a tactical missile in charge of concluding the engagement. In this work it will be referred to also as the pursuer. The interceptor firstly undergoes a boost-phase, where it quickly increases speed. During the successive midcourse phase, the interceptor flies away from the launch platform toward the direction of the target. During these two phases, the interceptor navigates exploiting the information from its inertial sensors and it can be guided from external, using information from surface-based radars [9]. When the distance between the interceptor and the ICBM is sufficiently small, the missile takes control over the mission and enters in the terminal phase of the engagement, or *end game*. Guidance in this phase is delegated to the information from an on-board terminal sensor, often referred to as *seeker*. The engagement is concluded when the interceptor hits the ICBM or when interception can not take place anymore. The former condition can be expressed as achieving a minimum relative distance (usually less than 1 or 2 meters). Once the relative distance has reached a minimum, it starts increasing. If the minimum value is not satisfactory, the engagement is over and interception cannot be achieved.

1.4 Outline

Next chapters deal with the issues related to guidance and control in the defense against ballistic missile. The work is organized as follows. The first part of the thesis (chapter 2 and 3) deals with strategic missiles issues. The second part (chapters from 4 to 7) deals with tactical missiles issues. Each chapter has a general introduction and a summary at the end. Numerical simulations have been included in every chapter to validate the theoretical considerations with practical results.

Chapter 2 describes the trajectory of an ICBM, including the derivation of the dynamical model for its motion and the formulation of a classical guidance law for the exo-atmospheric phase. Chapter 3 is dedicated to the problems ballistic threat detection and trajectory reconstruction by means of noisy measurements. The two tasks require the use of some state estimation algorithms, which are described concurrently.

Tactical guidance algorithms are introduced in chapter 4. Geometrical concepts related to each algorithm are explained along with the corresponding mathematical formulations. The discussion starts with the most intuitive guidance laws and ends presenting the more advanced ones. The issues related to the estimation of engagement related variables are

presented in chapter 5. Looking back to the state estimation algorithms previously defined, the implementation of a simple estimator in the loop is simulated with a simple guidance law. Then, a new guidance strategy is developed, that returns good engagement performances compared to other strategies in literature. The design of the interceptor vehicle is faced in Chapter 6. In particular, the aerodynamic configuration of the missile is analyzed, based on the short period response of the missile. An autopilot for the interceptor with the chosen configuration is derived in chapter 7. The control system is designed with linear techniques. The requirements for the design come from the new guidance strategy simulations, proposed in chapter 5. Final comments and conclusions are drawn in chapter 8.

Capitolo 2

Strategic missiles

Long-range strategic missiles are often referred to as ICBMs. They have large fuel supplies and extremely complex guidance and control systems. They are stored within specially designed areas, or even underground as a measure in case of an attack from an unfriendly nation. Apart from their use in military context, they can be integrated with space vehicles and payloads to be carried into outer space.
The trajectory of the ICBM undergoes several constraints, due to the critical conditions of the mission (high speed, high dynamic pressure). The trajectory can be scheduled off-line or can be calculated adaptively on-line, depending on the on-board computer capabilities and on the adopted strategy. During flight, the navigation system computes position, velocity and altitude. Navigation can be based on inertial systems or on celestial, terrestrial and magnetic references. The former systems do not depend on external equipments and send neither receive any signal and, therefore, can not be detected.
In this chapter the ICBM will be regarded as a rocket with solid engine. With a solid engine, thrust magnitude can not be modulated. Steering occurs by turning the thrust direction with a movable nozzle. This technique is known as Thrust Vector Control (TVC). TVC is the control input of the system. Aerodynamic control is not considered since it is in contrast with TVC and, furthermore, is not effective outside the atmosphere.
This chapter is organized as follows. First, the phases of the trajectory are studied. The dynamical model of ICBM motion is then derived and the mission of an ICBM is simulated. Eventually, a guidance law for the missile is described.

2.1 Trajectory phases

The trajectory of an ICBM can be split into two parts: the boost-phase and the free flight or ballistic phase. Reentry is the final phase of the free flight.

2.1.1 Boost-phase

The boost-phase is the powered phase of flight. It lasts from motor ignition and missile launch to motor burnout or cutoff. The final instant of the boost-phase is indeed indicated as time of burnout t_{bo}.
During this phase of flight, the rocket gains velocity by means of the thrust force obtained from a rocket engine. The vehicle travels through the atmosphere and eventually exits it, depending on mission and on cutoff altitude.
Boost phase can be divided in four arches of trajectory: the vertical trajectory, the pitch maneuver, the gravity turn trajectory and the guided phase.

- **Vertical trajectory** The vertical trajectory is usually a short arch of flight, necessary for range safety reasons (especially for ground launched rockets). During this phase the vehicle gains the velocity sufficient to overcome the gravity force that would otherwise draw it down. A roll maneuver might be performed to conveniently rotate the rocket so that, at the end of the vertical arch, its $\hat{y}_b$ body axis (orthogonal to the plane of symmetry of the rocket, *to the right of the pilot* in the aeronautic convention) is already pointed to the proper direction.

- **Pitch maneuver** With the pitch maneuver, the rocket bends along one of the planes passing for the vertical arch of the trajectory. The plane is identified by the relative azimuth angle. The bending motion originated by dedicated controls (e.g. TVC or aerodynamic controls) creates an initial incidence angle α that is subsequently reduced by the effects of thrust and gravity. When the incidence is completely nulled, the pitch maneuver is over ($pitch - over$ phase) and the velocity of the vector is restored along the longitudinal axis of the rocket. The kick angle χ is defined at this point as the angle between the local vertical direction and the velocity vector. χ is the complementary of the flight path angle γ at the pitch over.

- **Gravity turn** The gravity turn is a phase of flight where α is kept at an almost null value. Even small incidence angles, indeed, can cause large aerodynamic loads, especially on the nose of the rocket. The maximum load accepted by the rocket is expressed by the bound $\bar{q} \cdot \alpha$, where $\bar{q}$ is the dynamic pressure. Structural damage are likely to occur beyond this bound. The $q \cdot \alpha$ bound decreases with the altitude, due to the exponential decay of q. During this phase, thrust is always directed along the velocity vector. Therefore, it is evident that the kick angle heavily characterizes the remaining trajectory of powered flight.

- **Guided phase** When the rocket exits from the atmosphere, the bound $q \cdot \alpha$ is expired and the trajectory can be controlled in order to cover for the errors accumulated

in the previous phases. Guidance shall place the rocket on a trajectory with flight conditions that are appropriate for the mission. This trajectory shall end at burnout in a point that uniquely identifies position and velocity needed to reach the target on a free, unpowered flight. Suitable guidance laws can be perturbative or adaptive. A perturbative guidance law tries to steer the rocket towards a nominal trajectory, that has been previously calculated at ground. An adaptive guidance calculates at each instant a new trajectory starting from the actual flight conditions.

2.1.2 Free flight and reentry

After burnout, the rocket travels on a ballistic flight under the influence of gravity. The resulting trajectory is a conic trajectory (i.e., an ellipse). Usually, this phase takes place outside the atmosphere, so that the missile does not loose speed because of atmospheric drag. The initial conditions of the free flight, i.e. the flight conditions at burnout, determine the parameters of the trajectory.
The free flight phase ends when the rocket returns to the sphere centered at the center of Earth and with radius equal to the altitude reached at t_{bo}. No guidance is supposed to be needed, as the rocket was placed on a convenient elliptical trajectory that ends at the target.
The reentry phase starts when the rocket has returned to the reference sphere. More or less this coincides with the reentry in the atmosphere. Therefore, aerodynamic actions need to be considered again. Furthermore, heating must be taken into account due to the high reentry speed. These parameters limit the structural design of the rocket and the possible reentry trajectories for a given rocket.

2.2 Dynamical model

As it is evident from the description of the phases of flight of a rocket, there are three main forces that act on a rocket. They are the thrust, the gravity and the aerodynamic force. The equations of motion of a rocket can be derived expressing the contributions of these forces in a convenient reference frame.
The Earth Centered Inertial Frame (ECIF) is a Cartesian frame with basis $(\hat{c}_1, \hat{c}_2, \hat{c}_3)$ and origin O at the center of the Earth. It has the unit vector $\hat{c}_3$ aligned with the Earth axis of rotation; $\hat{c}_1$ belongs to the line in which the Earth equatorial plane intersects the ecliptic plane at a specified epoch t_{00} and is aligned with the vernal axis (i.e., the direction from the Sun to the first point in Aries) at t_{00}. The triple $(\hat{c}_1, \hat{c}_2, \hat{c}_3)$ forms a right-handed sequence of unit vectors.
An inertial reference frame system centered at the launch station is a suitable choice to

Tabella 2.1. Rocket model parameters

Parameter	Symbol	Definition	Dimensions
Initial thrust to weight ratio	n_0	$\frac{T}{gm_0}$	$[-]$
Reduced ballistic coefficient	β_0	$\frac{S}{2m_0}$	$\left[\frac{m^2}{Kg}\right]$
Specific impulse	I_{sp}	-	$[s]$
Structural over total mass ratio	u	$\frac{m_s}{m_0}$	$[-]$
Relative mass rate	q_0	$\frac{\dot{m}}{m_0} = \frac{n_0}{I_{sp}}$	$\left[\frac{1}{s}\right]$
Burn-out time	t_b	$\frac{1-u}{q_0}$	$[s]$
Thrust over weight ratio	$n(t)$	$\frac{n_0}{1-q_0 t}$	$[-]$
Ballistic coefficient	B	$C_D\frac{\beta_0}{1-q_0 t}$	$\left[\frac{m^2}{Kg}\right]$

describe the trajectory of a rocket. Such a frame is known as the *Local Horizon Frame*. Its basis are $(\hat{r},\hat{E},\hat{N})$ with $\hat{N}$ axis along the North direction of the launch station, $\hat{E}$ axis along the East direction of the launch station and $\hat{r}$ axis toward the centre of Earth, that is along the direction of the gravity vector. Therefore, gravity effects are easily expressed in this reference. On the other hand, the effects of thrust and aerodynamic forces are naturally expressed in a body fixed reference frame. Nevertheless, one can pass from the body reference to the inertial reference by means of simple angle transformations. The *Local Horizon Frame* is defined by two simple rotations about the center of mass:

$$\begin{pmatrix} \hat{r} \\ \hat{E} \\ \hat{N} \end{pmatrix} = \begin{pmatrix} \cos\lambda & -\sin\lambda & 0 \\ \sin\lambda & \cos\lambda & 0 \\ 0 & 0 & 1 \end{pmatrix} \begin{pmatrix} \cos L & 0 & -\sin L \\ 0 & 1 & 0 \\ \sin L & 0 & \cos L \end{pmatrix} \begin{pmatrix} \hat{c}_1 \\ \hat{c}_2 \\ \hat{c}_3 \end{pmatrix} \tag{2.1}$$

where λ and L are the absolute longitude and latitude of the center of mass, respectively. Having defined the position vector $\vec{R}$ in the *Local Horizon Frame* as $\vec{R} = \begin{pmatrix} x & y & z \end{pmatrix}$, the gravity force vector $\vec{G}$ can be defined as

$$\vec{G} = -\frac{\mu}{R^3}\vec{R} \tag{2.2}$$

where μ is the Earth' standard gravitational parameter.

The other forces can be written after the definition of some fundamental parameters. They are resumed in table 2.1 The aerodynamic force can be written starting from the knowledge of air density ρ and wind relative velocity $\vec{V}_R$. The former can be approximated by an

exponential model

$$\rho = \rho_0 e^{-k(R-R_\oplus)} \tag{2.3}$$

where ρ_0 and k are constant values and $R_\oplus$ is the Earth's radius. Wind relative velocity is the difference between the rocket velocity vector $\vec{V}$ and the wind velocity $\vec{V}_w$. The latter can be obtained assuming that the atmosphere is rotating with the same velocity $\vec{\omega}_\oplus$ as the Earth. Therefore,

$$\vec{V}_w = \vec{\omega}_\oplus \times \vec{R} \tag{2.4}$$

$$\vec{V}_R = \vec{V} - \vec{V}_w \tag{2.5}$$

Now the aerodynamic force vector $\vec{A}$ can be defined as

$$\vec{A} = -\rho V_R \frac{\beta_0}{1-q_0 t} \vec{V}_R \tag{2.6}$$

Thrust can be expressed as the product of thrust magnitude T times thrust direction $\hat{T} = \begin{pmatrix} l_1 & l_2 & l_3 \end{pmatrix}$. The former is given by

$$T = g \frac{n_0}{1-q_0 t} \tag{2.7}$$

The latter depends on the guidance strategy, and it is obviously varying with time. It is convenient to express thrust direction for each of the flight phases described in section 2.1.1.

During the vertical trajectory the thrust is aligned with the longitudinal axis of the rocket and, therefore, with the direction $\hat{r}$ to the center of the Earth

$$\hat{T}_{vert.} = \begin{pmatrix} 1 \\ 0 \\ 0 \end{pmatrix} \tag{2.8}$$

The roll and pitch maneuvers determine a plane for the trajectory and the kick angle. Thrust direction at the pitch over is thereby defined from the azimuth angle ψ and from χ.

$$\hat{T}_{pitchov.} = \begin{pmatrix} \cos\chi \\ \sin\chi \sin\psi \\ \sin\chi \cos\psi \end{pmatrix} \tag{2.9}$$

During the gravity turn, the thrust is aligned with the velocity vector in order to null the incidence [18]. Thrust direction is

$$\hat{T}_{grav.turn} = \hat{V} \tag{2.10}$$

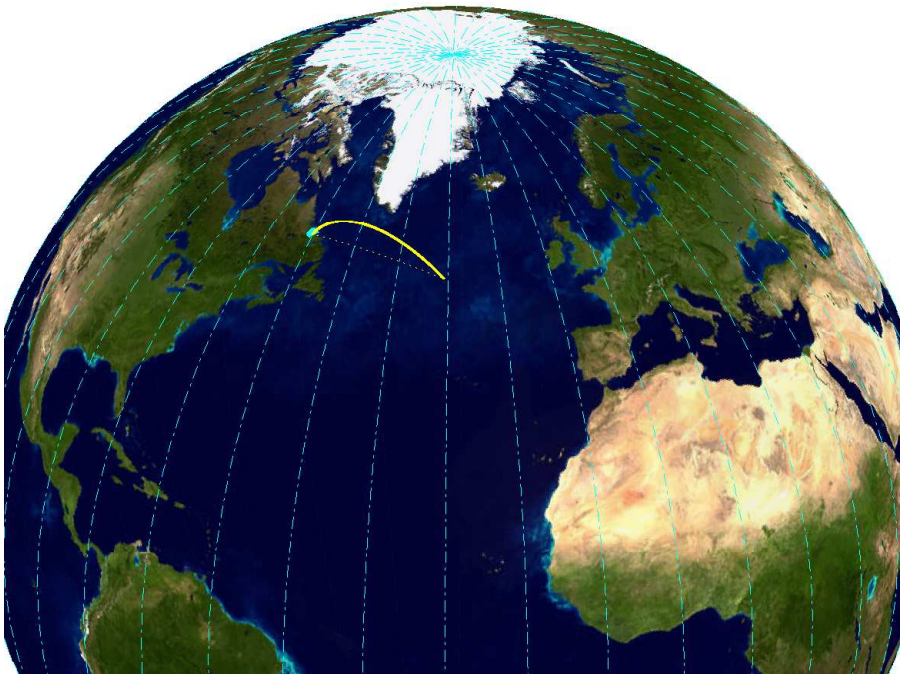

Figura 2.1. Rocket trajectory

After the gravity turn, thrust direction is defined by the particular guidance strategy adopted. The trajectory of a rocket is calculated integrating the following set of differential equations

$$\begin{cases} \dot{x} = u \\ \dot{y} = v \\ \dot{z} = w \\ \dot{u} = -\dfrac{\mu}{R^3}x - \rho V_R \dfrac{\beta_0}{1-q_0 t} V_{R_x} + g\dfrac{n_0}{1-q_0 t} l_1 \\ \dot{v} = -\dfrac{\mu}{R^3}y - \rho V_R \dfrac{\beta_0}{1-q_0 t} V_{R_y} + g\dfrac{n_0}{1-q_0 t} l_2 \\ \dot{w} = -\dfrac{\mu}{R^3}z - \rho V_R \dfrac{\beta_0}{1-q_0 t} V_{R_z} + g\dfrac{n_0}{1-q_0 t} l_3 \end{cases} \tag{2.11}$$

The trajectory of a medium range missile has been simulated by numerically integrating this dynamical model. The missile is identified by the parameters in table 2.2. The launch station and the $3D$ reconstruction of the trajectory are represented in Fig. 2.1.The missile flies initially along the launch vertical direction; then, it performs the pitch maneuver. The boost phase ends with the gravity turn trajectory.

Figs. 2.2 and 2.3 show the altitude and the velocity profiles for the missile. Flight time is about 1000 s. The missile reaches a maximum altitude of 800 Km, after 500 s. Some of the flight phases can be recognized in Fig. 2.3, which represents the velocity profile. The velocity of the missile is increasing due to thrust until t_{bo}. At $t = t_{bo}$, a discontinuity in the speed profile occurs. It indicates the end of the boost phase and the beginning of the

Tabella 2.2. Medium range missile parameters

Parameter	Value	Parameter	Value
n_0	2.2	I_{sp}	300 s
u_0	0.17	β_0	4.15e-05
q_0	7.33e-03	t_{bo}	113 s
L_0	55°	λ_0	−60°

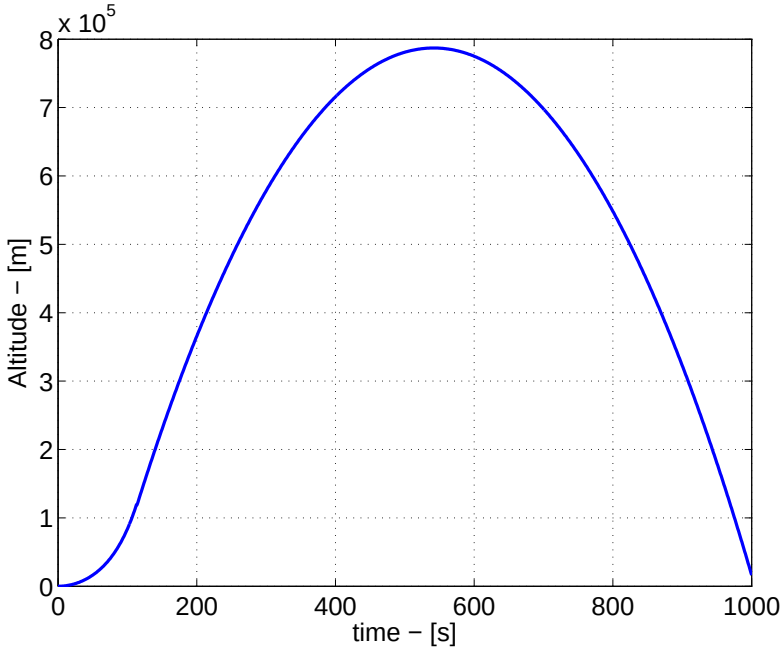

Figura 2.2. Rocket altitude

ballistic phase. The maximum speed is around 4 Km/s. At the beginning of the ballistic phase, the missile starts slowing down, until it reaches the apogee. The local minimum in the speed profile corresponds to the maximum in the altitude profile. From that point on, the missile is in free fall and it starts increasing its speed again. The maximum value of speed at reentry is a critical design criteria for the structure and the overall mission.

2.3 Guidance for strategic missiles

After the dynamic pressure bound has ceased to exist, strategic missiles usually performs some form of guidance to correct for errors and to arrive on the target point. The choice of the guidance law depends on the engine of the rocket. Liquid fueled engines can

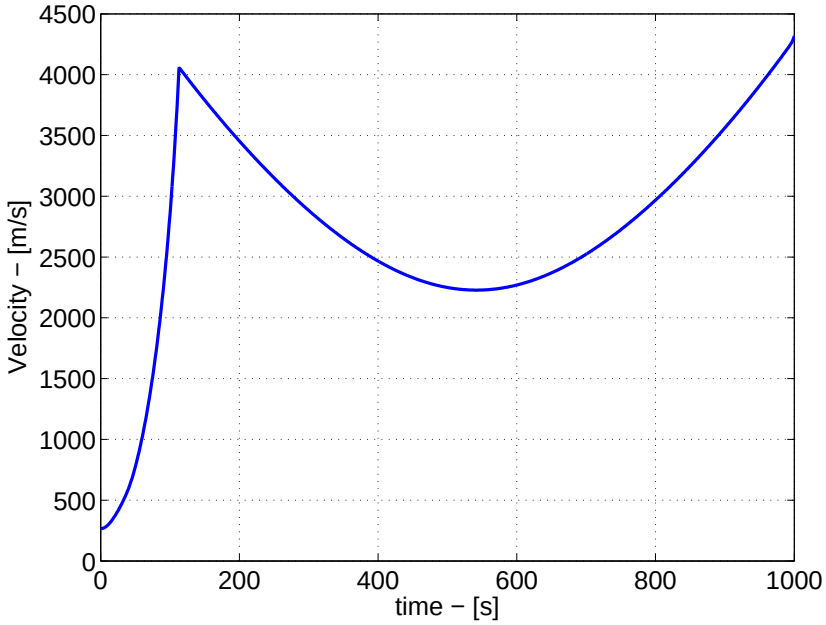

Figura 2.3. Rocket speed

terminate thrust before having burned all the propellant. Solid propellant engines can not terminate thrust before burn out and shall consume all the stored fuel before. The former rockets usually employ a form of Lambert guidance, the latter employ General Energy Management (GEM) steering to waste booster's fuel excess.
Both Lambert guidance and GEM are based on the numerical solution to Lambert's problem [6], [47]. According to Zarchan [68],

> At each instant of time, if you know where you are and where you want to go and how long it should take you to get to your destination, the solution to Lambert's problem tells you the magnitude and direction of the required velocity vector

Under certain assumptions, a simplified expression for Lambert guidance can be derived. In a two dimension, flat Earth, constant gravity scenario, given initial missile location x_0, y_0 and destination x_f, y_f and desired arrival time t_f, the goal of Lambert guidance is to find the velocity V required to fly ballistically from t_{bo} until t_f to the target point at t_f.
During free-flight, the missile flies on a elliptic trajectory. The general equation of a conic is

$$r = \frac{p}{1 + e\cos\theta_\star} \tag{2.12}$$

where r is the position of the missile along the elliptical trajectory, p is the semi-latus rectum of the ellipse, e is its eccentricity and $\theta_\star$ the true anomaly. It is well known [6] that

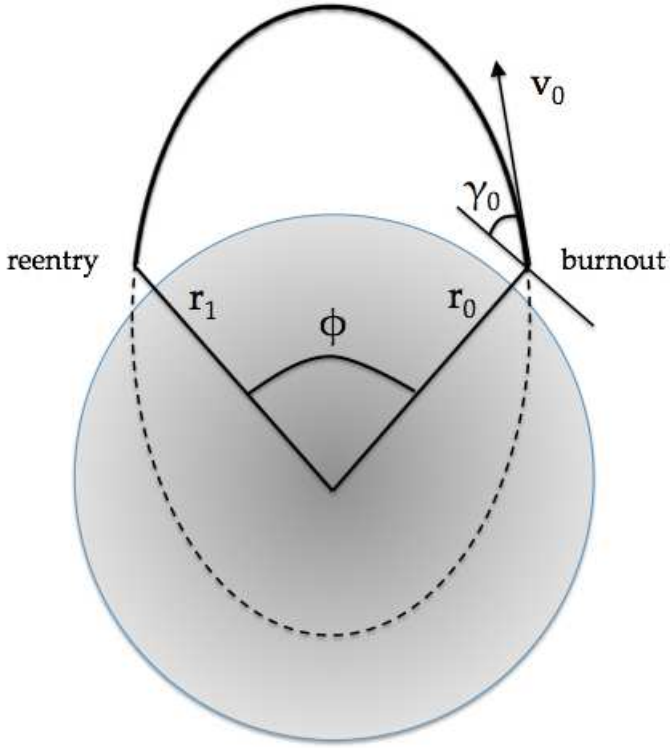

Figura 2.4. Ballistic trajectory geometry

the semi-latus rectum is related to the angular momentum h of the trajectory:

$$p = \frac{h^2}{\mu} \tag{2.13}$$

where μ is the planetary constant. The missile burnout will take place at some point r_0 on the ellipse with true anomaly θ_{art}, as it is shown in Fig. 2.4. If the missile has to fly to a point r_1 whose angular distance from r_0 is ϕ, the target point r_1 can be expressed as

$$\begin{cases} r_0 = \dfrac{p}{1+e\cos\theta_\star} \\ r_1 = \dfrac{p}{1+e\cos(\theta_\star+\phi)} \end{cases} \tag{2.14}$$

The velocity vector $\vec{V}$ of the missile on the ellipse can be expressed in the $\hat{p}\hat{e}$ plane:

$$\vec{V} = \frac{\mu}{h}\left(e\hat{p}+\hat{\theta}\right) \tag{2.15}$$

This vector can be decomposed in the radial and in the tangential direction. Remembering that the velocity $\vec{V}$ forms the *flight path angle* γ with the local horizon, one has

$$\begin{cases} V_r = V\sin\gamma = \dfrac{\mu}{h}(e\hat{p}\hat{r}) = \dfrac{\mu}{h}e\sin\theta_{ast} \\ V_\theta = V\cos\gamma = \dfrac{\mu}{h}\left(1+e\hat{p}\hat{\theta}\right) = \dfrac{\mu}{h}(1+e\cos\theta_{ast}) \end{cases} \tag{2.16}$$

From equations 2.16 one can derive expressions for the sine and cosine of θ_*:

$$\begin{cases} \sin\theta_\star = \dfrac{V\sin\gamma h}{e\mu} \\ \cos\theta_\star = \dfrac{1}{e}\left[\dfrac{h}{\mu}V\cos\gamma - 1\right] \end{cases} \tag{2.17}$$

At this point, it is useful to define the nondimensional parameter Q [5]

$$Q \triangleq \frac{V_0^2 r_0}{\mu} \tag{2.18}$$

Since the angular momentum of the orbit is defined as $h = rV\cos\gamma$, from the geometrical properties of the ellipse one can write

$$p = \frac{h^2}{\mu} = \frac{r_0^2 V_0^2 \cos^2\gamma_0}{\mu} = r_0 Q\cos^2\gamma_0 \tag{2.19}$$

Going back to equation 2.14 one can now write

$$r_1 = \frac{r_0 Q\cos{\gamma_0}^2}{1+e\cos(\theta_* + \phi)} \tag{2.20}$$

Using the trigonometric addition formulas, expressions 2.17 yields

$$\begin{aligned} r_1 &= \frac{r_0 Q\cos{\gamma_0}^2}{1+e\left[\cos\theta_\star\cos\phi - \sin\theta_\star\sin\phi\right]} \\ &= \frac{r_0 Q\cos{\gamma_0}^2}{1+e\left[\cos\phi\dfrac{1}{e}\left(Q\cos{\gamma_0}^2 - 1\right) - \sin\phi\dfrac{1}{e}Q\sin\gamma_0\cos\gamma_0\right]} \\ &= \frac{r_0 Q\cos{\gamma_0}^2}{1+Q\cos\phi\cos{\gamma_0}^2 - \cos\phi - Q\sin\phi\sin\gamma_0\cos\gamma_0} \\ &= \frac{r_0 Q\cos{\gamma_0}^2}{1-\cos\phi + Q\cos\gamma_0\left[\cos\gamma_0\cos\phi - \sin\phi\sin\gamma_0\right]} \\ &= \frac{r_0 Q\cos{\gamma_0}^2}{1-\cos\phi + Q\cos\gamma_0\cos(\gamma_0+\phi)} \end{aligned} \tag{2.21}$$

This equation expresses the trajectory of the missile in terms of the conditions at burn-out (i.e. r_0 and γ_0) and of the angle ϕ between r_0 and r_1. Substituting equation 2.18 in this expression, one obtains the velocity necessary for the missile to fly ballistically to r_1, starting from burn-out conditions. This velocity can be designated as Lambert's velocity V_{Lam}

$$V_{Lam} = \sqrt{\frac{\mu(1-\cos\phi)}{r_0\cos\gamma_0\left(r_0\cos(\gamma_0)/r_1 - \cos(\gamma_0+\phi)\right)}} \tag{2.22}$$

The task of the guided phase is to achieve this velocity at burn-out, so that the ICBM would fly ballistically to its target. The difference between V_{Lam} and the actual velocity of the ICBM is known as the velocity to be gained ΔV. If the thrust of the missile is aligned with

the velocity to be gained, then the V_{Lam} velocity will be obtained.
Defining the velocity to be gained on a plane *xy*, one has

$$\begin{aligned} \Delta V_x &= V_{Lam_x} - V_{M_x} \\ \Delta V_y &= V_{Lam_y} - V_{M_y} \\ \Delta V &= \sqrt{V_{Lam_x}^2 + V_{Lam_y}^2} \end{aligned} \tag{2.23}$$

If the magnitude of the current thrust acceleration is a_T, then the direction of the thrust at each instant should be aligned with the velocity to be gained vector

$$\begin{aligned} a_{T_x} &= \frac{a_T \Delta V_x}{\Delta_V} \\ a_{T_y} &= \frac{a_T \Delta V_y}{\Delta_V} \end{aligned} \tag{2.24}$$

2.4 Summary

This chapter has dealt with the trajectories of strategic missiles. During the atmospheric flight, a strategic missile must undergo a vertical segment and a gravity turn arch. When the missile is out of the atmosphere, and before the burn-out, the missile can be steered through the TVC. The task of the guided phase is to achieve the necessary condition (position, velocity and flight path angle) at burn-out, so that the missile would reach its target ballistically. Lambert guidance is a suitable method for missile steering during the boost-phase.
When the missile reenters the atmosphere, it experiences high drag forces and large heating. The structural design of the missile needs to take into account these constraints.
Tracking strategic missiles is the first task of the defense system and will be described in the next chapter. The knowledge of ICBM trajectories features is a prerequisite for tracking.

Capitolo 3

Threat localization

Now that the mission of an ICBM has been described, it is time to introduce the problem of intercepting an incoming ICBM. Interception involves target missile, interceptor and sensors for detection and tracking. The latter are the first phases of the interception. During them, the interceptor is provided with the information needed to start the engagement.
This chapter describes the systems employed for detection and tracking and how measurements are translated in useful information for the interceptor. Measurements can come from different sensing systems, such as radars or Infrared (IR) sensors. In order to reconstruct the trajectory of the missile, measurements are processed with an estimation algorithm.
The Kalman Filter is the optimal solution, in the sense of least-square estimation, to the problem of state estimation with noisy measurements, in the case of linear systems [37], [60], [41]. Other algorithms are employed in nonlinear contexts, where the estimation problem is infinite-dimensional. Extended Kalman Filter (EKF) [52] and Unscented Kalman Filter (UKF) [36] are two filters suitable for nonlinear problems.
This chapter is organized as follows: possible measurements for both the detection and the tracking phase will be introduced, including a modelization of the errors; then, two state estimation algorithms for nonlinear problems will be described; eventually, the simulation of an ICBM detection and tracking will be performed.

3.1 Measurements for detection and tracking

During the boost-phase, the missile exhaust generates a plume behind the vehicle as it travels through the atmosphere. This plume is composed by hot gases and it is a powerful source of IR radiation [59]. This radiation is visible from space. Therefore, a satellite equipped with an IR sensor can detect the plume of the missile. Furthermore, satellites can guarantee large-area coverage of the Earth, providing the defense system with early warning of missile launches. These features make space-based detection of ICBM very

interesting.

The DSP is a system that provides missile launches early warnings. It started in 1970, using satellites in Geosynchronous Earth Orbit (GEO). Its characteristics are described in [38]. Each satellite is equipped with a rotating telescope with detectors in the focal plane that locate the position of missile's plume. The precision of the DSP system is determined by the footprints of the pixels in its satellites' sensor array. The number of detectors suggest that the 1-σ position error is 500 m in all directions [4]. The three measurement from the space-based IR sensor are

$$\begin{aligned} X &= \tilde{X} + \nu_{IR} \\ Y &= \tilde{Y} + \nu_{IR} \\ Z &= \tilde{Z} + \nu_{IR} \end{aligned} \tag{3.1}$$

where X, Y, Z are the three position coordinates of the missile, expressed in an inertial reference, ν_{IR} is a zero-mean, Gaussian noise with variance σ_{IR}. The tilde sign stands for the true measurement.

Measurements for target tracking are usually provided in a 3D coordinate system. A ground-based radar can provide the necessary measurements. The measurements are easily expressed in the radar *Local Horizon Frame*, as it is shown in Fig. 3.1. The range R is the relative distance between the radar and the target; the azimuth ψ is the angle between the $\hat{N}$ direction and the projection of target position on the $\hat{N}\hat{E}$ plane; the elevation θ is the angle between the target position and its projection on the $\hat{N}\hat{E}$ plane. Doppler or range rate $\dot{r}$ measurements are not considered in this study.

The three measurements can be modeled in the following way

$$\begin{aligned} R &= \tilde{R} + \nu_R \\ \psi &= \tilde{\psi} + \nu_\psi \\ \theta &= \tilde{\theta} + \nu_\theta \end{aligned} \tag{3.2}$$

where the tilde symbol indicates the error-free true quantity and

$$\vec{\nu} = [\nu_R, \nu_\psi, \nu_\theta]'$$

is an additive noise vector. It is usually assumed that these noises are zero-mean, Gaussian distributed, and uncorrelated processes [43]

$$\begin{aligned} \vec{\nu} &\sim \mathcal{N}(0, \mathbb{R}) \\ \mathbb{R} &= diag\left(\sigma_R^2, \sigma_\psi^2, \sigma_\theta^2\right) \end{aligned} \tag{3.3}$$

For a surface radar such as the existing Aegis AN/SPY-1B, the variance of range noise can be taken as σ_R = 10 m. The variance of angular measurements noise can be considered as $\sigma_\psi = \sigma_\theta$ = 1 $mrad$ [4].

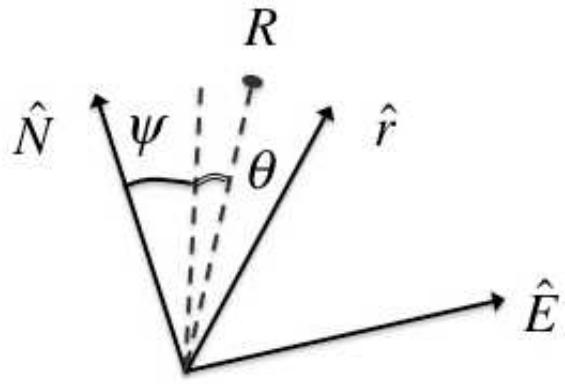

Figura 3.1. Radar measurements

3.2 Measurements processing

In this section the problem of processing the measurements from the radar is addressed. A dynamical filter is used to estimate the states of the missile, i.e. its position and velocity as it travels along its trajectory. A dynamical filter needs to know a dynamical model of missile motion, such as the one given in equation 2.11.

Due to the nonlinearity of this problem, a non linear filter needs to be employed. In the last 50 years, several filters for nonlinear estimation have been developed. Among them, the most widely known is the EKF, which is regarded as the *de facto* standard in the field [35]. The main feature of the EKF is the linearization of the dynamical model it performs around the actual conditions at each time step. This allows to approximate and propagate the mean and the covariance of the state variables.

The EKF works with a nonlinear discrete system in the form

$$\begin{aligned} x_{k+1} &= f(x_k) + g(u_k) + w_k \\ z_k &= h(x_k) + v_k \end{aligned} \tag{3.4}$$

where x is the state vector, u represents the control and z are the measurements. w and v are, respectively, the process and the measurements noise vectors with statistics

$$\begin{aligned} Q_k &= E[w_k w_k^T] \\ R_k &= E[v_k v_k^T] \end{aligned} \tag{3.5}$$

Linearizing the system at the k^{th} step around the actual state trajectory yields the definition of the matrices

$$F_k = \left.\frac{\partial f}{\partial x}\right|_{x_k} \quad G_k = \left.\frac{\partial g}{\partial u}\right|_{u_k} \quad H_k = \left.\frac{\partial h}{\partial x}\right|_{x_k} \tag{3.6}$$

Estimation is performed in two steps. In the first phase the value of the stochastic variable $\hat{x}$ is predicted according to the state model, by projecting the actual estimation and its covariance via the transition matrices. In the second step, the predicted estimation is corrected

with the information from the measurements. A gain vector K_k weights the difference between the real measurements and those one would obtain through the H matrix from the predicted state. The two phases can be summarized as follows

Prediction Predicted estimated state vector and its covariance matrix are denoted as $\hat{x}_{k|k-1}$ and $P_{k|k-1}$. The former can be obtained by propagating the old estimate $\hat{x}_{k-1|k-1}$ selecting the proper equations from the dynamical model of the process

$$\hat{x}_{k|k-1} = f(\hat{x}_{k-1|k-1}) + g(u_{k-1}) \tag{3.7}$$

$$P_{k|k-1} = F_{k-1}P_{k-1|k-1}F_{k-1}^T + Q \tag{3.8}$$

Correction The actual values of estimated state $\hat{x}_{k|k}$ and covariance $P_{k|k}$ are obtained after calculating the Kalman gain K_k and the estimated measurements $\hat{z}_k$

$$K_k = P_{k|k-1}H_k^T[HP_{k|k-1}H_k^T + R_k]^{-1} \tag{3.9}$$

$$\hat{z}_k = H_k\hat{x}_{k|k-1} \tag{3.10}$$

$$\hat{x}_{k|k} = \hat{x}_{k|k-1} + K_k(z_k - \hat{z}_k); \tag{3.11}$$

$$P_{k|k} = (I - K_kH)P_{k|k-1} \tag{3.12}$$

The main flaw of the EKF is in the propagation of the error covariance matrix P. Equation 3.8 assumes a linear evolution for P. This approximation can result very inappropriate in the case of non linear systems.

The UKF is another algorithm for state estimation of nonlinear systems, proposed by Julier and Uhlmann in the 1990's [34]. The main difference with the Kalman-like filters is in the prediction phase. This is based on the selection of a finite number of points from the state-space, the σ-points. The σ-points are picked up so that the σ-set has the same stochastic moments (mean and covariance) of the stochastic variable representing the actual state estimate. The nonlinear equations of the system can be directly applied to propagate the σ-points. After propagation, the mean and covariance of the estimated state can be calculated as the mean and covariance of the new set of points. This method was named [1] *Unscented transform* by its creator, Jeffrey Uhlmann [64].

The prediction and propagation steps of the UKF are stated in the following

[1] Apparently after a deodorant. See
`http://www.ieeeghn.org/wiki/index.php/First-Hand:The_Unscented_Transform`

Prediction If n is the dimension of the state-space, $2n+1$ points χ are selected to form the σ-set. Weight factors w_m and w_c are calculated for the mean and the covariance. The actual prediction of the state vector is the linear combination of the σ-points. The predicted measurements ζ_k are the measurements resulting from the σ-points. The predicted covariance is calculated from the deviations e_χ of each σ-point from the mean.

$$\hat{x}_{k|k-1} = \sum_{i=0}^{n} w_m^i \chi_k^i \tag{3.13}$$

$$e_{\chi_k} = \chi_k - \hat{x}_{k|k-1} \tag{3.14}$$

$$P_{k|k-1} = \sum_{i=0}^{2n} w_c^i e_{\chi_k}^i e_{\chi_k}^{i'} \tag{3.15}$$

$$\zeta_k = h(\chi_k) \tag{3.16}$$

$$\hat{z}_k = \sum_{i=0}^{n} w_m^i \zeta_k^i \tag{3.17}$$

Correction Correction is performed in the same fashion as in the case of the Kalman-like filters. A gain K_k is calculated from auxiliary covariance matrices Ψ_{zz} and Ψ_{xz} and it is then used to update the prediction of mean and covariance.

$$e_{\zeta_k} = \zeta_k - \hat{z}_k \tag{3.18}$$

$$\Psi_{zz_{k|k-1}} = \sum_{i=0}^{2n} w_c^i e_{\zeta_k}^i e_{\zeta_k}^{i'} + R_k \tag{3.19}$$

$$\Psi_{xz_{k|k-1}} = \sum_{i=0}^{2n} w_c^i e_{\chi_k}^i e_{\zeta_k}^{i'} \tag{3.20}$$

$$K_k = \Psi_{xz_{k|k-1}} \left(\Psi_{zz_{k|k-1}} \right)^{-1} \tag{3.21}$$

$$\hat{x}_{k|k} = \hat{x}_{k|k-1} + K_k(z_k - \hat{z}_k); \tag{3.22}$$

$$P_{k|k} = P_{k|k-1} - K_k \Psi_{zz_{k|k-1}} K_k^{'} \tag{3.23}$$

To obtain the σ-points for the next step one has to build a matrix $S = \|0 \vdots M \vdots M\|$, with M being defined as

$$M = \sqrt{\Lambda} \quad \Lambda = (n + \bar{k}) \left[P_{k|k} + Q_k \right] \tag{3.24}$$

The σ-points are updated as

$$\chi_k = \hat{x_{k|k}} + \sigma_i \tag{3.25}$$

where σ_i is the i^{th} column of S.

3.3 Strategic missile tracking

In this section, the missile tracking problem using the space-based IR sensor and the surface-based radar is analyzed. An UKF is used to estimate the states of the missile, i.e. its position and velocity in a inertial reference. The estimation is performed on a set of 200 Monte Carlo samples. Each sample differs from the others by the initial guesses given to the estimator. The simulation covers the boost-phase of the ICBM trajectory.
The trajectory to be estimated is the one simulated in section 2.2. The filter is provided with the model of equation 2.11. The identification phase, when the missile is tracked by the space-based IR sensor, lasts until t = 30 s. After that, the surface-based radar acquires the target missile and tracks it.
The process noise is originated from acceleration disturbances. Since the kinematic model corresponds to the differentiation of the position, the external noise on the process can enter only as an acceleration signal. The process noise covariance matrix Q is defined as

$$Q = \int_0^{T_s} \Phi(\eta)\Omega\Phi(\eta)^T d\eta \tag{3.26}$$

where Ω is a 6×6 matrix whose only non-zero element is a 3×3 diagonal block in the lower right position.

$$\Omega = \begin{pmatrix} 0 & 0 \\ 0 & 1 \end{pmatrix} \cdot q_0 \tag{3.27}$$

where q_0 is a numerical value found by experiment. Φ is the state transition matrix that, for a system such as the one from equation 2.11, is composed by 3×3 blocks

$$\Phi = \begin{pmatrix} 1 & T_s \\ 0 & 1 \end{pmatrix} \tag{3.28}$$

where T_s is the sampling time of the measurements. Carrying out calculation for Q, one yields a block matrix

$$Q = q_0 \begin{pmatrix} T_s^3/3 & T_s^2/2 \\ T_s^2/2 & T_s \end{pmatrix} \tag{3.29}$$

The filter is initialized with a vector of guesses $\hat{x}_{0|0}$ and with a $P_{0|0}$ matrix. The initial guesses belong to a Gaussian distribution with the true value of x_0 as mean and the elements of the $P_{0|0}$ matrix as variances

$$\begin{gathered} \hat{x}_{0|0} \sim \mathcal{N}(x_0, \sqrt{P_{0|0}}) \\ P_{0|0} = diag\begin{bmatrix} 2000^2 & 2000^2 & 2000^2 & 10^2 & 10^2 & 10^2 \end{bmatrix} \end{gathered} \tag{3.30}$$

The parameters of the simulation are reported in Table 3.1

Tabella 3.1. Simulation parameters

Parameter	Value	Parameter	Value
σ_{IR}	500 m	σ_R	10 m
σ_ψ	0.001 rad	σ_θ	0.001 rad
ω	1	T_s	0.02 s

3.3.1 Results

Figs. 3.2, 3.3, 3.4, 3.5, 3.6, 3.7 show the results of the estimation process, plotted against time. The red line is the mean estimation error; the green line is the error from a sample run; the blue line is the error standard deviation; the black lines are the 1σ bounds calculated by a sample run of the filter.

During the detection phase the filter is able to estimate correctly the trajectory of the ICBM: the estimation error expected from the filter (the black lines) is converging to a value around 50 m for the position and around few m/s for the velocity. During the tracking phase the expected errors are even smaller: around 10 m for the position and around 1 m/s for the velocity.

Furthermore, the filter is well tuned. The standard deviation of the errors is almost identical to the 1-σ bounds from the filter (blue and black lines superimposed). The mean error on the set of samples is near zero, meaning that the filter has no bias. The sample error stays satisfactorily inside the 1-σ bounds.

3.4 Summary

This chapter has dealt with detection and tracking of an ICBM. The measurements from space-based IR sensors and a surface-based radar have been employed to estimate missile's trajectory in a numerical simulation.

Trajectory estimation has been carried out using an UKF. This is a suitable algorithm for nonlinear estimation. The simulation has been conducted on a set of Monte Carlo samples. Each sample differs from the others by the initial guess provided to the filter.

A good reconstruction of target's trajectory allows to set up an effective defense strategy. The interceptor will be guided towards the target thanks to the tracking information. When the distance between the interceptor and the target will be reduced to few kilometers, the task of estimating target's trajectory will be demanded to the interceptor itself. The issues related to this estimation problem will be dealt with in chapter 5, after having described guidance laws for the interceptor.

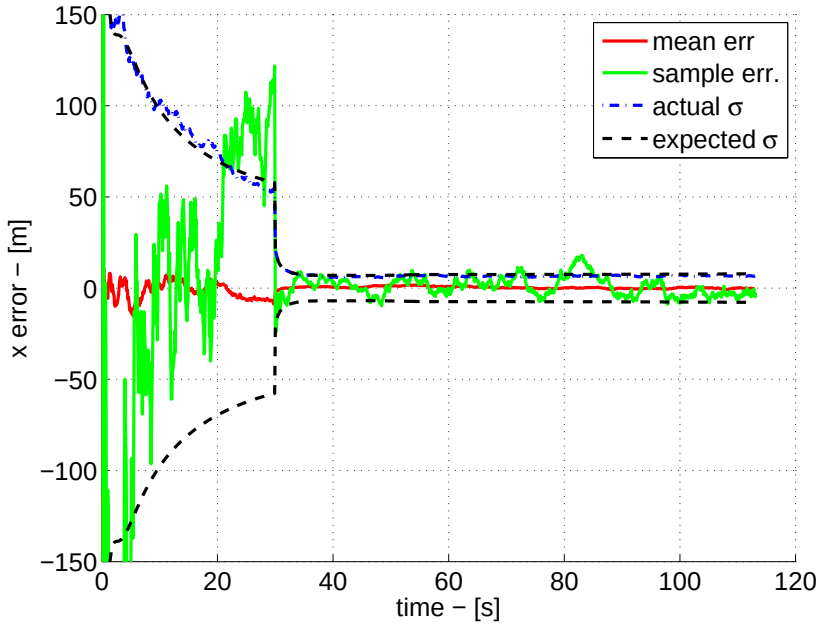

Figura 3.2. Estimated X

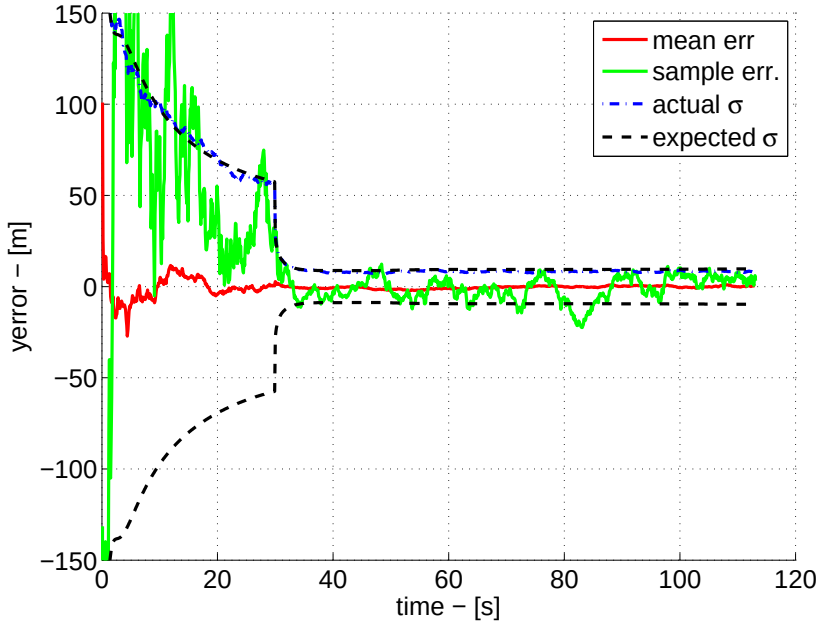

Figura 3.3. Estimated Y

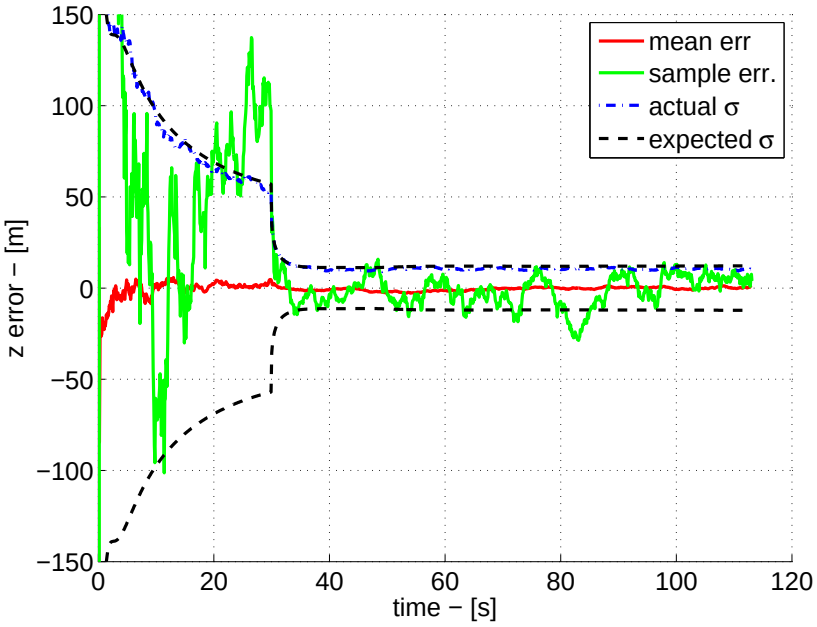

Figura 3.4. Estimated Z

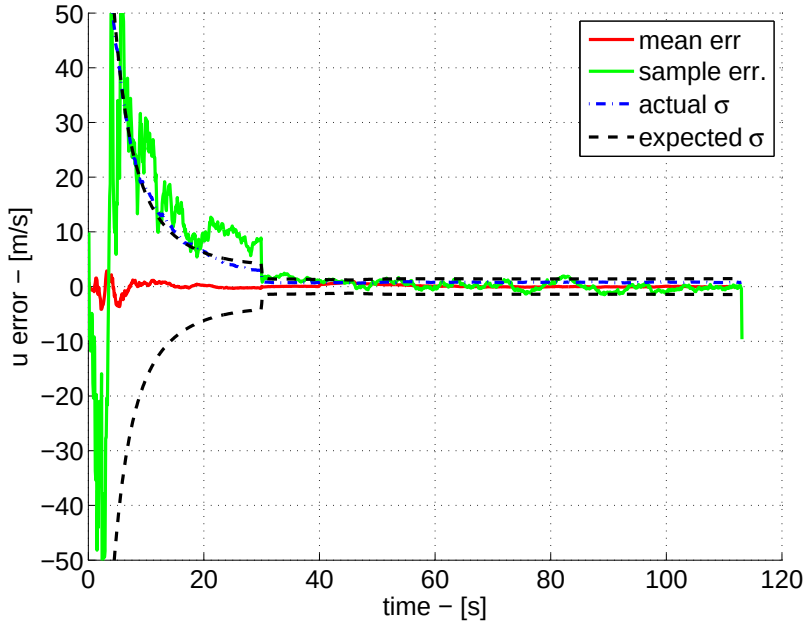

Figura 3.5. Estimated U

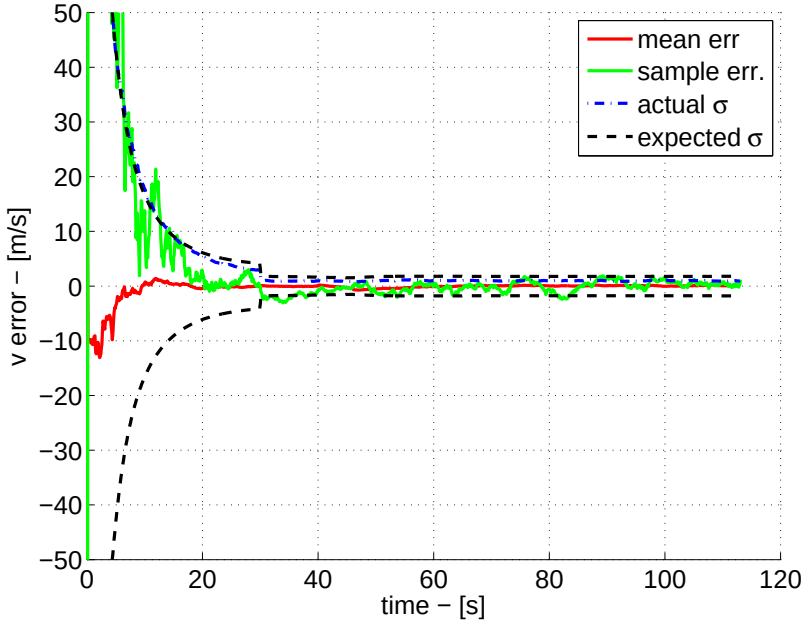

Figura 3.6. Estimated V

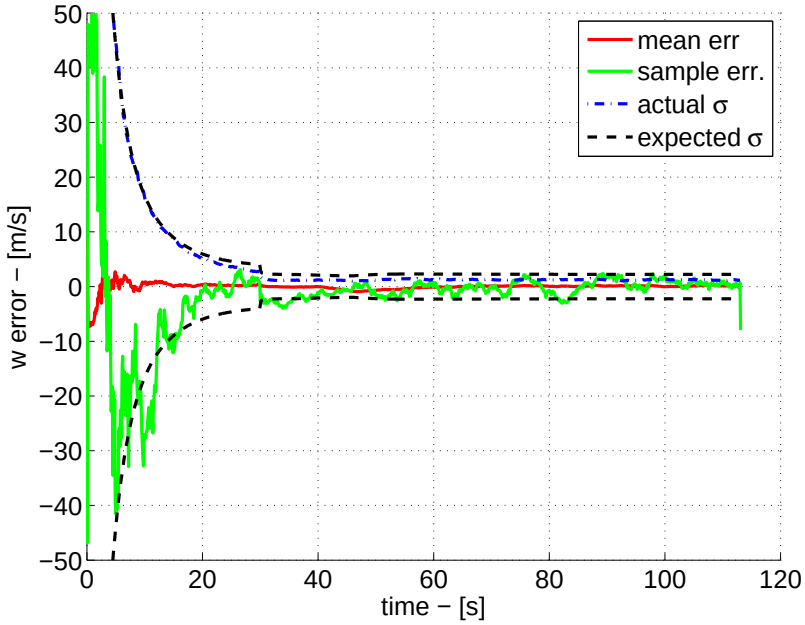

Figura 3.7. Estimated W

Capitolo 4

Tactical missile guidance laws

The discussion has dealt so far with threat related issues. Detecting an incoming missile and being able to track its trajectory is the first requisite for a defense system. The next requisite is to have a system able to tackle missile threat. As explained in chapter 1, this system is based on a missile that should hit the incoming ballistic missile. A major necessity for the interceptor is to be able to steer its trajectory depending on the ballistic missile.
This chapter presents an overview of the basic concepts for tactical missiles guidance systems. Guidance is a process that involves two subjects, an interceptor (later on defined also as *pursuer*) and a target (also referred to as *evader*). The task of the guidance system is to drive the missile towards the target until interception. When the missile hits the target the engagement is concluded.
Missiles can be guided in all the phases of the mission. During the boost phase the missile can be either guided or not. During the midcourse, guidance, if active, should bring the missile onto the desired course and maintain it on course until it enters in the last phase of the engagement. Guidance is crucial during the terminal phase of the engagement. In this phase, high accuracy from the guidance system is required to intercept the target. Small errors can result in large miss distance at the end of the engagement.
In this chapter a classification of the most common guidance techniques will be first given. Then the geometrical and mathematical aspects of the principal guidance laws will be introduced. The guidance laws will be described starting from the most simple and traditional algorithms, such as Pure Pursuit (PP) and Proportional Navigation (PN). Then, more advanced laws will be derived as extension of the previous algorithms by adding new elements to the analysis. Optimal control theory and differential games frameworks will be employed in the description of guidance laws. At the end of the chapter, an introduction to estimation in the loop issues will be given. Numerical examples will support the description of the algorithms.

4.1 Classification of guidance techniques

Missiles guidance systems are classified in three main groups [61]: homing, nonhoming and direct. The *homing* term refers to a missile that tracks the target thanks to some form of energy emitted by the latter. Homing can be *passive*, if the source of energy is the target itself (RF transmissions, acoustic noise, heat, etc.), *active*, if the target reflects energy beamed at it from the missile or *semiactive*, if the missile exploits the reflection of energy from the target, with the latter being illuminated by an external source. In the following, the guidance control system will be often referred to as the *homing loop*.
A missile like the *Sidewinder*, which will be used in the simulation in chapter 5, is an an example of a passive homing guided missile. It uses an infrared device to identify the target against the background. This kind of devices are useful against any target with large temperature differentials with respect to the surroundings.
Examples of homing systems can be found not only in engineering applications, but also in nature. Hawks catch their preys using their sight and thus performing passive homing. Bats perform active homing, because they emit ultrasound pulses.
Nonhoming techniques include *inertial* guidance. This is mostly related to ballistic missiles, since it is not based on sending and receiving signals, but rather on computing position and velocity. Corrections are provided by measurements from on board equipment.
Direct guidance techniques are based on commands calculated at the ground controlling site and transmitted to the missile. Both the missile and the target must be tracked by some tracking system (e.g. a radar). If guidance commands are sent directly to the missile the technique is called *command guidance*. *Beam rider guidance* is another direct technique where the target is tracked by an electromagnetic beam. The missile senses the beam by means of a on board antenna. Variations in the beam correspond to changes in target's relative positioning and can be translated to guidance command.

4.2 Line of sight and Pure Pursuit

The first geometrical concept to be introduced in missile guidance is related to the Line of Sight (LOS). This is defined as the ray that starts from some reference point O and passes through the target T. Considering a fixed reference frame one can define the LOS by the angle λ which it forms with the horizontal, as in Fig. 4.1.

Under certain assumptions (no target maneuvers, constant velocity for both M and T, ideal actuation of required acceleration), one can write a set of three equations which describes the engagement. The variables are the range R, the angle λ and the missile flight path angle

γ_M (see Fig. 4.1)

$$\begin{cases} \dot{R} = v_T \cos(\gamma_T - \lambda) - v_M \cos(\gamma_M - \lambda) \triangleq V_R \\ \dot{\lambda} = \dfrac{v_T \sin(\gamma_T - \lambda) - v_M \sin(\gamma_M - \lambda)}{R} \triangleq \dfrac{V_\lambda}{R} \\ \dot{\gamma_M} = \dfrac{a_M}{v_M} \end{cases} \tag{4.1}$$

This set of equations captures the motion of both the missile and the target, provided that the latter has constant speed v_T and heading γ_T. If this is not, one shall consider a larger number of variables. The term a_M refers to missile acceleration.

The first guidance law that can be considered in this framework is called Pure Pursuit (PP) [58]. Its purpose is to have the missile velocity vector v_M always pointed along the LOS, i.e. along R. This means that one can assume $\gamma_M = \lambda$ and, consequently, $\dot{\gamma}_M = \dot{\lambda}$. Then, a_M turns out to be

$$a_{M_{PP}} = v_M \dot{\gamma}_M = v_M \dot{\lambda} \tag{4.2}$$

Due to its simplicity, this rule was widely employed by the first generation of two-point guided weapons until the early 50's. It is interesting to note that also animals seem to know this law: ants use the PP rule to follow one another [12].

A modified version of this rule has an addictive term for error compensation, which is needed in case v_M is not aligned with the LOS:

$$a_{M_{PPm}} = v_M \dot{\lambda} + K_{PP}(\gamma_M - \lambda) \tag{4.3}$$

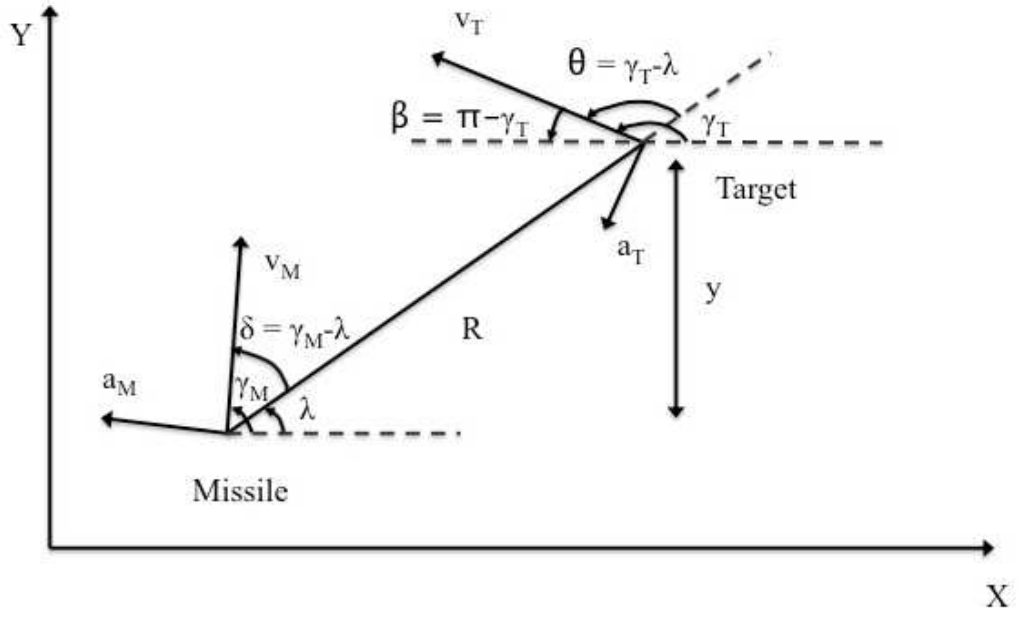

Figura 4.1. Two dimensional engagement scenario

K_{PP} is a gain that is chosen according to the desired performance, in terms of time and control effort.
In order to evaluate the issues related to the PP rule expressed in 4.2 an engagement simulation was conducted. The engagement is planar, with M's initial position in the origin of the reference. The initial range R_0 between M and T is 10000 m and the initial LOS angle λ_0 is 10°. T has constant speed v_T = 500 m/s and constant flight path angle $\gamma_T = 90°$. M's initial flight path angle is 20° and the constant speed is v_M = 200 m/s.
Fig. 4.2 shows M's and T's trajectories and the range R vs time. It can be seen that M hits T from behind: this is a peculiarity of the PP engagement, which is often referred to as *tail chase* or *dog chase*.

4.3 Collision triangle and Proportional Navigation

With the assumptions of constant heading and constant speed for both M and T, one can derive conditions under which the collision is guaranteed. This is related to the concept of Parallel Navigation, which aims to keep the LOS rate always constant ($\dot{\lambda} = 0$). From the set of equations 4.1 and with reference to the angles in Fig. 4.1 one sees that constant LOS rate results in

$$v_M \sin\delta = v_T \sin\theta \tag{4.4}$$

Another obvious condition for the engagement is that $\dot{R} < 0$, otherwise we will have M receding from T. This means that

$$v_M \cos\delta > v_T \cos\theta \tag{4.5}$$

Conditions 4.4 and 4.5 are called *Collision Course (CC) conditions*. They allow to introduce the geometrical concept of *collision triangle*, represented in figure 4.3. Here v_C is the closing velocity, defined as $v_C = -\dot{R} = v_M cos(\gamma_M - \lambda) - v_T cos(\gamma_T - \lambda)$.
Achieving and maintaining $\dot{\lambda} = 0$ is the purpose of PN, one of the most widely known and employed guidance law. PN commands are always proportional to $\dot{\lambda}$ and to the closing velocity. The expression of the PN law is

$$a_{M_{PN}} = N v_C \dot{\lambda} \tag{4.6}$$

N is a unit-less gain, called *Navigation constant*, that has to be chosen with respect to some performance index.
In order to evaluate the differences between PP and PN a simulation was run with both guidance laws. The engagement is planar, with M initial position in the origin of the reference. The initial range R_0 is 10000 m and λ_0 is 10°. T has constant speed $v_T = 500$ m/s and

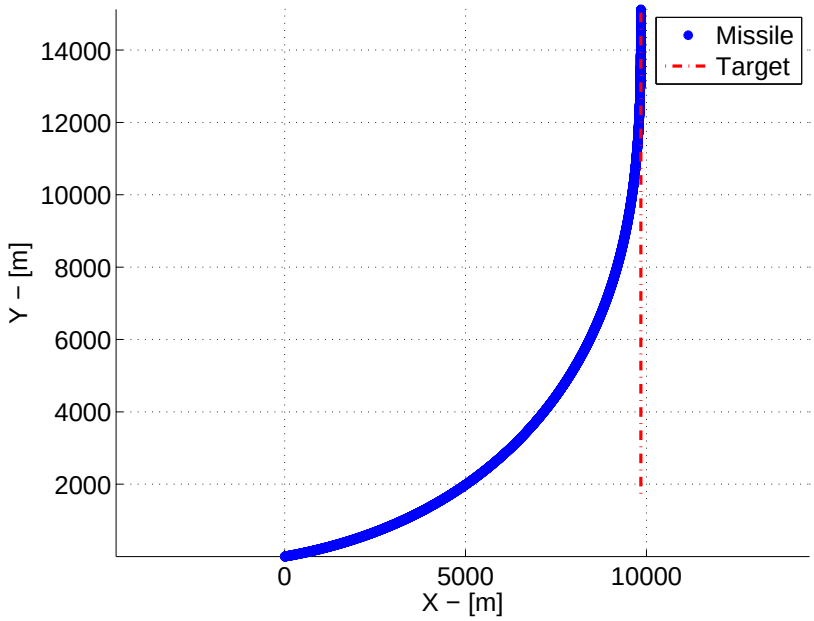

(a) Trajectory

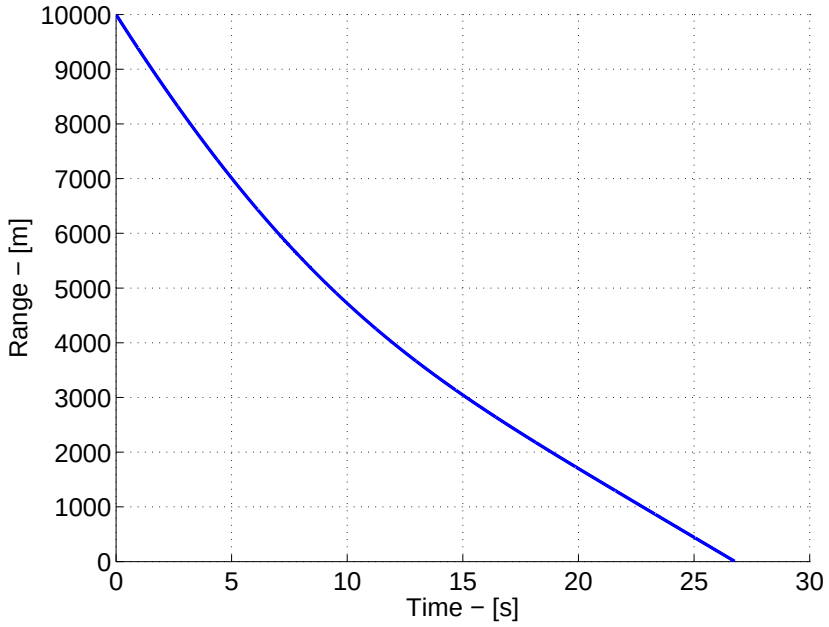

(b) Relative distance

Figura 4.2. PP engagement

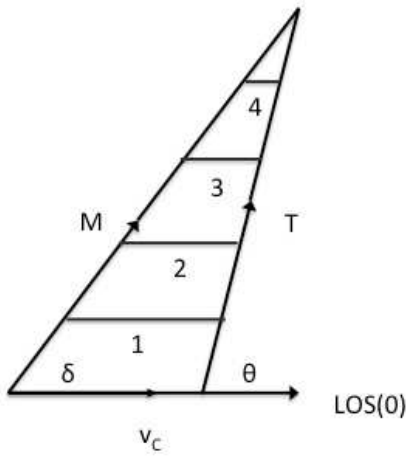

Figura 4.3. Collision triangle

constant flight path angle $\gamma_T = 90^\circ$. M's velocity is not initially aligned with the LOS, as $\gamma_M = 20^\circ$. v_M is constant and its value is 750 m/s. A number of simulations has been run, varying the values of the navigation gains from expressions 4.3 and 4.6.

Figs. 4.4 and 4.5 show the results of the simulations. In all the cases M hits T. Unlike PP, PN does not generally hit the target from behind: the trajectory is more *'straight'*. The only exception is when $N = 2$: this time the missile's trajectory is similar to those from the PP. It is also interesting to observe the different behaviors of the control history, which is the acceleration required from the guidance system: gain variations seem not to affect the level of required acceleration in the case of PP, while they are very significant in the case of PN. Furthermore, PN required acceleration has a peak at the beginning, but then it goes asymptotically to zero towards the end, meaning that the correction is performed as soon as possible. Higher gains highlight this trend.

4.4 Linearization and miss distance

Usual engagement conditions for *head on* or *tail chase* cases admit small flight path angles and almost constant bearing. This allows to perform some linearization in the guidance law derivation.

In the scenario of Fig. 4.1 y is the relative separation between M and T, perpendicular to the fixed reference. Having constant bearing means to have $\dot{\lambda} = 0$. Therefore, one can choose a small λ such that

$$y = R\sin\lambda \simeq R\lambda \tag{4.7}$$

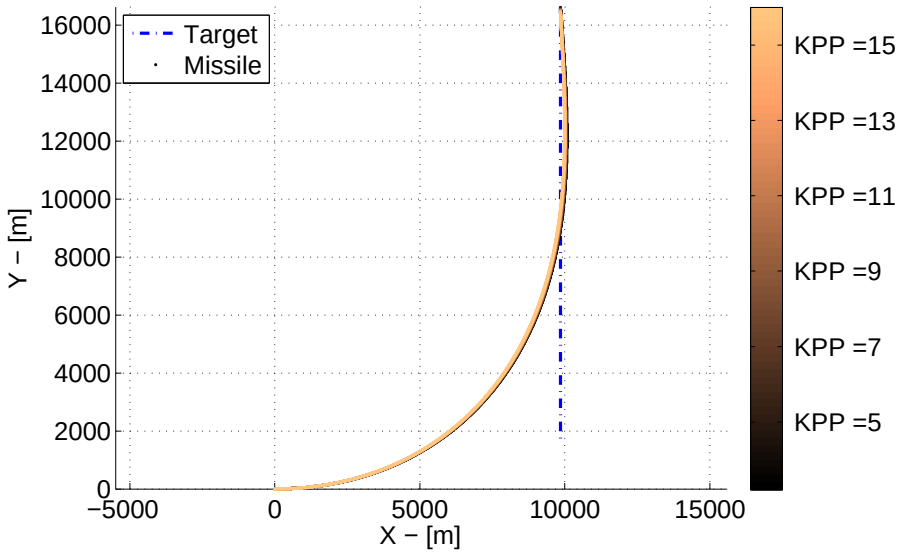

(a) PP trajectory

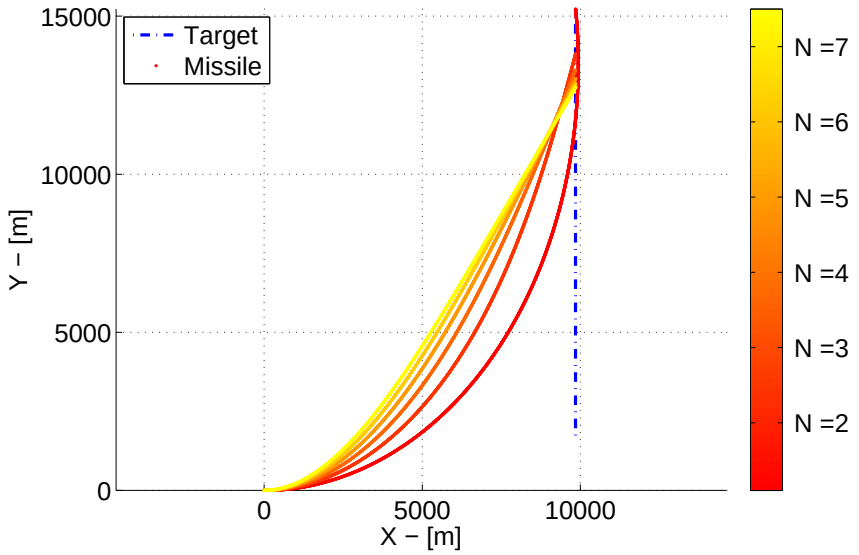

(b) PN trajectory

Figura 4.4. Comparison between PP and PN - trajectories

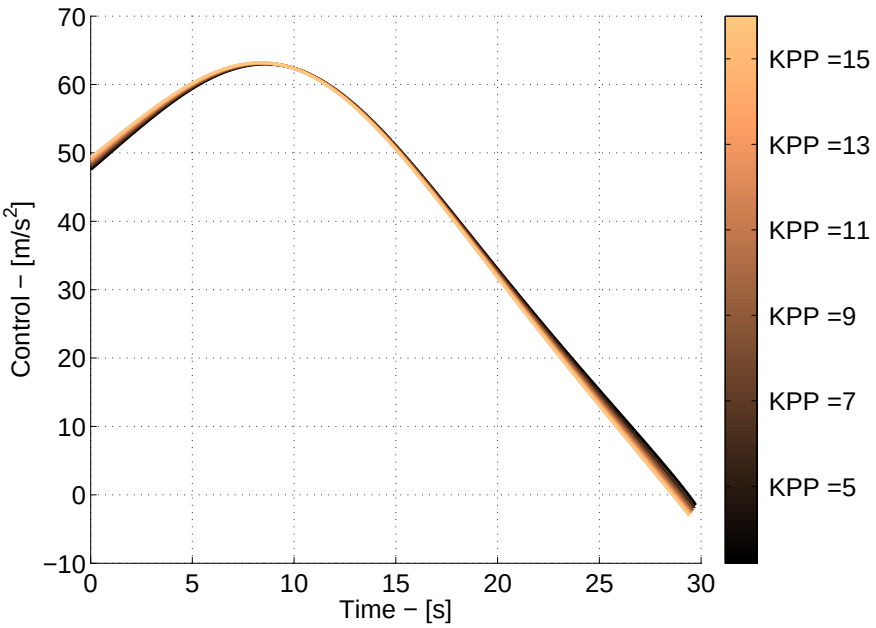

(a) PP control

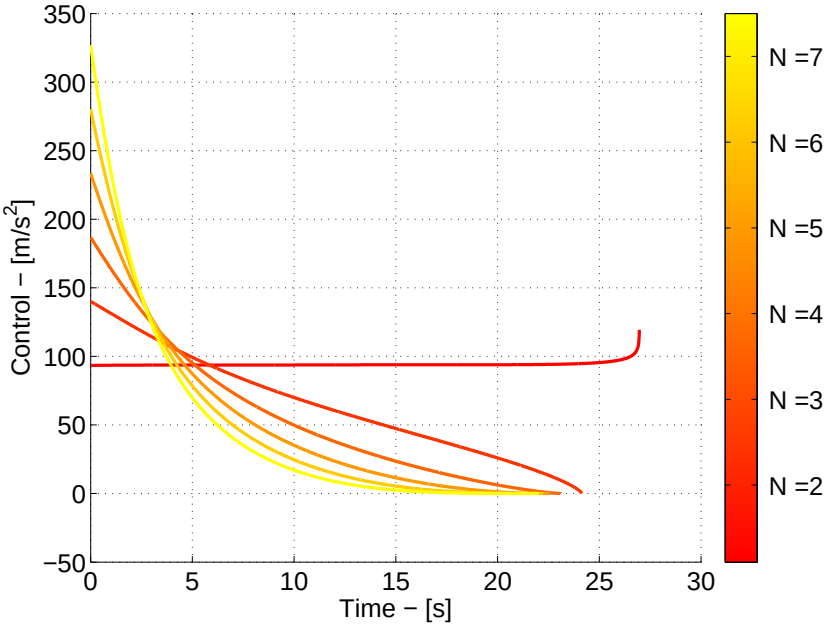

(b) PN control

Figura 4.5. Comparison between PP and PN - control efforts

This leads to the definition of the *miss distance* as the relative separation between M and T at the end of flight

$$miss = y(t_f) \tag{4.8}$$

Here t_f is a constant, *a priori* chosen. The quantity $t_f - t$ is defined as the time to go t_{go} until the end of flight. R is then the distance covered at a velocity V_C in the interval [t, t_f]

$$R = V_C(t_f - t) = V_C t_{go} \tag{4.9}$$

$V_C = V_M \pm V_T$ is called closing velocity, respectively for a *head on* or a *tail chase*. Differentiating y twice, one obtains

$$\begin{aligned} \dot{y} &= \dot{R}\lambda + R\dot{\lambda} \\ &= -V_C\lambda + V_\lambda \\ \ddot{y} &= -V_C\dot{\lambda} + -\dot{V}_C\lambda + \dot{V}_\lambda \\ &= \dot{V}_\lambda \end{aligned} \tag{4.10}$$

since λ and V_C are assumed to be constant and their derivatives are therefore null. Going back to the definition of y, λ can be expressed as

$$\lambda = \frac{y}{R} \tag{4.11}$$

Differentiating this expression one obtains

$$\begin{aligned} \dot{\lambda} &= \frac{R\dot{y} - y\dot{R}}{R^2} \\ &= \frac{R\dot{y} + yV_C}{V_C^2 t_{go}^2} \\ &= \frac{y + \dot{y}\dfrac{R}{V_C}}{V_C t_{go}^2} \\ &= \frac{y + \dot{y}t_{go}}{V_C t_{go}^2} \end{aligned} \tag{4.12}$$

The quantity $y + \dot{y}t_{go}$ is defined as the Zero Effort Miss (ZEM). At each instant the ZEM is the miss distance that would result if both the missile and the target made no further maneuver from then on. The PN law can now be written as

$$a_{M_{PN}} = Nv_C\dot{\lambda} = N\frac{ZEM}{t_{go}^2} \tag{4.13}$$

It can be demonstrated [8] that PN with $N = 3$ turns to be the optimal solution in the case of a linearized problem, under the assumptions of nonmaneuvering target and zero-lag (i.e. ideal) guidance system.

4.5 Corrections to the PN law

A restrictive hypothesis considered so far is to have a target with constant speed and heading. This simplification might result too strong in real applications, since targets can perform evasive maneuvers at any point of the engagement. Thus, it is useful to take into account target acceleration in the definition of the guidance laws.

Augmented Proportional Navigation (APN) is a modification of the PN law which explicitly takes into account target acceleration. This new law can be derived by means of analytical analyses. In particular, it can be derived applying optimal techniques that will be dealt with in section 4.6. Mathematical proofs of the solution can be found in [40] and [8].

Nevertheless, the APN law can also be inferred in a more intuitive way, by remembering equation 4.13. There the ZEM was defined as the distance that would result in case both the missile and the target made no further correction. In the case of a maneuvering target, this quantity can be modified in order to take into account the effects of target maneuver. The new definition of the ZEM is

$$ZEM_{APN} = y + \dot{y} t_{go} + \frac{1}{2} a_T t_{go}^2 \tag{4.14}$$

because the resulting distance is that of an uniformly accelerated motion with acceleration a_T. The APN law is now modified as

$$a_{M_{APN}} = \frac{K_{APN} \cdot ZEM_{APN}}{t_{go}^2} \tag{4.15}$$

The implementation of APN inside the homing loop is shown in the block diagrams in Fig. 4.6 along with the PN law. The only difference among the two loops is the target acceleration term that feeds the commanded missile acceleration. In order to compare these two algorithms against a maneuvering target, the models of Fig. 4.6 were run. The initial value for the miss is 500 m and the target performs an evasive 3 g maneuver. Results of the simulations are shown in Fig. 4.7. Accelerations are normalized with the level of target maneuver. The maximum level of required acceleration with APN is almost half the level of PN. Furthermore $a_{M_{APN}} < a_{M_{PN}}$ for more than half t_f.

Another assumption that has been made so far is that the missile is able to implement instantaneously any acceleration command calculated from the guidance system. However, in real missile applications, commands actuation by the autopilot takes a finite time. This lag is a very important feature of the guidance system: large times can result in large miss distances.

The lags of the guidance systems can be approximated with transfer functions of a certain order. The simplest representation is a first order transfer function with a certain time constant τ. Indicating the commanded acceleration with u and the actual missile acceleration

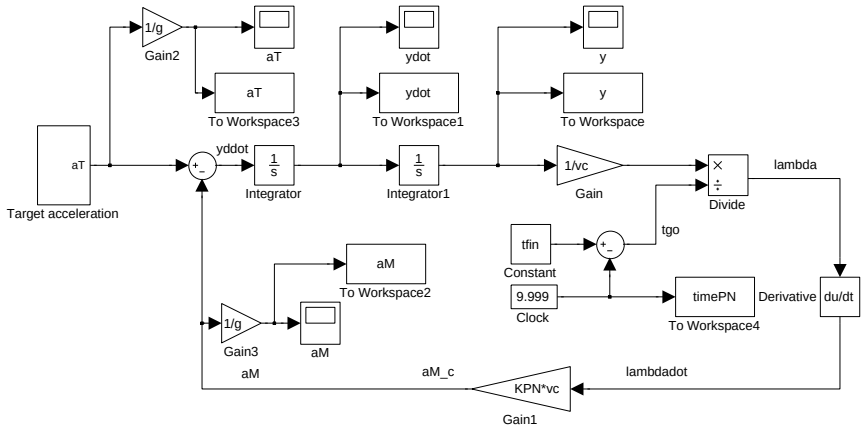

(a) PN

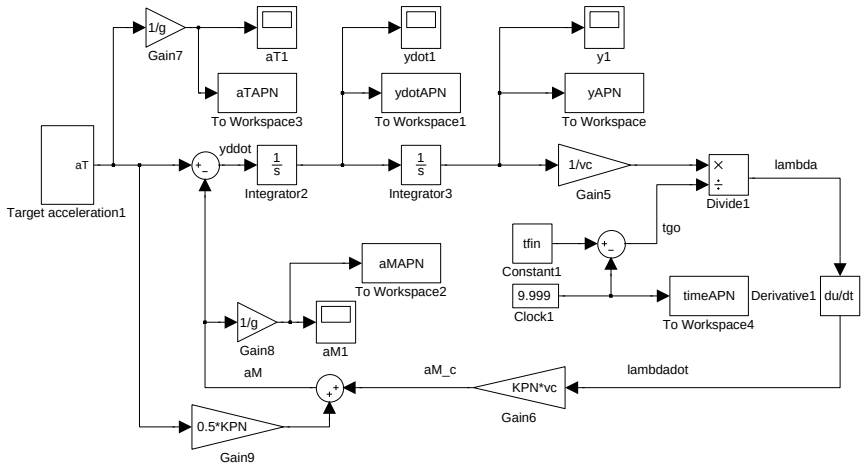

(b) APN

Figura 4.6. PN and APN block diagrams

with $a_M^{'}$ one has

$$\dot{a}_M = \frac{u - a_M}{\tau} \tag{4.16}$$

Time constant value varies from missile to missile, but generally ranges between 0.1 and 1 s. A larger time constant would be hardly tolerable for the guidance system.
To test the effects of the guidance system lag on the engagement, the previous simulation was run again, this time considering equation 4.16. Results are shown in figure 4.8. The maximum level of required acceleration is almost the same in both cases, although APN requires less acceleration for more than half t_f as in the zero order lag guidance system. The lag does not significantly affect the outcome of the two algorithms, even if it makes acceleration profiles less *'straight'*.

4.6 Optimal guidance laws

The guidance laws described so far are derived from geometric considerations. They work well in the ideal cases of nonmaneuvering targets and zero-lag guidance systems. At the end of the 1950's the optimal control theory approach started to be employed to derive optimal guidance laws [30], [13], [39], [14]. However, it was just in the 1990's that the newly derived guidance laws found real applications in air defense, thanks to the advances in the numerical techniques and to the diffusion of microprocessors [58].
In this section expressions for optimal guidance laws will be derived in the case of a zero-lags guidance system and of a single lag guidance system. In order to implement the optimal guidance law in a feedback control loop inside the homing loop, it has to be a function of system variables. Among the many possible formulation of the cost functional, the most practical definition for the optimal law is to minimize the miss distance and the required acceleration. The requirement is

$$y(t_f) = 0 \quad \text{subject to minimizing} \quad \int_0^{t_f} u^2(t)dt \tag{4.17}$$

where u is the missile acceleration, here considered as a control.
The linear variables introduced in Sec. 4.4 form a practical and useful set of equations to work with. Three state variables describe the engagement. The state vector is defined as

$$x = [\ x_1 \quad x_2 \quad x_3\ ] = [\ y \quad \dot{y} \quad a_T\ ] \tag{4.18}$$

If the guidance system has no lags, the dynamical model is

$$\begin{cases} \dot{x}_1 = x_2 \\ \dot{x}_2 = x_3 - u \\ \dot{x}_3 = 0 \end{cases} \tag{4.19}$$

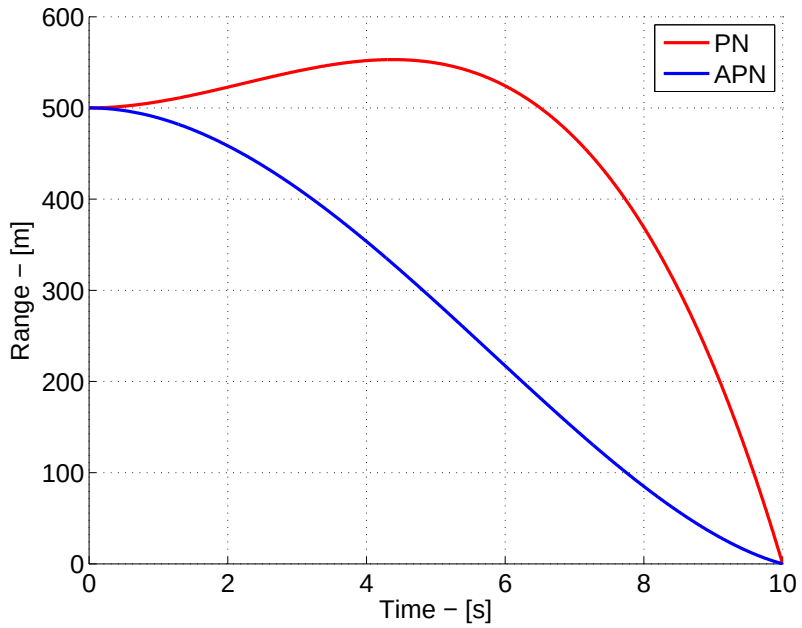

(a) miss

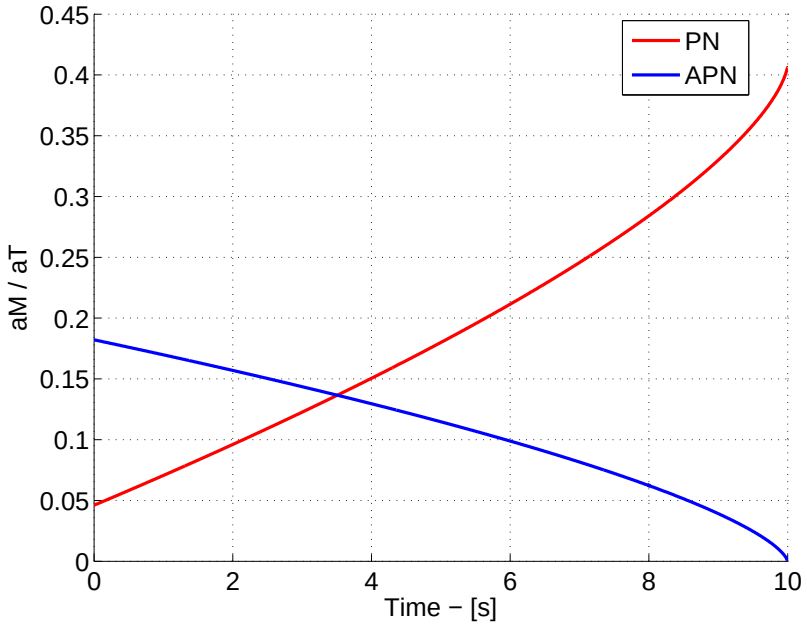

(b) acceleration

Figura 4.7. PN and APN against target maneuver

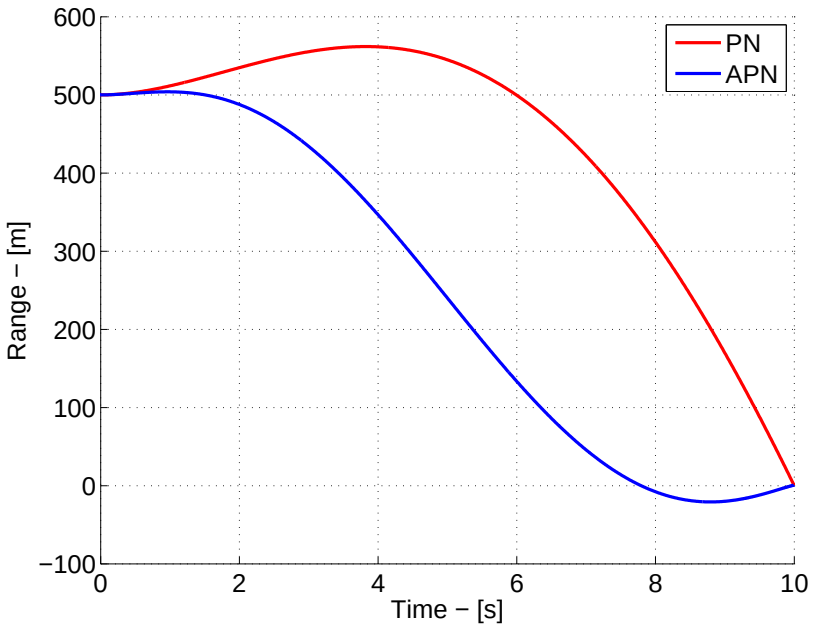

(a) miss

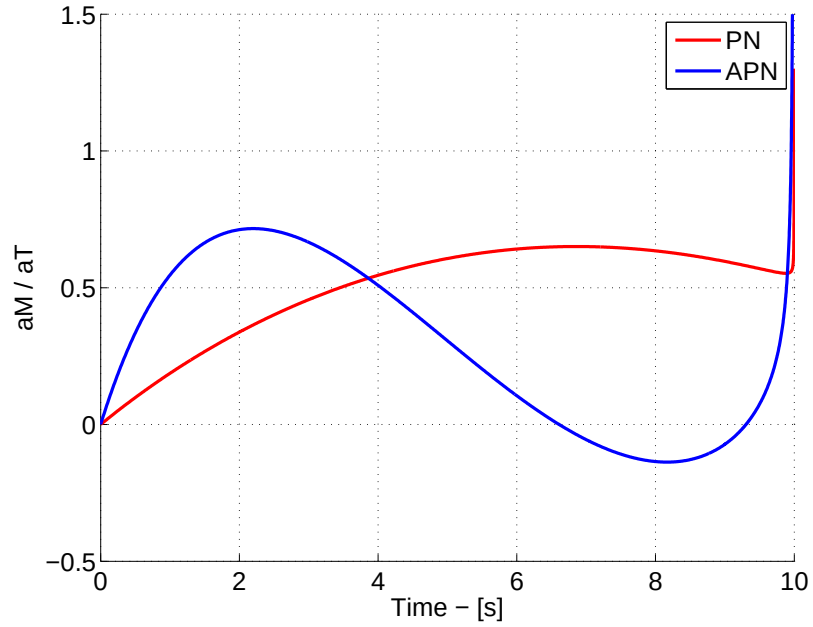

(b) acceleration

Figura 4.8. PN and APN against target maneuver - first order lag

This model can be easily written in the state space form

$$\dot{x} = Fx + Gu \tag{4.20}$$

Usually this type of problems is solved using techniques from optimal control theory [15]. In this case, however, the solution can be found more easily using the Schwartz inequality [40], [67]. Due to the linearity of the system, the value of the state vector at $t = t_f$ is

$$x(t_f) = \Phi(t_f - t)x(t) + \int_t^{t_f} \Phi(t_f - \lambda)Gu(\lambda)d\lambda \tag{4.21}$$

where Φ is the state transition matrix of the system, calculated as

$$\Phi = \mathscr{L}^{-1}[sI - F]^{-1} \tag{4.22}$$

For the model 4.19 Φ is

$$\Phi = \begin{pmatrix} 1 & t & 0.5t^2 \\ 0 & 1 & t \\ 0 & 0 & 1 \end{pmatrix} \tag{4.23}$$

The miss at $t = t_f$ can be expressed as

$$y(t_f) = y(t) + \dot{y}(t_f)(t_f - t) + 0.5a_T(t_f - t)^2 - \int_t^{t_f} (t_f - \lambda)u(\lambda)d\lambda \tag{4.24}$$

Writing 4.24 in a more compact way yields

$$\begin{gathered} y(t_f) = f_1(t_f - t) - \int_t^{t_f} h_1(t_f - \lambda)u(\lambda)d\lambda \\ f_1(t_f - t) = y(t) + \dot{y}(t_f)(t_f - t) + 0.5a_T(t_f - t)^2 \\ h_1(t_f - \lambda) = t_f - \lambda \end{gathered} \tag{4.25}$$

To have zero miss distance means to have $y(t_f) = 0$ and thus

$$f_1(t_f - t) = \int_t^{t_f} h_1(t_f - \lambda)u(\lambda)d\lambda \tag{4.26}$$

The Schwartz inequality states that the inner product of two vectors is less than or equal to the product of their norms. Furthermore, the equality is valid if and only if the two vectors are linearly dependent. In formulas one has

$$| < x, y > | \leqslant \|x\| \cdot \|y\| \tag{4.27}$$

$$| < x, y > | = \|x\| \cdot \|y\| \Leftrightarrow y = kx \tag{4.28}$$

Applying the Schwartz inequality to equation 4.26 one has

$$f_1^2(t_f - t) \leqslant \int_t^{t_f} h_1^2(t_f - \lambda)d\lambda \int_t^{t_f} u^2(\lambda)d\lambda \tag{4.29}$$

which yields

$$\int_t^{t_f} u^2(\lambda)d\lambda \geqslant \frac{f_1^2(t_f-t)}{\int_t^{t_f} h_1^2(t_f-\lambda)d\lambda} \tag{4.30}$$

Equation 4.30 sets a lower bound on the commanded acceleration. Clearly, u is minimized when the equality sign of 4.30 holds. Remembering equation 4.28, this means that u and $h_1(t_f-\lambda)$ are linearly dependent, i.e.

$$u(\lambda) = kh_1(t_f-\lambda) \tag{4.31}$$

Substituting 4.31 in equation 4.30 and taking out k from the integral one can define the value of k that minimizes u

$$k = \frac{f_1(t_f-t)}{\int_t^{t_f} h_1^2(t_f-\lambda)d\lambda} \tag{4.32}$$

The optimal control is given by

$$u = \frac{f_1(t_f-t)}{\int_t^{t_f} h_1^2(t_f-\lambda)d\lambda} h_1(t_f-t) \tag{4.33}$$

Substituting the terms from 4.25 and considering that

$$\int_t^{t_f} h_1^2(t_f-\lambda)d\lambda = \frac{3}{(t_f-t)^3} \tag{4.34}$$

one has the expression for the optimal guidance law, suitable for feedback implementation

$$u = \frac{3(y+\dot{y}t_{go}+0.5a_T t_{go}^2)}{t_{go}^2} \tag{4.35}$$

This is the same expression of the APN law, defined in equation 4.15. Thus it is demonstrated that, under the assumption of a constant target maneuver, APN is the optimal solution to the interception problem. This law was first derived by Bryson in a general way [13].
Considering a lag in the guidance system, the state vector shall be augmented with one new variable

$$x = [\ x_1 \quad x_2 \quad x_3 \quad x_4\ ] = [\ y \quad \dot{y} \quad a_T \quad a_M\ ] \tag{4.36}$$

If the guidance system has no lags, the dynamical model is

$$\begin{cases} \dot{x}_1 = x_2 \\ \dot{x}_2 = x_3 - x_4 \\ \dot{x}_3 = 0 \\ \dot{x}_4 = \dfrac{u-x_3}{\tau_M} \end{cases} \tag{4.37}$$

where u is the missile acceleration, here considered as a control, and τ_M is the time constant of the missile guidance system. Commands are then actuated with a certain delay, due to the real implementation of the guidance system.

The previously defined procedure can be used again to derive the optimal law with the new system. This time the Φ matrix can be found to be

$$\Phi = \begin{pmatrix} 1 & t & 0.5t^2 & -t\tau + \tau^2(1-e^{-t/\tau}) \\ 0 & 1 & t & \tau(1-e^{-t/\tau}) \\ 0 & 0 & 1 & 0 \\ 0 & 0 & 0 & e^{-t/\tau} \end{pmatrix} \tag{4.38}$$

The expression for $y(t_f)$ is slightly changed with respect to 4.24

$$\begin{aligned} y(t_f) = y(t) + \dot{y}(t_f)(t_f - t) + 0.5a_T(t_f - t)^2 - \tau^2 a_M \left[e^{-t_f/\tau} + \frac{t_f - t}{\tau} - 1 \right] + \\ - \int_t^{t_f} (t_f - \lambda - \tau[1 - e^{-(t_f - \lambda)/\tau}]) d\lambda \end{aligned} \tag{4.39}$$

Thus, the new expressions for f_1 and h_1 are

$$\begin{aligned} f_1(t_f - t) = y(t) + \dot{y}(t_f)(t_f - t) + 0.5a_T(t_f - t)^2 - \tau^2 a_M \left[e^{(t_f - t)/\tau} + \frac{t_f - t}{\tau} - 1 \right] \\ h_1(t_f - \lambda) = (t_f - \lambda - \tau[1 - e^{-(t_f - \lambda)/\tau}]) \end{aligned} \tag{4.40}$$

These expressions can be substituted in equation 4.33. Calculating the integral term one has

$$\int_t^{t_f} h_1^2(t_f - \lambda) d\lambda = \tau^3 \left(0.5 - 0.5e^{-2t_{go}/\tau} - \frac{2t_{go}e^{-t_{go}/\tau}}{\tau} - \frac{t_{go}^2}{\tau^2} + \frac{t_{go}}{\tau} + \frac{t_{go}^3}{3\tau^3} \right) \tag{4.41}$$

Defining

$$x = \frac{t_{go}}{\tau} \tag{4.42}$$

after some algebra, one has that

$$\frac{h_1(t_f - t)}{\int_t^{t_f} h_1^2(t_f - \lambda) d\lambda} = \frac{6x^2(x - 1 + e^{-x})}{t_{go}^2(2x^3 - 6x^2 + 6x - 3e^{-2x} - 12e^{-x} + 3)} \tag{4.43}$$

Hence, the optimal guidance law can be written

$$u = \frac{N'}{t_{go}^2} \left[y(t) + \dot{y}(t_f)t_{go} + 0.5a_T t_{go}^2 - \tau^2 a_M \left[e^x + x - 1 \right] \right] \tag{4.44}$$

The quantity in the brackets is the ZEM. The navigation ratio is not a constant as in the other laws, but is changing with t_{go} and the guidance system time constant

$$N' = \frac{6x^2(x - 1 + e^{-x})}{2x^3 - 6x^2 + 6x - 3e^{-2x} - 12e^{-x} + 3} \tag{4.45}$$

To test the behavior of this optimal guidance law against a maneuvering target, a simulation was run. The results of the optimal guidance law are compared with those from PN and APN. The initial miss is 500 m and the target performs a constant 3 g evasive maneuver. The lag of the guidance system is represented by a first order transfer function, with time constant τ = 1 s. The block diagram of this simulation is shown in Fig. 4.9. The guidance law is implemented through the blocks

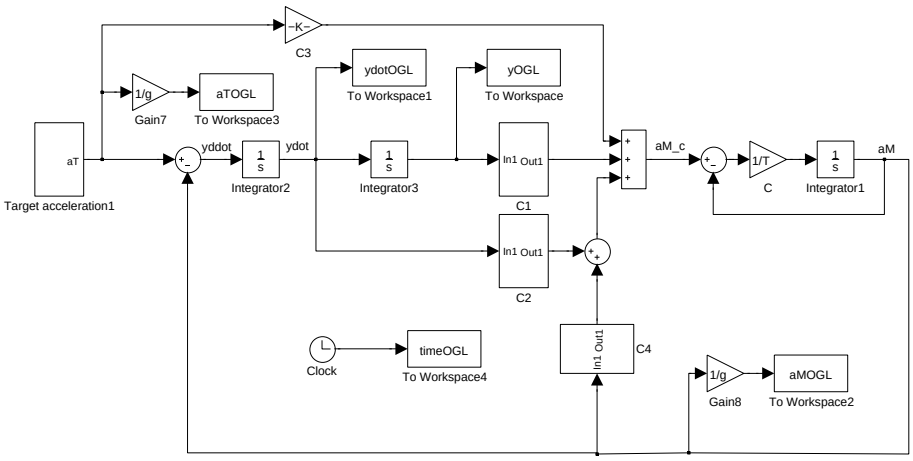

Figura 4.9. OGL block diagram

- $C_1 = \dfrac{N}{t_{go}^2}$
- $C_2 = \dfrac{N}{t_{go}}$
- $C_3 = 0.5N$
- $C_4 = \dfrac{-N\tau^2(e^{-t_{go}/\tau} + t_{go}/\tau - 1)}{t_{go}^2}$

Results are shown in figure 4.10. The obtained miss is zero and the required acceleration is most of the time lower than the one required by PN.

4.7 Differential games missile guidance

Some of the laws described so far consider explicitly the effect of target maneuvers and some do not. A target maneuver can be estimated, but not predicted, as it is controlled independently by the target. Thus, the previously formulated assumptions on target acceleration can be untrue and result in a very large miss distance. Furthermore, actual missiles presents saturations on the maximum level of lateral acceleration. The so called zero-sum pursuit evasion game is a suitable solutions [33] for such problems.

A pursuit evasion game is a non−cooperative differential game. The pursuer's task is to maneuver in order to minimize the miss distance and its control effort, while maximizing the evader's control effort. The evader plays to do the opposite. An advantage with this

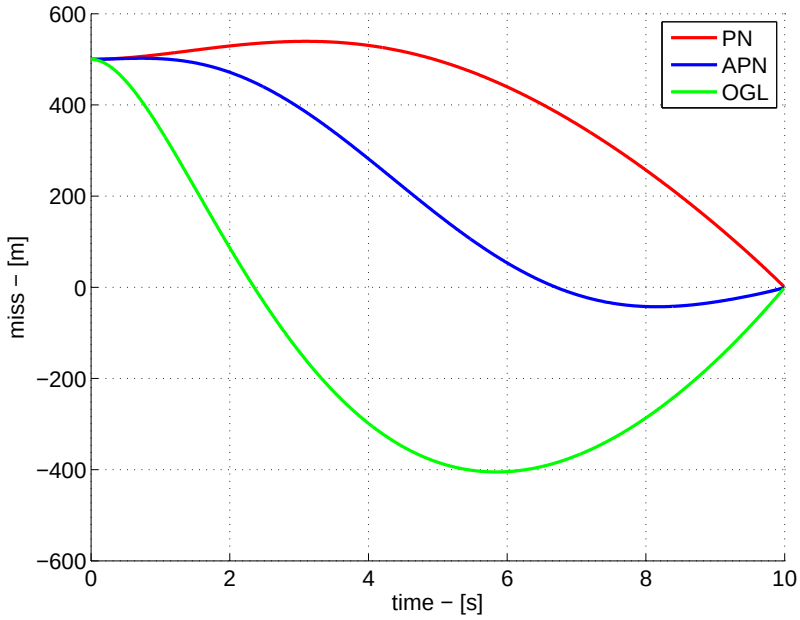

(a) miss

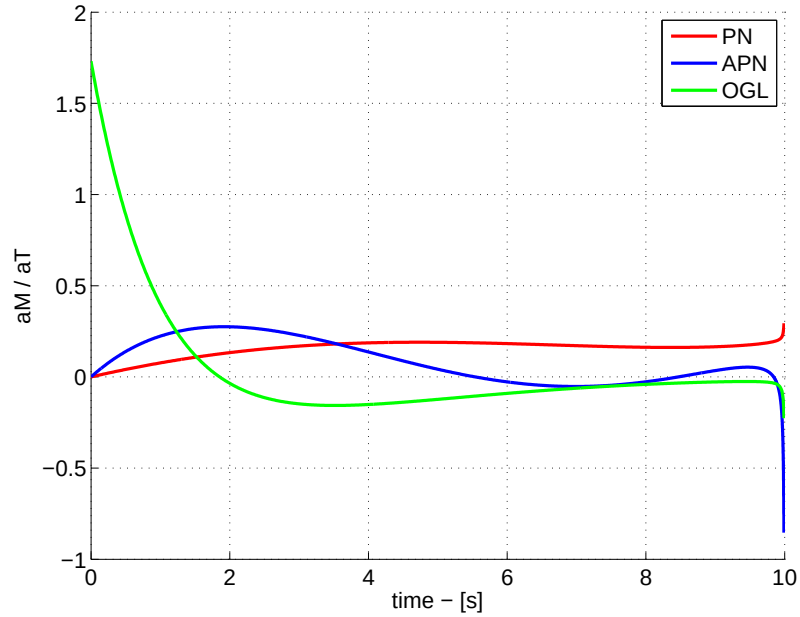

(b) acceleration

Figura 4.10. PN, APN and OGL against target maneuver - first order lag

particular formulation is that it does not require the knowledge of the opponent's strategy by the missile guidance system. Rather, it takes into account the evader's maneuver capabilities. The game outputs are the optimal strategies for both agents, guidance commands $u^*(t)$, $v^*(t)$, respectively, and the value of the game, i.e. the guaranteed miss distance. A very useful feature of this formulation is the game space partitioning to capture and avoidance zones.

Within the capture zone, finite miss distance is guaranteed, as Gutman and Leitmann [24] first showed. They proposed a simple pursuit evasion game between two players with constant speeds and constant bounds on lateral acceleration in the neighborhood of a collision course. Later formulations include first-order pursuer dynamics [23] and evader dynamics [56]. Recently, Conway and Pontani proposed a numerical solution for a game with realistic dynamics [17].

The model for the game can be written starting from a linear model. The state vector is

$$X = \begin{bmatrix} y & \dot{y} & a_M(t) & a_T & \gamma_M & \gamma_T \end{bmatrix}^T \tag{4.46}$$

The dynamical model is

$$\dot{X} = A(t)X + B(t)u + C(t)v \tag{4.47}$$

with

$$A(t) = \begin{bmatrix} 0 & 1 & 0 & 0 & 0 & 0 \\ 0 & 0 & -1 & 1 & -a_M(t) & a_T(t) \\ 0 & 0 & -1/\tau_M & 0 & 0 & 0 \\ 0 & 0 & 0 & -1/\tau_T & 0 & 0 \\ 0 & 0 & 1/V_M & 0 & 0 & 0 \\ 0 & 0 & 0 & 0 & 0 & 0 \end{bmatrix} \tag{4.48}$$

$$B(t) = \begin{bmatrix} 0 & 0 & a_{M_{max}}/\tau_M & 0 & 0 & 0 \end{bmatrix}^T \tag{4.49}$$

$$C(t) = \begin{bmatrix} 0 & 0 & 0 & a_{T_{max}}/\tau_T & 0 & 0 \end{bmatrix}^T \tag{4.50}$$

where u and v are the normalized controls

$$\begin{aligned} u &= a_M^{comm}/a_{M_{max}} \\ u &= a_T^{comm}/a_{T_{max}} \end{aligned} \tag{4.51}$$

a_M^{comm} and a_T^{comm} are the guidance commands, $a_{M_{max}}$ and $a_{T_{max}}$ are the saturation level of lateral acceleration. This dynamic model with first order transfer functions for both pursuer and evader guidance systems is known in literature as DGL/1 [56].

The state vector 4.46 can be reduced to a scalar using the terminal projection transformation described by Bryson and Ho [15]:

$$Z(t) = D\Phi(t_f, t)X(t) \tag{4.52}$$

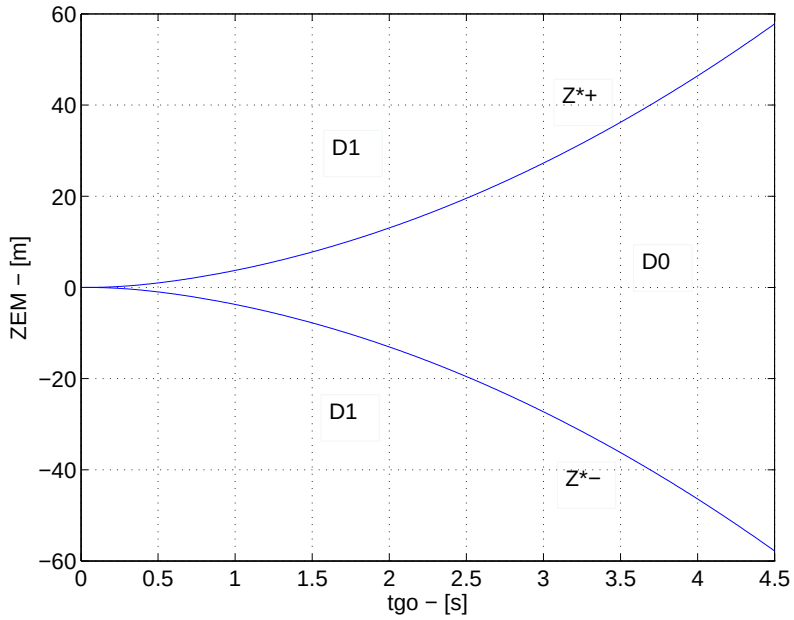

Figura 4.11. DGL/1 game structure with $\mu \geqslant 1$ and $\mu\varepsilon \geqslant 1$

where $\Phi(t_f,t)$ is the state transition matrix and

$$D = \begin{pmatrix} 1 & 0 & 0 & 0 & 0 & 0 \end{pmatrix}^T \tag{4.53}$$

The cost function can now be written as

$$J = |D^T X(t_f)| = |y(t_f)| \tag{4.54}$$

The optimal solution for this differential game was derived by Shinar [56]. The optimized game dynamics is

$$\begin{aligned} \dot{Z}^* &= \Gamma(t_f,t)sign\{Z(t_f)\} \\ \Gamma(t_f,t) &= (B(t_f,t)+C(t_f,t)) \end{aligned} \tag{4.55}$$

where

$$\begin{aligned} B(t_f,t) &= D^T\Phi(t_f,t)B(t) \\ C(t_f,t) &= D^T\Phi(t_f,t)C(t) \end{aligned} \tag{4.56}$$

Integrating backward this equation yields a candidate optimal trajectory $Z(t)$. The game solution is a decomposition of the (Z, t_{go}) reduced game space into a *regular* (the avoidance zone) and a *singular* region (the capture zone). Regions that cannot be filled by candidate optimal trajectories are singular. The decomposition is determined by the form of $\Gamma(t_f,t)$, depending on the dynamic model of the game.

Generally speaking, a capture zone (called D_0) is a region of the state space where optimal strategies are arbitrary. No matter what the two agents do, the granted miss is finite, as

long as the ZEM trajectory stays in this region. The value of the game in this region can be either zero or not, depending on the game structure. Avoidance zone (called D_1) is a region where the optimal strategies are

$$\begin{aligned} u^*(t) &= a_{M_{max}} \cdot sign\{ZEM\} \\ v^*(t) &= a_{T_{max}} \cdot sign\{ZEM\} \end{aligned} \tag{4.57}$$

and the value of the game is a function of initial conditions. The bounds Z_+^* and Z_-^* between the two zones are semipermeable symmetric surfaces, i.e. that each player can prevent the adversary from penetrating the surface. Depending on the assumptions of ideal or real guidance systems for the missile and the target and on the maximum values of lateral acceleration, a number of game structures can be described [55].

The parameters of the game are the pursuer-evader maneuverability ratio, defined as $\mu = a_{M_{max}}/a_{T_{max}}$ and the evader-pursuer dynamics ratio, defined as $\varepsilon = (a_{M_{max}} \cdot \tau_T)/(a_{T_{max}} \cdot \tau_M)$. Fig. 4.11 represents the game structure of DGL/1 under the assumptions that $\mu \geqslant 1$ and $\mu\varepsilon \geqslant 1$. Trajectories that starts in D_0 have a zero guaranteed miss; trajectories that starts in D_1 do not have finite guaranteed miss.

4.8 Summary

This chapter has presented various guidance laws for tactical missiles in the terminal phase of the engagement. Along with the description of the laws, numerical simulations have been reported to support the theoretical analysis with examples and results. Traditional laws have been employed in missilry since the first half of the 20^{th} century. They are easy to implement and to design, being based on few parameters. PP and PN were firstly described starting from geometrical considerations. The linearization of the engagement equations was derived to introduce the concepts of miss distance and ZEM. Miss distance and ZEM are used to derive the expressions of APN.

Thanks to the technological improvement in the electronic equipments, more complex laws have been employed in the last decades. The starting point for these formulations is the optimal control theory and the game theory. Modern laws can deal with more realistic scenarios than the traditional laws.

Capitolo 5

Estimation issues in guidance laws implementation

In the previous chapter the main issues related to guidance laws have been analyzed. Going through the description of the laws, it was possible to notice how geometrical concepts gave way to mathematical ones. Modern guidance laws are more complicated and less intuitive than traditional. However, they can deal with more complex scenarios and this can result in an overall supremacy in performance.

The hypothesis of having perfect knowledge of all the variables involved in the engagement is not realistic in real missile applications and it will be relaxed in this chapter. While presenting the guidance laws, the actual values of miss distance, bearing, accelerations and all their derivatives have been considered in the formulation and in the numerical examples. In some cases analytical expressions for some of these quantities can be derived. In some others, though, one must rely only on measurements. Exact values are not disposable anymore, because real measurements are corrupted with noise. Therefore, in order to use available measurements, one needs some kind of processing.

Automatic measurements processing inside the homing loop is performed through dynamical filtering. The EKF described in chapter 3 is a suitable algorithm for the engagement nonlinear environment. Due to its particular formulation for the error covariance matrix, this algorithm will be preferred in this chapter to the already employed UKF.

Using estimation, both traditional and modern laws can be implemented starting from a single bearing measurement, no matter how complex they are from the mathematical point of view. This allows to reduce the impact of guidance systems costs and to ease their realization.

This chapter is dedicated to the problems related to estimation inside the homing loop. An introduction to measurement related notions will be firstly given. After that, the homing

loop presented in chapter 4 will be implemented along with a noisy seeker sensor and an estimator. Particular attention will be paid to the unobservability problem that raises in the presence of bearings-only measurements. An innovative strategy combining guidance and estimation will be presented that enhances range estimation and improves the overall performance of the engagement. The supremacy of this new guidance strategy over the classical approach will be demonstrated by means of nonlinear simulations.

5.1 Measurements for the engagement

In guided missile systems a seeker is used to sense and track the target. Seeker can be active, if the missile itself illuminates the target; semi-active, if the illumination source is external (e.g. a ground based radar); passive, if the illumination source is the target itself. The motion of the target is used in the mechanization of the guidance law, feeding the guidance system with a bearing measurement. The tracking is performed with an antenna or another energy-receiving device (e.g. a radar, an infrared, a laser, or an optical sensor).
The seeker is usually composed of up to three gimbals on which are mounted gyroscopes and an antenna. In an active radio frequency seeker or passive infrared seeker, two gimbals are commonly used. There are also fixed antenna systems which use electronic beam steering by means of a phased array antenna. The radome composes the nose of the missile. It has the task to cover the radio-frequency or infrared devices of the seeker. The design of the radome involves electro-magnetic, mechanical, thermal and aerodynamical issues.
Semi-active RF seekers used to be boarded on missiles in the past. They were large and heavy devices, in accordance with electronic equipments from the pre-miniaturized era. As low cost, small and reliable electronics have become available, higher-accuracy infrared or high-frequency RF seekers have been employed [9]. The *AIM-9X Sidewinder* is equipped with a high-resolution rotate-to-view seeker [61], mounted on a body-fixed, two-axis gimbal. The outer seeker casing rotates 360° to provide a clear viewing path for the seeker.
The seeker is not the only sensor boarded on the missile. Data from an Inertial Measurement Unit (IMU) and a Global Positioning System (GPS) system, properly processed, provide the missile navigation system with the necessary information. Telemetry data from the actuators and from the other subsystems of the missile are used from the on board computer to keep everything under control. However, for the purposes of this chapter, the only significant measurement is the one from the seeker. Nominal values for pursuer inner variables such as flight path angle γ_M, actual acceleration a_M and velocity v_M will be taken into account in the following examples. They are meant to be the output of some internal pursuer subsystem, so that there is no need to filter them.
On the other hand, noise on the bearing is a crucial factor in seeker's performance. It can

occur due to target effects or missile effects. The radome itself constitutes a bias error due to diffraction; this effect is called *boresight error*. Receiver noise is mostly due to thermal noise by the antenna and missile integrated electronics. It increases with the range, because the signal to noise ratio of the target lowers when range is larger.
An exhaustive description of seeker's characteristics or noise sources in the bearing signal is out of the purposes of this work. More material can be found in the book from Siouris [61]. For estimation studies in this work, the bearing measurement $\tilde{\lambda}$ from the seeker will be regarded as the nominal line of sight angle λ plus an additive noise v. The noise will be white Gaussian noise with variance σ_v = 0.001 *rad*

$$\begin{aligned} \tilde{\lambda} &= \lambda + v \\ v &\sim \mathcal{N}(0rad, 0.001rad) \end{aligned} \tag{5.1}$$

5.2 Estimator in the loop

Considering the linearized formulation of the engagement, the system is in the form

$$\begin{aligned} \dot{x} &= Fx + Gu + w \\ z &= Hx + v \end{aligned} \tag{5.2}$$

where x is the state vector, u represents the control (in this case the lateral acceleration) and z are the measurements. w and v are, respectively, the process and the measurements noise vectors with statistics

$$\begin{aligned} Q &= E[ww^T] \\ R &= E[vv^T] \end{aligned} \tag{5.3}$$

In reality, the filter works with discrete signals, because measurements are available only at fixed time instants. Discretizing 5.2 yields

$$\begin{aligned} x_{k+1} &= \Phi x_k + \Gamma_k u_k + w_k \\ z_k &= H_k x_k + v_k \end{aligned} \tag{5.4}$$

$$\Phi = \Phi_{T_s} = e^{FT_s}\Gamma_k = \int_0^{T_s} \Phi(\tau) G d\tau \tag{5.5}$$

As explained in chapter 3, estimation is performed in two steps. The equations of an EKF can be summarized as follows

Prediction Predicted estimated state vector and its covariance matrix are denoted as $\hat{x}_{k|k-1}$ and $P_{k|k-1}$. The former can be obtained by propagating the old estimate $\hat{x}_{k-1|k-1}$ selecting the proper equations from the dynamical model of the process 5.4

$$\hat{x}_{k|k-1} = \Phi \hat{x}_{k-1|k-1} + \Gamma_k u_k \tag{5.6}$$

$$P_{k|k-1} = \Phi P_{k-1|k-1} \Phi^T + Q \tag{5.7}$$

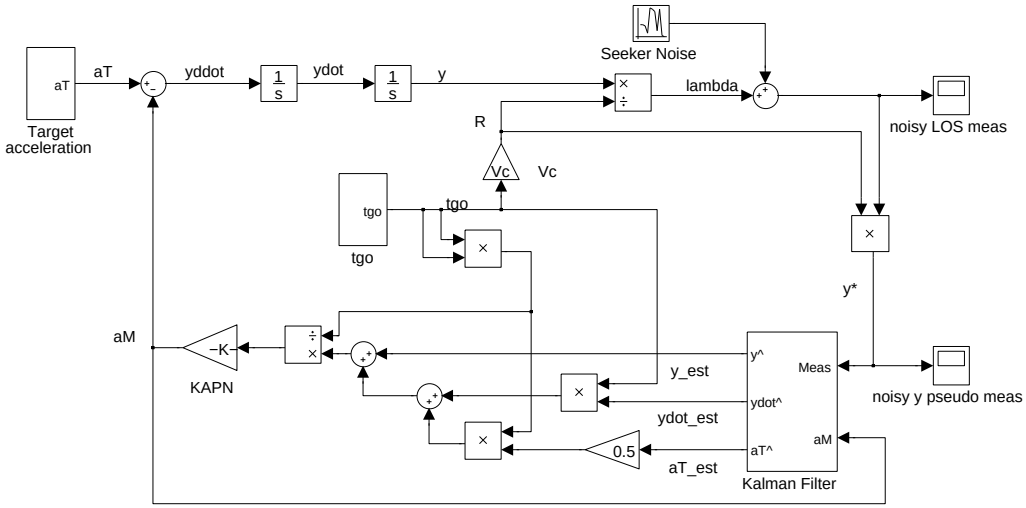

Figura 5.1. Homing loop with estimator

Correction The actual values of estimated state $\hat{x}_{k|k}$ and covariance $P_{k|k}$ are obtained after calculating the Kalman gain K_k and the estimated measurements $\hat{z}_k$

$$K_k = P_{k|k-1}H^T[HP_{k|k-1}H^T + R]^{-1} \tag{5.8}$$

$$\hat{z}_k = H\hat{x}_k \tag{5.9}$$

$$\hat{x}_{k|k} = \hat{x}_{k|k-1} + K_k(z_k - \hat{z}_k); \tag{5.10}$$

$$P_{k|k} = (I - K_k H)P_{k|k-1} \tag{5.11}$$

These equations can be implemented inside the guidance system to provide it with the estimates of the necessary state variables. Fig. 5.1 shows the block diagram of a homing loop with an integrated Kalman filter. The implemented guidance law is the APN from equation 4.15. Sample and hold devices are employed in the Kalman filter block in order to discretize the continuos inputs. In the presence of nonlinear systems, the EKF algorithm can be used instead of the Kalman Filter (KF). The structure of the EKF algorithms is the same as the one of the KF. The only difference is in the prediction phase. Correction phase is not reported for the sake of brevity.

Prediction Predicted estimated state vector is obtained propagating the equation from the nonlinear model. The covariance is propagated through the state transition matrix of the system

$$\hat{x}_{k|k-1} = f(\hat{x}_{k-1|k-1}, t_k, u_k, 0) \tag{5.12}$$

$$P_{k|k-1} = \Phi P_{k-1|k-1}\Phi^T + Q \tag{5.13}$$

5.3 PN implementation through a 2 states Kalman filter

PN from equation 4.6 is at the same time one of the principal and simple guidance laws. It works well with zero-lags guidance systems and with a not maneuvering target. If both the missile and the target have constant speeds the closing velocity of the engagement is constant. Assuming that v_C is known from some external source, in the terminal phase of the engagement PN needs only to know $\dot{\lambda}$.
A 2 states Kalman filter is then sufficient to implement PN. The state vector of the estimator is $x = \begin{bmatrix} x_1 & x_2 \end{bmatrix}^T = \begin{bmatrix} \lambda & \dot{\lambda} \end{bmatrix}^T$. The dynamical model for the filter is

$$\begin{cases} \dot{x}_1 = x_2 \\ \dot{x}_2 = 0 \end{cases} \tag{5.14}$$

The only target measurement for the missile is the bearing angle λ; measurements are updated every T_s seconds. Measurements at the instant k can be obtained through equation

$$z_k = Hx + v \tag{5.15}$$

where H is the vector

$$H = \begin{bmatrix} 1 & 0 \end{bmatrix} \tag{5.16}$$

The bearing measurement is corrupted by a white Gaussian noise v with variance σ_v. In chapter 3, the process noise covariance matrix Q for this example was found to be

$$Q = q_0 \begin{pmatrix} T_s^3/3 & T_s^2/2 \\ T_s^2/2 & T_s \end{pmatrix} \tag{5.17}$$

To test the Kalman filter implementation a simulation was run on a set of 200 Monte Carlo samples. Each sample differs from the other by the value of the initial guess. The initial guesses belong to a Gaussian distribution whose mean and variance are specified in Table 5.1 along with other initial values and parameters of the simulation. The engagement starts on a collision triangle, so that PN is able to drive the missile to interception. The model employed for simulation is

$$\begin{cases} \dot{R} = v_T \cos(\gamma_T - \lambda) - v_M \cos(\gamma_M - \lambda) \\ \dot{\lambda} = \dfrac{v_T \sin(\gamma_T - \lambda) - v_M \sin(\gamma_M - \lambda)}{R} \\ \dot{\gamma}_M = \dfrac{a_M}{v_T} \\ \dot{\gamma}_T = \dfrac{a_T}{v_T} \\ \dot{a}_T = 0 \end{cases} \tag{5.18}$$

Tabella 5.1. PN simulation initial values and parameters

Parameter	Value	Parameter	Value
R_0	10 km	λ_0	0°
γ_{T_0}	50°	T_s	0.02 s
v_M	3 km/s	v_T	1 km/s
a_{M_0}	0 m/s^2	a_{T_0}	0 m/s^2
σ_v	0.001 rad	q_0	0.001
$\lambda_{0\|0}$	$\sim \mathcal{N}(0^\circ, 5^\circ)$	$\dot{\lambda}_{0\|0}$	$\sim \mathcal{N}(0^\circ, 5^\circ)$

Figs. 5.2, 5.3 show the results of estimation. The red line is the mean estimation error; the green line is the error from a sample run; the blue line is the error standard deviation; the black lines are the 1σ bounds calculated by a sample run of the filter. Variables are plotted against t_{go}. The mean estimation error from the set of Monte Carlo samples is almost zero. The standard deviation of the samples is almost superimposed to the 1σ bounds from the filter. Hence, the filter is well tuned and the estimation result is correct.
Fig. 5.4 shows the achieved miss distance by means of the cumulative distribution function. The axis of abscissae is the miss distance, while the ordinates indicate the percentage of samples with a miss smaller than or equal to the value reported on the x axis. The 90% accuracy of this simulation is 0.12 m. This means that if the missile designer would like to achieve a 90% kill probability then a warhead lethal radius of 0.12 m is needed.

5.4 Target maneuver estimation

In chapter 4 it was shown that more advanced laws such as APN are more effective than traditional PN against target maneuvers. To implement such laws, one needs to have more information on target's behavior. In particular, the guidance system has to be provided with an estimate of target maneuver. This is impossible to determine without external measurements such as radar based range and range-rate, in addition to the bearing measurement from the seeker. In a simple seeker-only configuration missile, target maneuver estimation has to be tackled with a deeper mathematical approach.
The concept of *shaping filter* was introduced by Fitzgerald [21] to represent signals with known form $h(t)$ but random starting time t_{st}. Fitzgerald proved that the output of a shaping filter excited by white noise has the same mean and autocorrelation function as those of the signal $x(t)$

$$x(t) = h(t - t_{st})u(t - t_{st}) \tag{5.19}$$

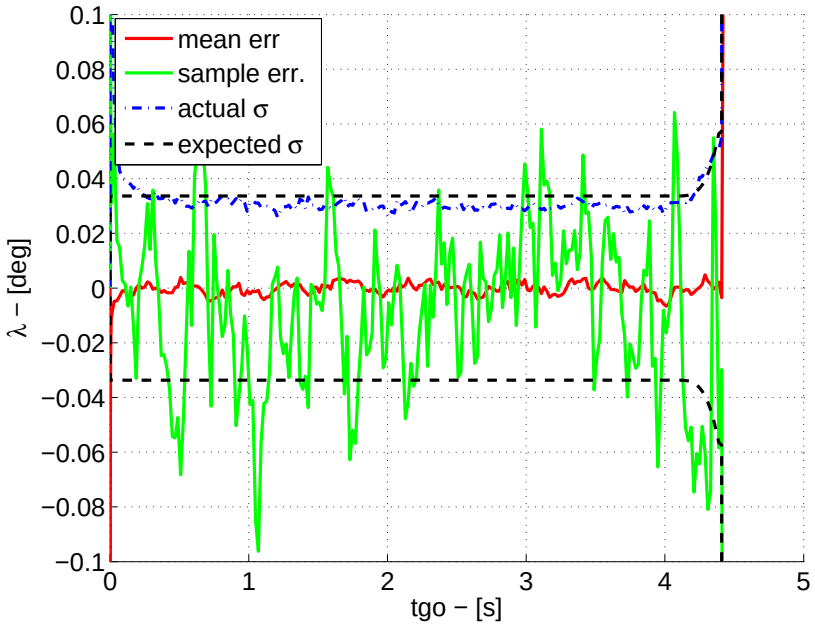

Figura 5.2. Estimated λ

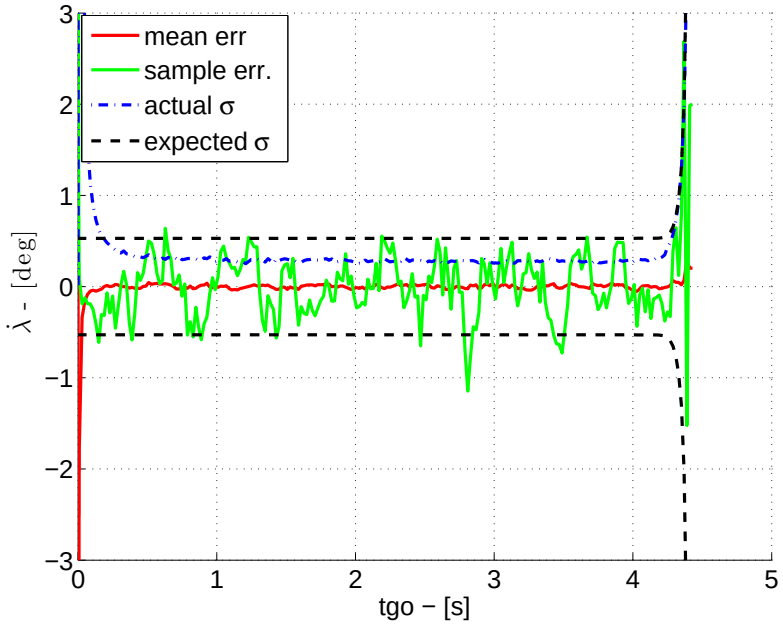

Figura 5.3. Estimated $\dot{\lambda}$

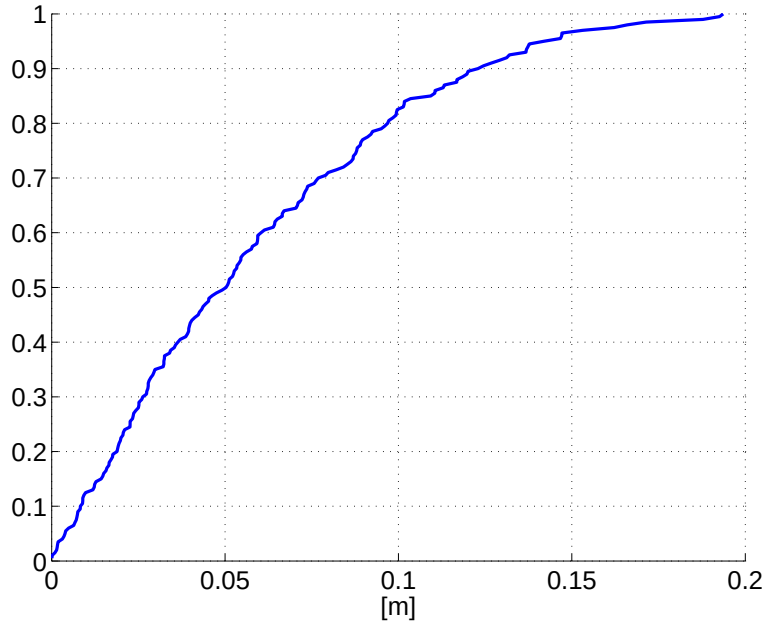

Figura 5.4. CDF - MT

where $u(t-t_{st})$ is the unit step. The shaping filter representation $H(s)$ is the Laplace transform of the signal $h(t)$

$$H(s) = \mathscr{L}[h(t)] \tag{5.20}$$

The process of equation 5.19 and the output of the shaping filter are then statistically equivalent in the sense that they have the same second-order statistics (i.e. root mean square value). Thus, passing either of them through a physical system, they are indistinguishable if their second order statistics are being observed.

Zarchan applied shaping filters to represent various realistic missile maneuvers [66], [67]. Once the ballistic missile is identified by the defense system, its maximum level of maneuverability is known. Assuming that the evasive maneuver will be performed constantly at the maximum acceleration, the form of the target maneuver signal is also known and the only unknown quantity remains its starting time. The starting time can be assumed as uniformly distributed over the flight time t_f. Hence, a target maneuver can be represented as a stochastic process with probability density function

$$P_T = 1/t_f \tag{5.21}$$

The signal that drives the shaping filter is a white noise with power spectral density

$$\Psi = a_T^2 P_T = a_T^2/t_f \tag{5.22}$$

To implement the shaping filter in the estimator inside the homing loop, one has to add a state for a_T and the term Ψ to the process noise covariance matrix Q.

5.5 Bearings-only issues

The introduction of Kalman filtering and shaping filters has shown how to implement a simple law such as PN and to identify a target maneuver. Nevertheless, realistic engagement features such as lags in the guidance systems have not been taken into account, yet. Passing to a more down-to-earth description of the engagement, more advanced laws such as APN [67] or Minimum Effort (Guidance) Law (MEL) [8] are needed. Their implementation, however, requires more complex structures.

An essential information is the t_{go} to the interception. In the case of bearings-only, such a measure is unobservable as the range is not directly available. Furthermore, the bearing measurement turns out to be not sufficient to reconstruct also the range, because it contains no information on how fast the missile is approaching to the intercept point. It is like if one has to travel in a certain time from one point to another, but he only knows the direction to go: he would surely arrive on the point, but there is a chance that he might miss the right time. The process remains unobservable prior to a maneuver from the observer [45], [20]. Aidala showed [1] that bearing and range estimation errors can interact to cause estimator instability. He suggested a proper estimator initialization procedure to make the estimator stable.

A solution to improve range observability is to maneuver away from the collision triangle: this causes the line of sight to rotate and gives some insights about the relative range. The Cramer-Rao lower bound was used in [20] to demonstrate that it is impossible to estimate range without maneuvers and to analyze the effects of such maneuvers on estimation accuracy. Optimal maneuvers that increase the observability of the t_{go} have been studied in [31] and [27]. Optimality sensitivity to errors in t_{go} estimation can be mitigated by weighting the terminal relative velocity, and possibly the missile terminal acceleration as well as the usual miss distance [7]. The maneuver defines a new course for the interceptor, that increases the observability of the range and also the miss distance. This is adequate and somehow desirable until a certain point, when the missile should aim at decreasing the miss distance. The maneuver can be also optimized with respect to the determinant of the Fisher information matrix. Numerical methods [26], [49] were employed to design suboptimal maneuvers with numerical techniques. Song and Um [62] proposed to add in the APN expression a term proportional to the range and to the heading, which forces the line of sight to rotate: this term is dominant at the beginning of the engagement, while it goes to zero at its end, having terminal performance as the traditional APN. Hexner and Weiss [28] derived a feed-

back guidance policy that initially describes the t_{go} through a probability density and then updates it by a Kalman filter from the interceptor's observations. In this case, the interceptor does not maneuver to improve the observability.

In the following a new strategy for missile guidance with bearings-only measurements is introduced, based on the evaluation of the Kalman filter (KF) error covariance matrix eigenvalues. They are, in fact, a measure of the level of the estimated system's observability [25]. The information obtained from the eigenvalues will be exploited in the framework of a pursuit-evasion game.

Considering a single lag in the guidance systems of both missile and target, the differential equations that fully describe the engagement are

$$\begin{cases} \dot{R} = v_T \cos(\gamma_T - \lambda) - v_M \cos(\gamma_M - \lambda) \triangleq V_R \\ \dot{\lambda} = \dfrac{v_T \sin(\gamma_T - \lambda) - v_M \sin(\gamma_M - \lambda)}{R} \triangleq \dfrac{V_\lambda}{R} \\ \dot{a}_M = \dfrac{u - a_M}{\tau_M} \\ \dot{\gamma}_M = \dfrac{a_M}{v_M} \\ \dot{a}_T = \dfrac{v - a_T}{\tau_T} \\ \dot{\gamma}_T = \dfrac{a_T}{v_T} \end{cases} \tag{5.23}$$

where R is the relative distance between missile and target; λ is the line of sight angle; γ_M and γ_T are, respectively, missile and target flight path angles; v_M and v_T their speeds; u and v the missile's and the target's commanded accelerations; a_M and a_T the actual ones. The lags are represented by a first order transfer function with time constants τ_M and τ_T, respectively. The geometry of the engagement is represented in Fig. 5.5.

In this particular study, an extended Kalman filter will be employed to reconstruct the parameters that cannot be measured directly. The estimated state $\hat{x}$ is defined as

$$\hat{x} = \begin{bmatrix} \hat{R} & \hat{\lambda} & \hat{\gamma}_T & \hat{a}_T & \hat{v}_T \end{bmatrix}' \tag{5.24}$$

Missile related parameters (i.e. a_M, v_M and γ_M) are not estimated since they are directly measured or *a priori* known. A shaping filter is used to detect target maneuvers. The complete model for estimation is

$$\begin{cases} \dot{R} = v_T \cos(\gamma_T - \lambda) - v_M \cos(\gamma_M - \lambda) \\ \dot{\lambda} = \dfrac{v_T \sin(\gamma_T - \lambda) - v_M \sin(\gamma_M - \lambda)}{R} \\ \dot{\gamma}_T = \dfrac{a_T}{v_T} \\ \dot{a}_T = \omega \\ \dot{v}_T = 0 \end{cases} \tag{5.25}$$

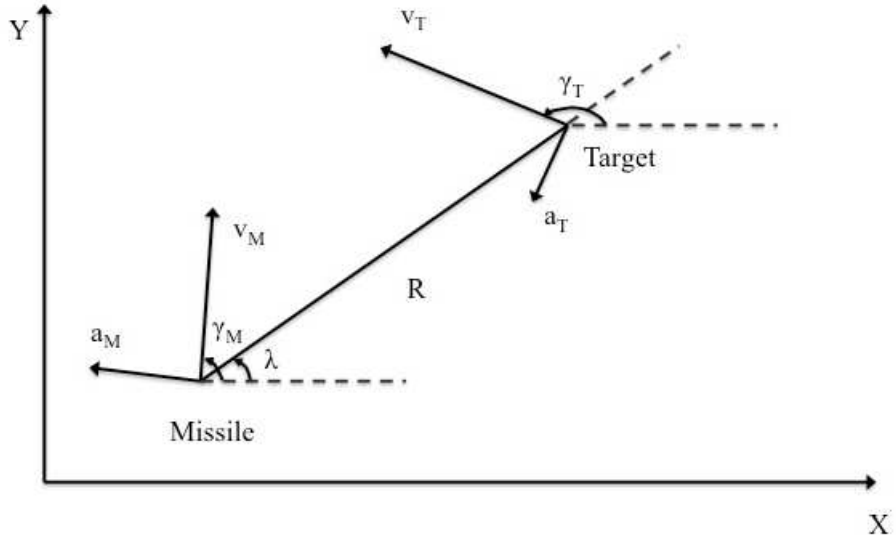

Figura 5.5. Engagement geometry

5.6 Combined guidance-estimation problem

In a scenario with guidance systems lags and target maneuvers, guidance laws like MEL and differential-games-based guidance laws are needed. They require an accurate estimate of the engagement's t_{go}. This is related to the knowledge of the relative distance R and of the collision speed V_C between the missile and the target. If a collision triangle is maintained, t_{go} can be estimated as

$$\hat{t}_{go} = \frac{R}{V_C} \tag{5.26}$$

If CC conditions hold, the range cannot be reconstructed from bearings-only measurements and therefore the guidance law cannot be properly implemented. There is a conflict between the optimal guidance strategy and range estimation: the better the former is applied, the worst the latter results. A poor range estimation will result in a poor engagement performance.

In order to solve this issue, information from the outputs of the filter can be exploited. Ham et al. [25] outlined a relationship between the eigenvalues of the filter error covariance matrix P, properly normalized, and the observability of the system. This relationship will be very important in the rest of this study, and it is therefore repeated here for the reader's convenience.

Let $\tilde{x}$ be the estimation error from a Kalman filter and define it as

$$\tilde{x} = \hat{x} - x \tag{5.27}$$

where $\hat{x}$ is the estimated state and x is the true state vector. Being $\tilde{x}$ a stochastic variable, each linear combination w of its components through a basis v has an associated variance σ_w^2. This can be related to the error covariance matrix P of the filter in the following way

$$\begin{aligned} w &= v_1\tilde{x}_1 + \ldots + v_n\tilde{x}_n = v^T\tilde{x} \\ \sigma_w^2 &= \sum_{i=1}^{n}\sum_{j=1}^{n} v_i v_j p_{ij} = v^T P v \end{aligned} \tag{5.28}$$

By selecting the canonical basis

$$v = \{[1,0,\ldots,0]^{'},[0,1,\ldots,0]^{'},\ldots,[0,\ldots,0,1]^{'}\}$$

one can obtain the covariances associated with the single states.

A large value of σ_w^2 implies a large error in the estimation, meaning that the filter cannot reconstruct the linear combination of states associated to v, or the single state in the case of canonical v. Unless the filter is not well-tuned, this is related to the intrinsic unobservability of the state. Thus, a large σ_w^2 can be regarded as a measure of bad observability.

Therefore, the largest eigenvalue of P corresponds to the variance of the state or to the linear combination of the states that is poorly observable. The smallest eigenvalue, instead, is associated to the most observable states. To look for the largest value of σ_w^2 means to maximize it subject to the constraint

$$v^T v = 1$$

This problem can be solved with the Lagrangian multiplier method [15]. The condition to find the maximum is σ_w^2 is

$$\frac{\partial}{\partial v}(\sigma_w^2 - \lambda(v^T v - 1)) = 0 \tag{5.29}$$

where λ is the Lagrangian multiplier. Using relation 5.28 and carrying out the differentiation one has

$$\begin{aligned} \frac{\partial}{\partial v}(v^T P v - \lambda(v^T v - 1)) = 0 \\ \Rightarrow (P - \lambda I)v = 0 \end{aligned} \tag{5.30}$$

Multiplying both sides of 5.30 by v^T yields

$$\begin{aligned} v^T(P - \lambda I)v = v^T P v - v^T \lambda v = 0 \\ \sigma_w^2 = \lambda \end{aligned} \tag{5.31}$$

since $v^T P v = \sigma_w^2$ and $v^T v = 1$.

In order to compare eigenvalues in the same range, a normalization of P is necessary. Being n the dimension of the state vector, the normalization procedure can be expressed as

$$\begin{aligned} P_{norm} &= n\frac{P0_{norm}^{-1} P P 0_{norm}^{-1}}{trace(P0_{norm}^{-1} P P 0_{norm}^{-1})} \\ P0_{norm} &= diag\left(\left[\frac{1}{\sqrt{P_{11}(0)}}, \frac{1}{\sqrt{P_{22}(0)}}, \cdots, \frac{1}{\sqrt{P_{nn}(0)}}\right]\right) \end{aligned} \tag{5.32}$$

As seen before in this chapter and in chapter 3, the error covariance matrix of a Kalman filter at the k^{th} iteration is calculated in two steps

$$P_{k|k-1} = \Phi P_{k-1|k-1}\Phi^T + Q_{k-1} \tag{5.33}$$

$$P_{k|k} = (I - \Gamma_K H)P_{k|k-1} \tag{5.34}$$

The prediction step in equation 5.33 is a projection of the old value of P along the direction of Φ, the state transition matrix. The correction phase in equation 5.34 updates the predicted covariance with the Kalman gain K and the measurements matrix H. For the set of equations 5.25, Φ can be calculated starting from the Jacobian matrix F:

$$F = \begin{pmatrix} 0 & V_\lambda & -v_T\sin(\gamma_T-\lambda) & 0 & \cos(\gamma_T-\lambda) \\ \dfrac{-V_\lambda}{R^2} & \dfrac{-V_R}{R} & \dfrac{v_T\cos(\gamma_T-\lambda)}{R} & 0 & \dfrac{\sin(\gamma_T-\lambda)}{R} \\ 0 & 0 & 0 & \dfrac{1}{v_T} & -\dfrac{a_T}{v_T^2} \\ 0 & 0 & 0 & 0 & 0 \\ 0 & 0 & 0 & 0 & 0 \end{pmatrix} \tag{5.35}$$

$$\Phi = e^{FT_s} \tag{5.36}$$

Due to the nonlinearity of the system, the effect of a maneuver on the eigenvalues can be calculated starting from the Jacobian matrix 5.35 and then applying equation 5.33.
A maneuver is originated by a variation of γ_M which results in a variation of V_λ and V_R (see equation 5.23). Different maneuvers are characterized by different Jacobian matrices and eventually by different eigenvalues of P. The smallest value among the range associated eigenvalues of P corresponds to the maneuver, which mostly improves range observability. Given that $a_{M_{max}}$ is missile's maximum level of lateral acceleration, a finite set of guidance commands ranging between -1 and 1 can be considered. The one that returns the best observability conditions can be identified evaluating the eigenvalues. Nevertheless, not all the commands can be applicable, because some of them might drive the missile $too\ far$ from the nominal engagement trajectory. The pursuit evasion game framework can help decide when to prefer observability and when to go straight for the target.

5.7 A new guidance strategy

Recalling section 4.7, the resulting game structure for the considered first order dynamics model for the adversaries 4.47-4.50 is known as DGL/1 and it is represented in Fig. 5.6. The D_0 region is the one comprised between the boundaries Z_+^* and Z_-^*. Z_+^* and Z_-^* are

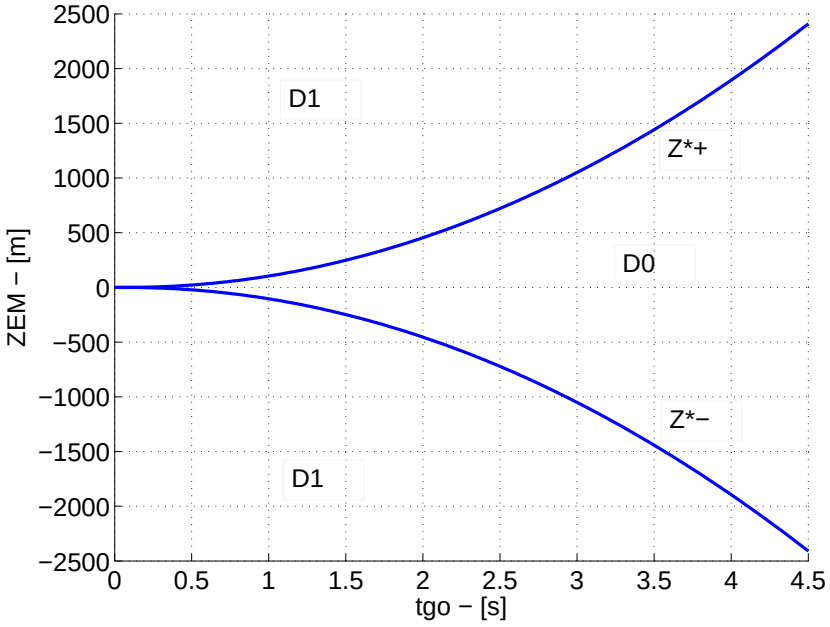

Figura 5.6. DGL/1 game structure

calculated [56] as the solution of the differential equation, integrating backwards in time from a certain initial condition

$$\frac{dZEM^*}{dt} = \Gamma \cdot sign\{ZEM^*(t)\} \tag{5.37}$$

where

$$\begin{aligned}\Gamma = -a_{M_{max}} \cos(\gamma_{M0} - \lambda_0)\Xi\left(t_{go}/\tau_M\right)\tau_M + \\ a_{T_{max}} \cos(\gamma_{T0} - \lambda_0)\Xi\left(t_{go}\tau_T\right)\tau_T\end{aligned} \tag{5.38}$$

with

$$\Xi(x) = \left(e^{-x} + x - 1\right) \tag{5.39}$$

The cosine terms have been introduced in order to take the proper contribution of the accelerations perpendicular to the line of sight. The perpendicular direction is calculated at the beginning of the end-game engagement and the derived structure is considered for the rest of the engagement. Integrating the differential equation from the condition $Z^*_+ = 0$ one obtains

$$\begin{aligned}Z^*_+ = -a_{M_{max}} \cos(\gamma_{M0} - \lambda_0)\left(-\tau_M e^{-t_{go}/\tau_M} + \frac{t_{go}^2}{2\tau_M} - t_{go} + \tau_M\right)\tau_M \\ + a_{T_{max}} \cos(\gamma_{T0} - \lambda_0)\left(-\tau_T e^{-t_{go}/\tau_T} + \frac{t_{go}^2}{2\tau_T} - t_{go} + \tau_T\right)\tau_T\end{aligned} \tag{5.40}$$

Thanks to the pursuit-evasion game formulation, two different guidance strategies can

now be defined. The first strategy will be referred to as *deterministic*, while the second as *stochastic*.

The deterministic guidance is based on the optimal strategy 4.57. The commanded acceleration in this case is [56]

$$a_{comm_{DET}} = a_{M_{max}} \cdot sign\{\widehat{ZEM}\} \tag{5.41}$$

where $\widehat{ZEM}$ is the estimated *Zero Effort Miss*. Under imperfect observations this law is not optimal anymore. Still, it is of common practice to use deterministic guidance laws in a stochastic setting, relying on the certainty equivalence principle [57].

For the considered problem the ZEM is expressed as

$$\begin{aligned} ZEM = -\dot{R}\dot{\lambda}t_{go}^2 + a_T \cos(\gamma_T - \lambda)\Xi(t_{go}/\tau_T)\,\tau_T^2 \\ -a_M \cos(\gamma_M - \lambda)\Xi(t_{go}/\tau_M)\,\tau_M^2 \end{aligned} \tag{5.42}$$

The stochastic strategy is a new approach to guidance. It is split in two cases, depending on whether we are in the D_0 or in the D_1 region. As mentioned before, the value of the game in D_0 does not depend on the applied strategy. This allows choosing the guidance command that returns the best observability conditions, when in D_0. Maneuvering away from the collision triangle will increase the ZEM. This can be tolerated until it reaches the value of the bound Z^*. From then on the guidance command shall let the ZEM follow the Z^* bound, thus remaining with a finite guaranteed miss distance.

When in the D_0 region, a finite set of acceleration command is considered, ranging from $-a_{M_{max}}$ to $+a_{M_{max}}$. Then the normalized error covariance matrix is computed along with its eigenvalues for each entry of the set of commands. This involves the computation of the Jacobian matrix of the filter, which depends on γ_M and, therefore, on a_M. The acceleration command is the one that results with the smallest among the set composed by the largest eigenvalues of P_{norm} for each command. When in the D_1 region the applied command is again the one expressed in 5.41. The stochastic strategy is given in Table 5.2. Due to computational constraints, the maneuver is determined at each time step over a unit time step horizon. Due to noise, eventually the ZEM trajectory will leave the D_0 region and miss distance will occur. In order to delay this departure as much as possible, a conservative approach has been chosen: the Z^* bounds have been reduced by an amount Δ of the punctual value of equation 5.40; furthermore, when t_{go} is smaller than a certain t_{sw}, the guidance switches to the deterministic strategy. This way, at the end of the engagement, the missile tries to reduce its ZEM and not to move away from the collision triangle.

Δ and t_{sw} values are specified in Table 5.3. They can be considered as the guidance tuning parameters. Their significance can be understood in the light of the division of the game space between capture and avoidance zones. It is extremely important not to cross to the

Tabella 5.2. Algorithm for stochastic strategy

1: **if** $|\widehat{ZEM}| < (1 - \Delta) \cdot Z^{*+}$ & $t_{go} > t_{sw}$ **then**
2: calculate resulting γ_M for each command u from a finite set $\in [-a_{M_{max}}\ a_{M_{max}}]$
3: for each command u, find P_{norm} largest eigenvalue and store it in the set Σ
4: choose the command u^* associated with the smallest eigenvalue from the set Σ
5: $a_{comm_{STO}} = u^*$
6: **else**
7: $a_{comm_{STO}} = a_{M_{max}} \cdot sign\{\widehat{ZEM}\}$
8: **end if**

D_1 region, because there would be no finite guaranteed miss. The miss distance is therefore very sensitive to these two parameters.

5.8 Nonlinear stochastic simulations

Two nonlinear simulations were conducted to test the validity of the strategies, one without target maneuvers and one with target maneuvers. Being the latter a more general case, the former is nevertheless interesting because it is more difficult from the observability point of view. The engagement performances of the two strategies will be compared also to that of PN. PN does not require the knowledge of t_{go} and it is seems interesting to test it against two algorithms highly dependent on t_{go}. The estimator integrated in the PN simulation is the one described in section 5.3
The two different scenarios are described in section 5.8.1. The performances of the two strategies will be compared in terms of miss distance. The comparison will be made on a set of 200 Monte Carlo samples. Each sample differs from the others by the initial guesses given to the estimator and by the initial value of γ_T and γ_M. The stopping criterion for the simulation is when $\dot{R} > 0$.

5.8.1 Engagement scenarios

The scenarios of the engagement start with the missile and the target on a collision triangle. In the first scenario (Not Maneuvering Target - NMT) the target does not perform any maneuvers, while in the latter (Maneuvering Target - MT) it starts maneuvering at its maximum capability at a uniformly distributed random time. Both missile and target have constant speed.
Initial values and parameters of the simulation are resumed in Table 5.3. The values of γ_{T_0} for all the samples belong to a Gaussian distribution with mean of 50° and variance 10°.

The initial values of γ_M belong to a Gaussian distribution with values corresponding to a perfect collision triangle as mean and variance 1°.

5.8.2 Estimation

The only target measurement for the missile is the bearing angle λ; measurements are updated every T_s seconds. Measurements at the instant k can be obtained through equation

$$z_k = Hx + v \tag{5.43}$$

where H is the vector

$$H = \begin{bmatrix} 0 & 1 & 0 & 0 & 0 \end{bmatrix} \tag{5.44}$$

The bearing measurement is corrupted by a white Gaussian noise v with variance σ_v. The process noise covariance matrix Q is defined as

$$Q = \int_0^{T_s} \Phi(\eta)\Psi\Phi(\eta)^T d\eta \tag{5.45}$$

where Ψ is a matrix whose only non-zero element is $\Psi(4,4) = \psi$. The filter is initialized with the $P_{0|0}$ matrix and with a vector of guesses $\hat{x}_{0|0}$

$$\begin{gathered} \hat{x}_{0|0} \sim \mathcal{N}(x_0, \sqrt{P_{0|0}}) \\ P_{0|0} = diag\begin{bmatrix} 500^2 & \left(\frac{5\pi}{180}\right)^2 & \left(\frac{5\pi}{180}\right)^2 & (5g)^2 & 100^2 \end{bmatrix} \end{gathered} \tag{5.46}$$

The only tuning parameter of the estimator is ψ, that was chosen by numerical simulations. Noise on the measurements was taken as an input. $P_{0|0}$ elements were chosen according to the variances of the Monte Carlo samples.

Tabella 5.3. Simulation initial values and parameters

Parameter	Value	Parameter	Value
R_0	$10\ km$	λ_0	10°
γ_{T_0}	$\sim \mathcal{N}(50^\circ, 10^\circ)$	T_s	$0.02\ s$
v_M	$3\ km/s$	v_T	$1\ km/s$
a_{M_0}	$0\ m/s^2$	a_{T_0}	$0\ m/s^2$
τ_M	$0.1\ s$	τ_T	$0.2\ s$
$a_{M_{max}}$	$30\ g$	$a_{T_{max}}$	$5\ g$
σ_v	$0.001\ rad$	$\sigma_{\omega_{a_T}}$	$\frac{a_{T_{max}}^2}{tf}\ m/s^2$
$t_{sw}\ (NMT)$	$2\ s$	$t_{sw}\ (MT)$	$2.5\ s$
$\Delta\ (NMT)$	0.3	$\Delta\ (MT)$	0.35

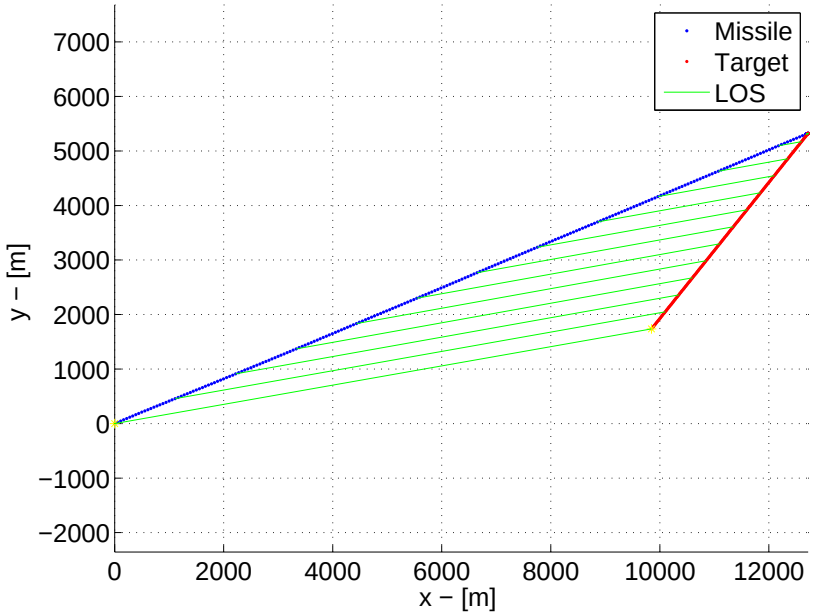

Figura 5.7. Missile and target trajectories - deterministic strategy - NMT

5.8.3 Results - No target maneuvers

The missile remains on the collision triangle in the case of the deterministic strategy, while in the other case it maneuvers away and breaks the collision course conditions. As it can be seen from Figs. 5.7 and 5.8, in fact, in the latter the trajectory of the missile is slightly curved, while in the former is straight as expected.

Figs. 5.9 and 5.10 show the estimated ZEM, the actual ZEM, the commanded acceleration and the actuated one for a sample run. The represented t_{go} is calculated after the end of the simulation, by subtracting each time instant from the final time. One should keep in mind that the acceleration command (black line) is driven by the estimated ZEM (red line). After the estimated ZEM has reached the 0 level, the command exhibits the typical bang-bang behavior, as the strategy tries to maintain the estimated ZEM around 0. In the stochastic case the command is less chattering than in the former: this is better from the actuators point of view. Both the estimated and the true ZEM are increasing at the beginning, until they reach near the threshold of the Z^* bound. Then, they start to chatter around the bound, until $t_{go} \leqslant t_{sw}$, when the strategy switches to the deterministic one and the command is no longer based on the solution that mostly enhances observability.

It is interesting to note that the commands are $bang - bang$. This confirms that, in order to enhance observability, the best option is to maneuver away from the collision triangle.

Fig. 5.11 shows the results of range estimation, plotted against t_{go}. The red line is the

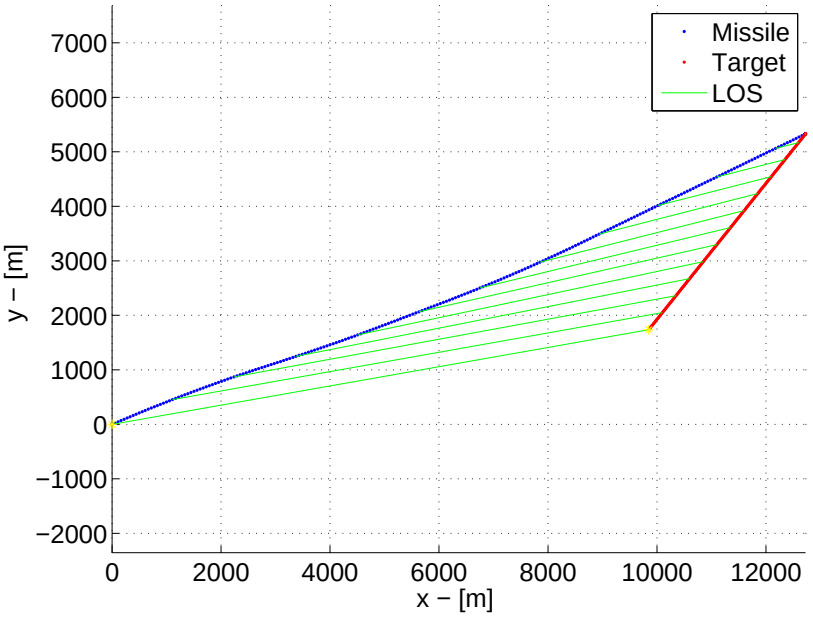

Figura 5.8. Missile and target trajectories - stochastic strategy - NMT

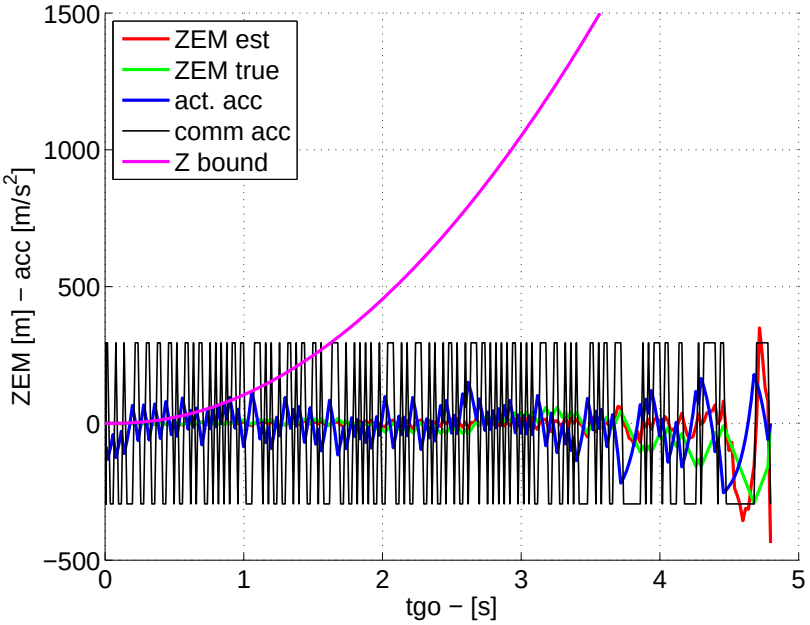

Figura 5.9. Sample accelerations and ZEM - Deterministic NMT

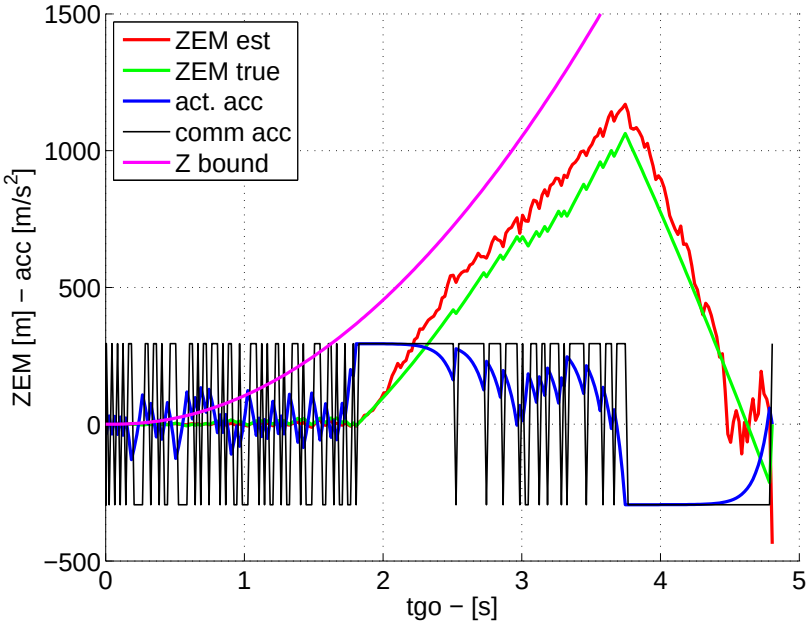

Figura 5.10. Sample accelerations and ZEM - Stochastic NMT

mean estimation error; the green line is the error from a sample run; the blue line is the error standard deviation; the black lines are the 1σ bounds calculated by a sample run of the filter.

The results of range estimation in the deterministic case show that the system is not observable: the bounds of the covariance matrix diverge until $t_{go} > 0.5\ s$. On the other hand, they converge in the stochastic case, meaning that the maneuvering strategy affects the estimation results. The jumps in the standard deviation at the end of the simulation mean that there are some samples whose estimation is very bad. This is more evident with the deterministic strategy.

Shaping filter effectiveness can be evaluated in Fig. 5.14. The filter is able to detect target's maneuver as the mean error is around the zero level. The computed bounds from the filter are consistent with the standard deviation of the error. As with the range estimation, the jumps at the end of the engagement are due to bad estimated samples. The jump in the deterministic strategy case is greater than in the other case.

Figs. 5.12, 5.13 and 5.15 show the estimation results for λ, γ_T and v_T. These results shows a small improvement in the stochastic strategy, in terms of convergence of the expected filter boundaries and in terms of jumps in the standard deviation at the end of the engagement. Arguably, the improvement of range estimation has positive effects on the overall filter behavior. It shall be remembered, in fact, that the EKF is a numerical tool and thus can suffer from numerical conditioning when there is something wrong. It can be concluded that the

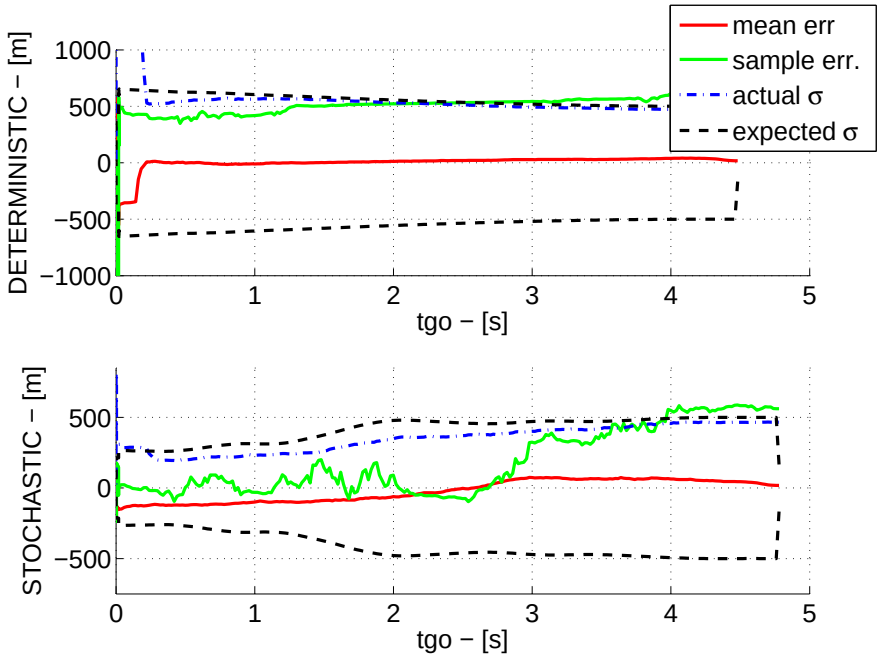

Figura 5.11. Estimated R - NMT

new strategy is helpful to enhance the overall estimation.

Fig. 5.16 shows the achieved miss distance by means of the cumulative distribution function. The axis of abscissae is the miss distance, while the ordinates indicate the percentage of samples with a miss smaller than or equal to the value reported on the x axis. The two strategies obtain almost the same results in 35% of the cases, with a miss around 0.05 m. From that until 97% of the cases, the stochastic strategy is more precise, having an accuracy smaller or equal to 0.32 m in 90% of the cases, while the deterministic strategy has an accuracy of 0.50 m in 90% of the cases. PN reaches the performance levels of the deterministic strategy in 70% of the cases and of the stochastic strategy in 25% of the cases. In the rest of the cases, its results are less precise. Clearly, despite the independence from t_{go} advantage, PN is not adequate to deal with a scenario with lags in the guidance system.

If the missile designer would like to achieve a 90% kill probability then using the stochastic strategy a warhead lethal radius of 0.32 m is needed while in the other case it is 56% larger. A 90% kill probability with the PN requires a lethal radius of 1.5 m.

5.8.4 Results - Target maneuvers

Missile and target trajectories from a sample run are shown in Figs. 5.17 and 5.18 for both the strategies. This time the trajectory of the target (red line) is curved and thus the missile has already an insight on range estimation. Figs. 5.19 and 5.20 show, respectively, the

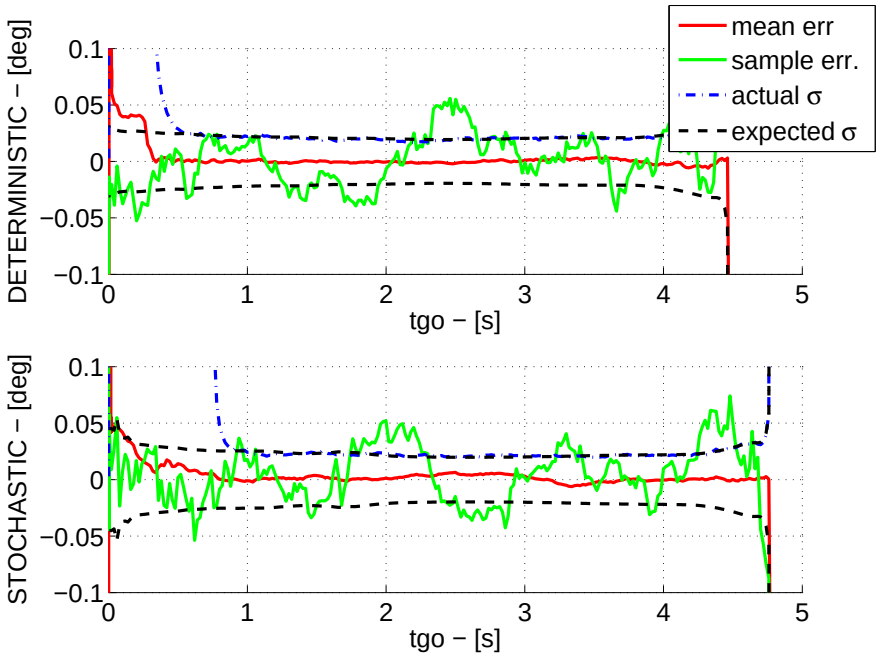

Figura 5.12. Estimated λ - NMT

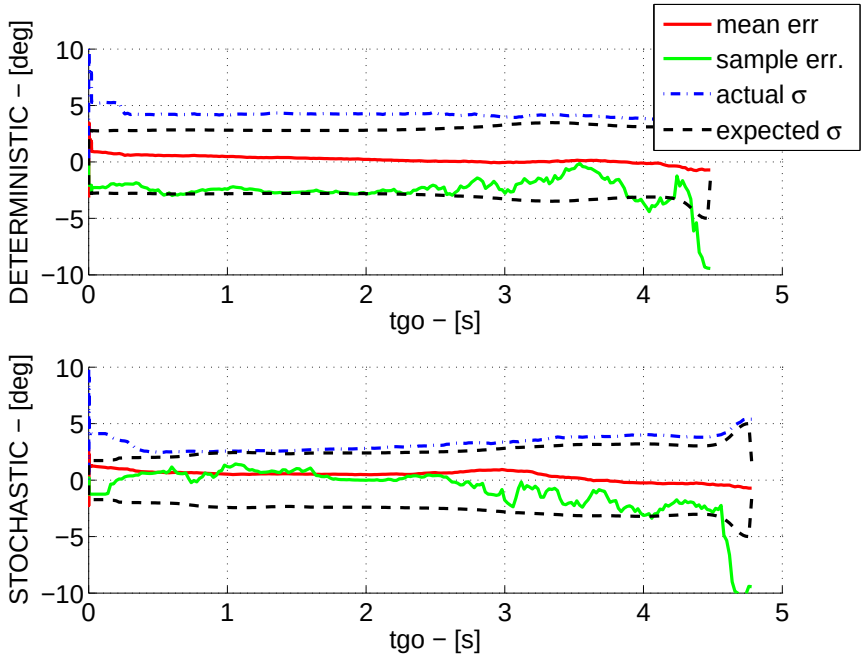

Figura 5.13. Estimated γ_T - NMT

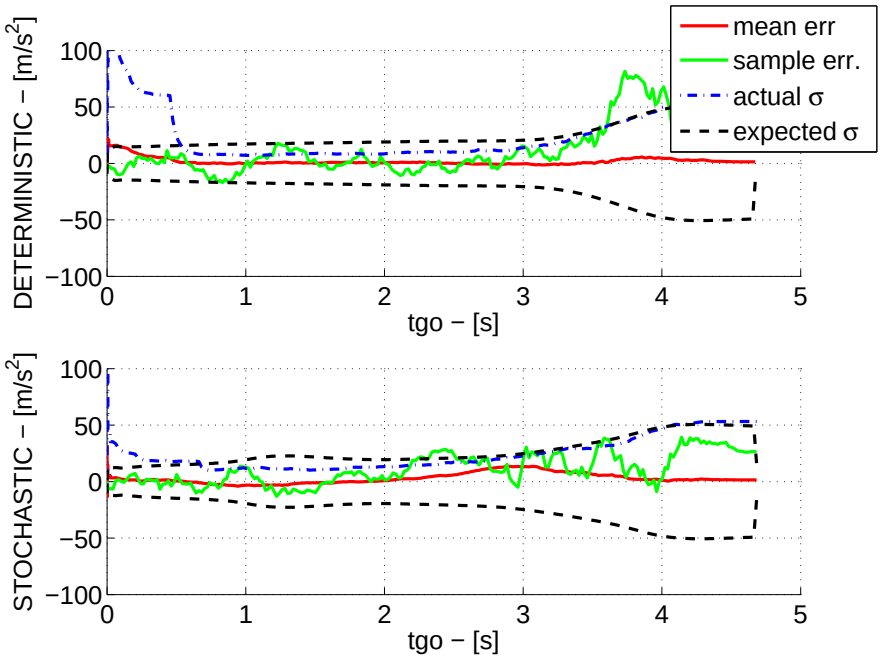

Figura 5.14. Estimated a_T - NMT

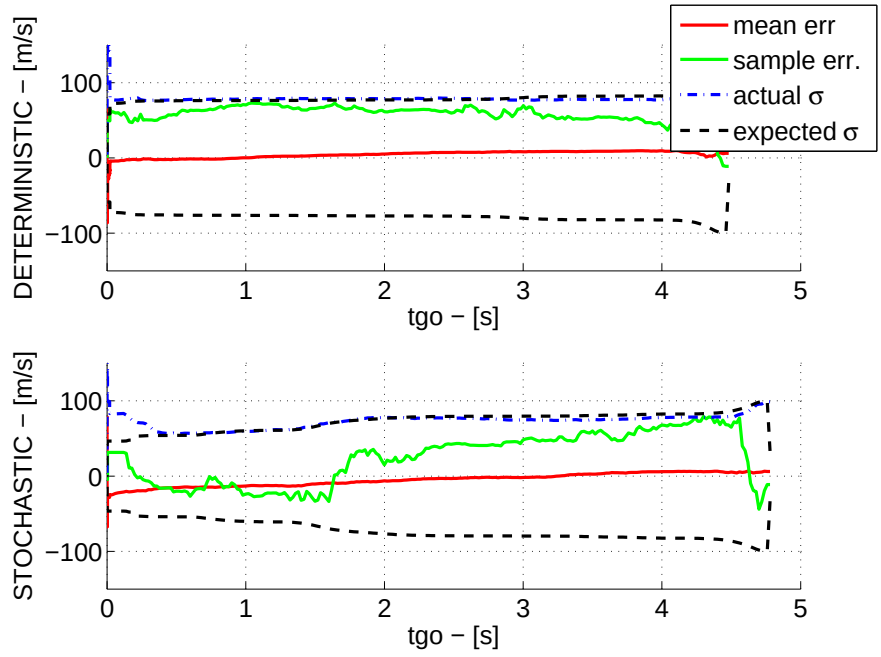

Figura 5.15. Estimated v_T - NMT

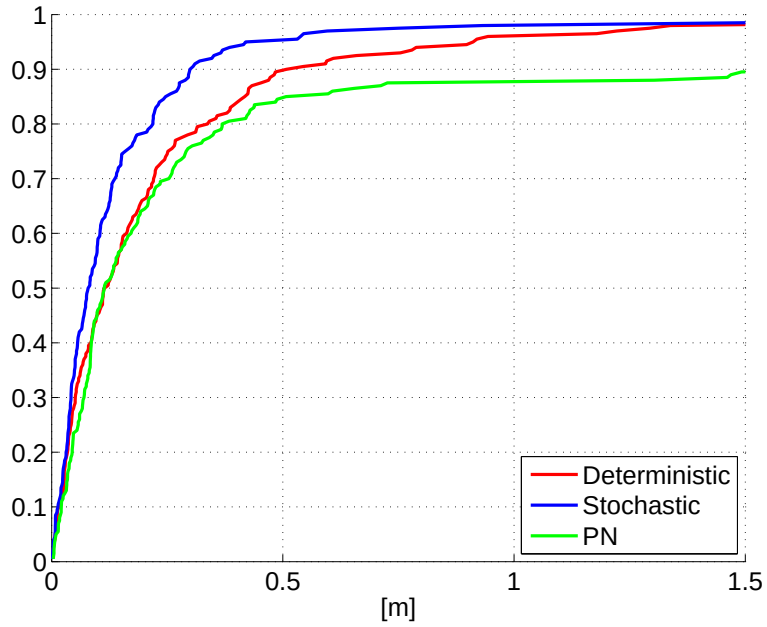

Figura 5.16. CDF - NMT

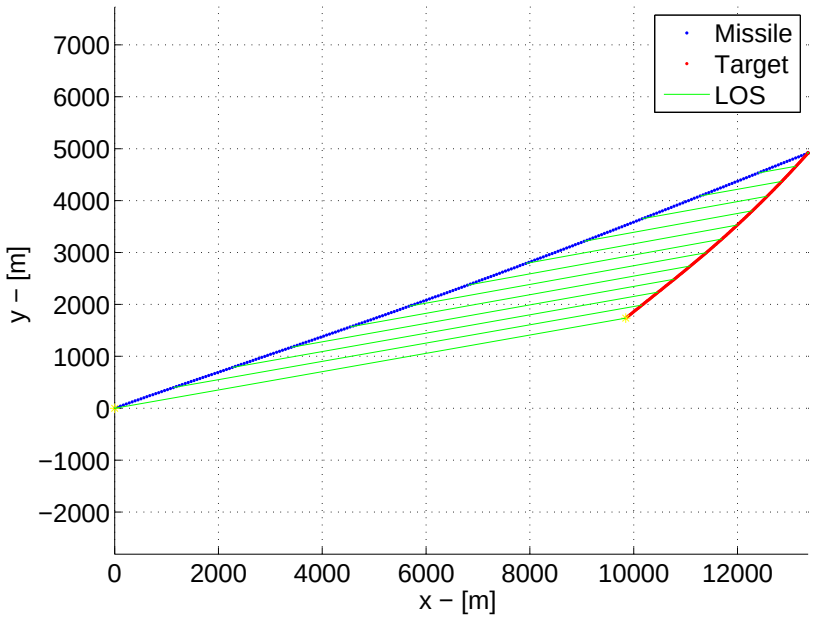

Figura 5.17. Missile and target trajectories - deterministic strategy - MT

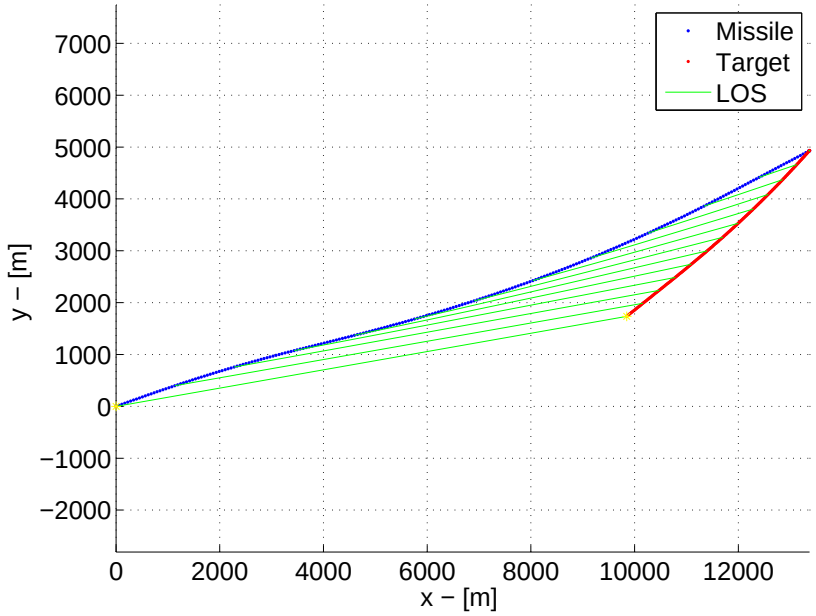

Figura 5.18. Missile and target trajectories - stochastic strategy - MT

computed Z^* bounds, the estimated ZEM and the actual one, along with the acceleration command and the actuated acceleration for the case of target maneuvers. These plots look almost the same as in the case with no target maneuvers. The stochastic case has almost no chattering in the first 3 seconds of engagement. The results of range estimation are shown in Fig. 5.21. With the deterministic strategy the range is again unobservable, as in the NMT case. Only at the end of the engagement the 1σ bounds converge, arguably because the missile is missing the target and thus the line of sight rotates very fast. With the stochastic strategy the estimation is more precise, meaning that the range is more observable than with the other strategy.

Fig. 5.24 shows the results of target's acceleration estimation. As in the NMT case, the shaping filter is effective and target's maneuvers are well estimated. The jump in the standard deviation at the end of the simulation is more noticeable in the deterministic case.

Figs. 5.22, 5.23 and 5.25 show the estimation results for λ, γ_T and v_T. As in the NMT case, the results with the stochastic strategy are better than with the deterministic strategy: the expected bounds from the filter converge better and the jumps in the standard deviation at the end of the engagement are less evident. Even in this case the stochastic strategy has resulted effective in improving the estimation performance of the engagement with respect to the deterministic strategy.

Fig. 5.26 shows the cumulative distribution function of the miss distance over the 200 Monte Carlo runs. The two strategies give almost the same performance until 0.03 *m* (20%

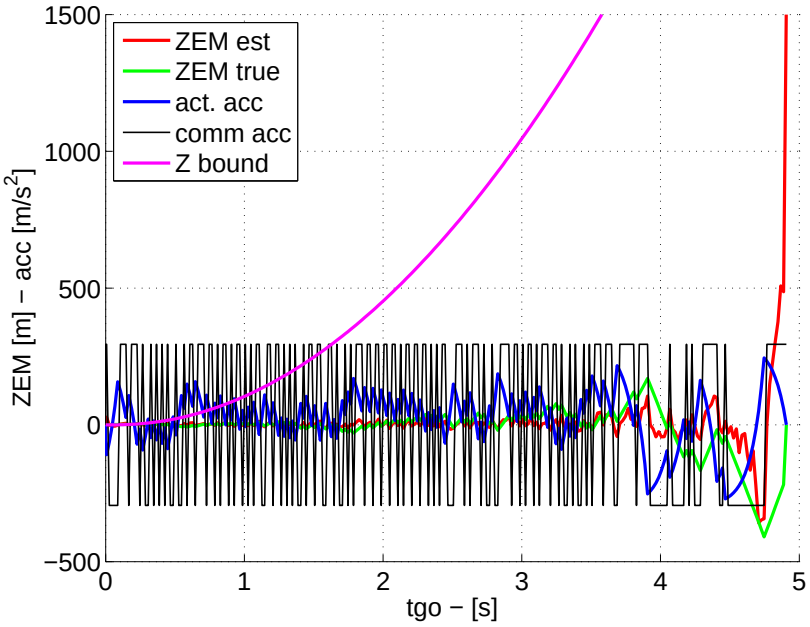

Figura 5.19. Sample accelerations and ZEM - Deterministic MT

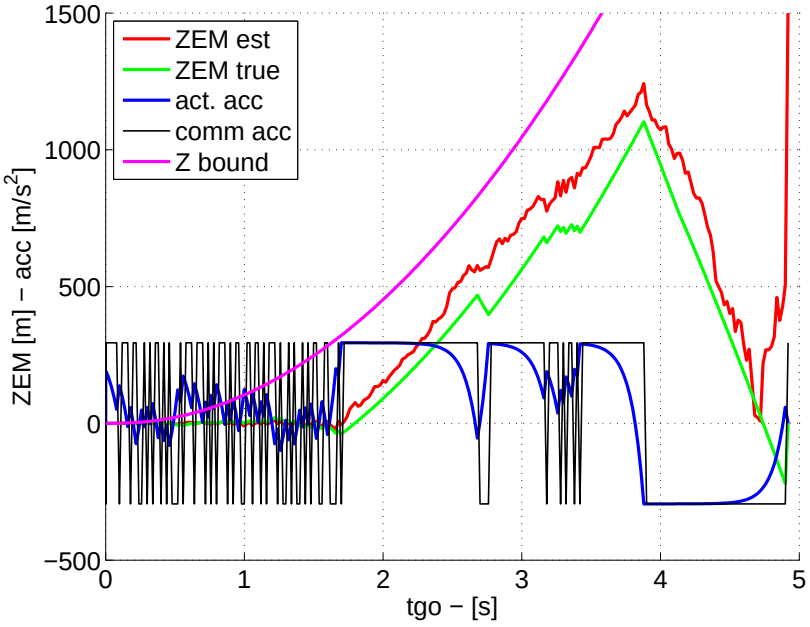

Figura 5.20. Sample accelerations and ZEM - Stochastic MT

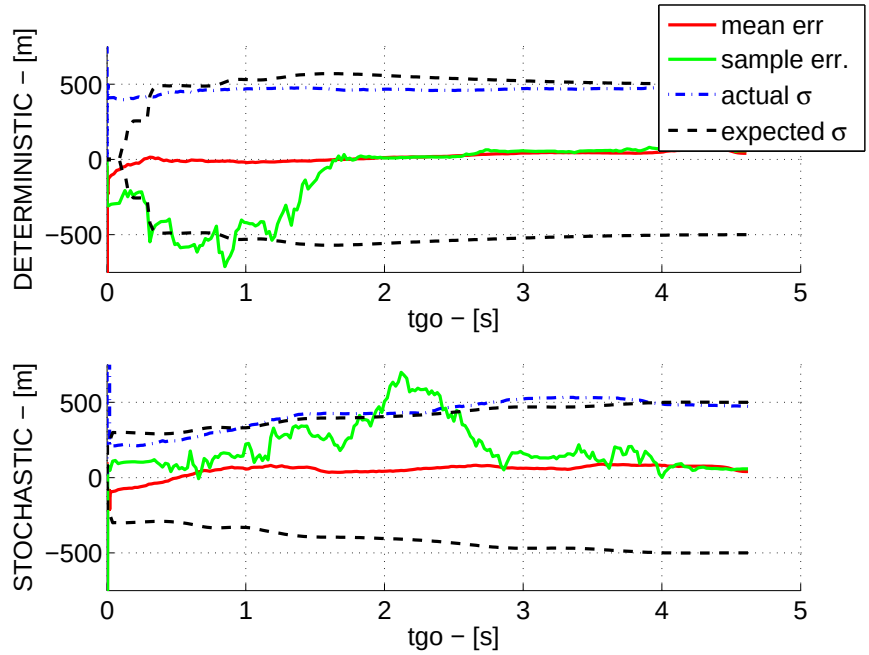

Figura 5.21. Estimated R - MT

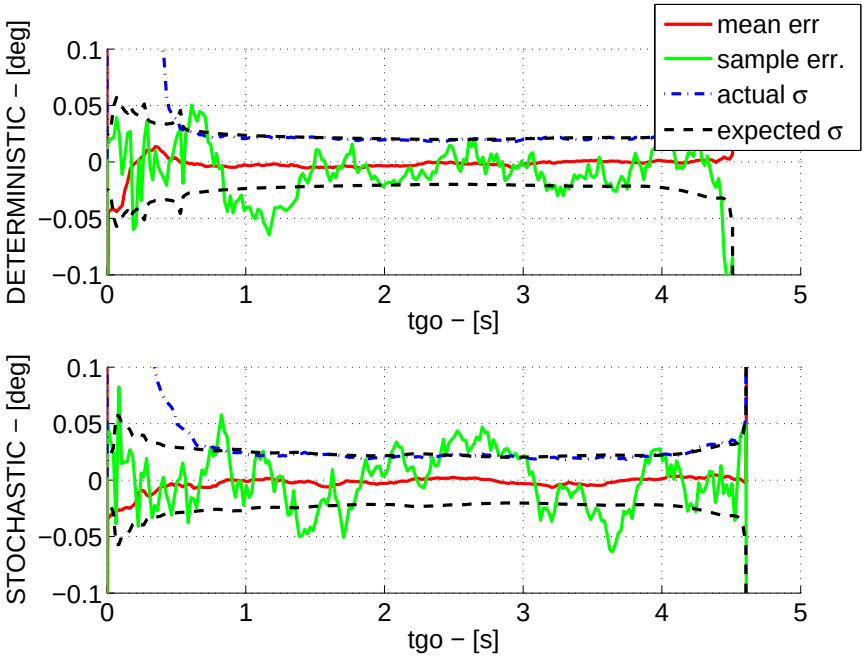

Figura 5.22. Estimated λ - MT

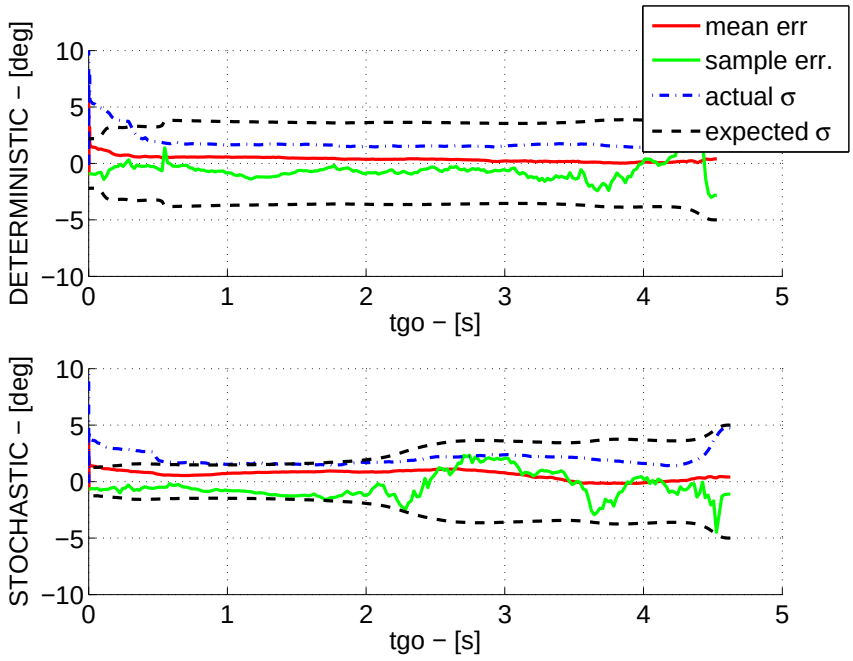

Figura 5.23. Estimated γ_T - MT

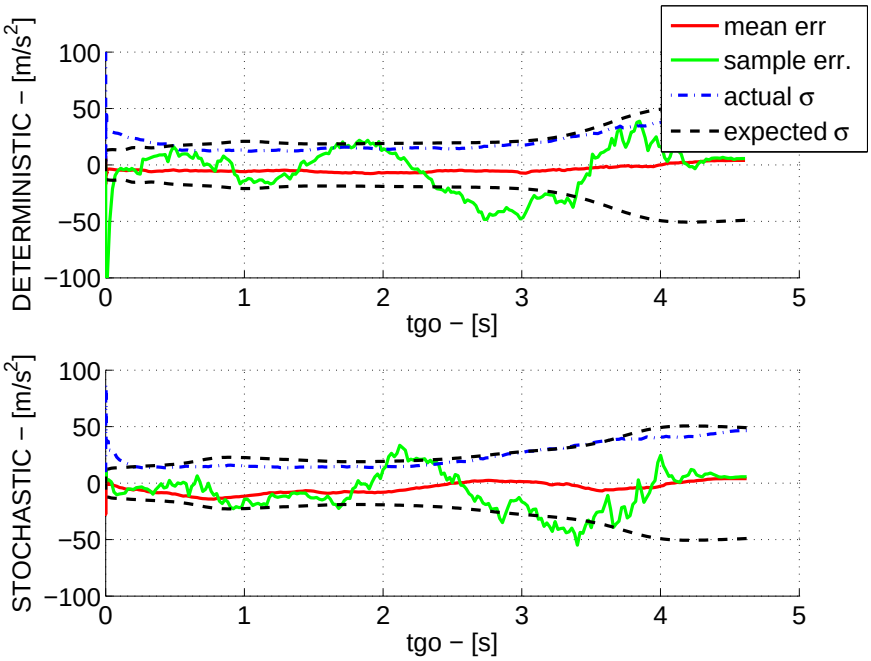

Figura 5.24. Estimated a_T - MT

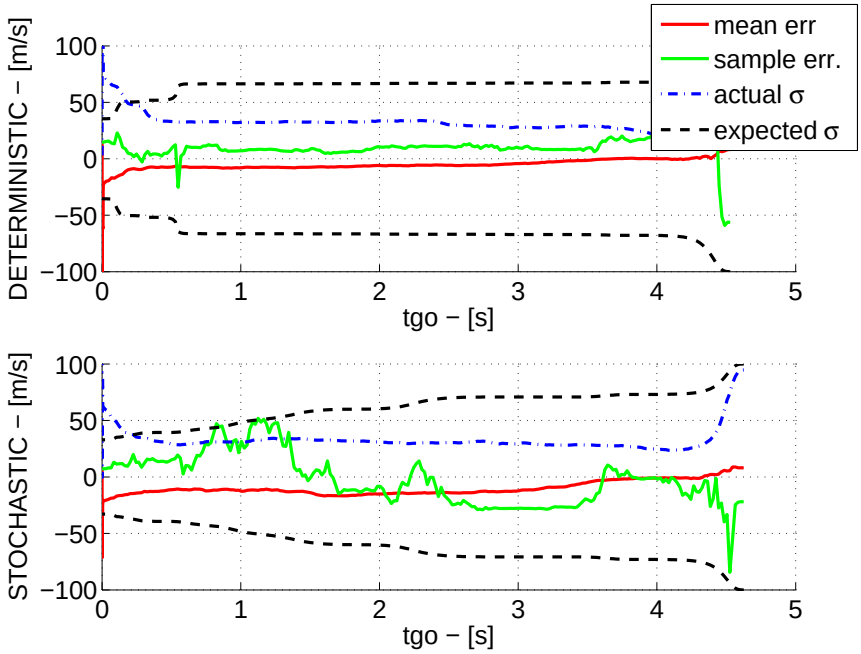

Figura 5.25. Estimated v_T - MT

of the runs). From then on the stochastic strategy is more precise than the deterministic. In 90% of the cases the stochastic strategy reaches an accuracy of 0.44 *m*, while for the deterministic the accuracy is 0.60 *m*. These results are slightly worse than in the case with no target maneuvers, presented in Fig. 5.11. Target maneuvers facilitate range estimation, but they also help the target to escape and thus increase the miss distance. This is even more evident when it comes to PN results, that are hardly comparable to the formers. This is easily understandable because of the presence of target maneuvers, which have a large impact on miss distance if not taken into account [67].

5.9 Summary

This chapter has dealt with the problem of estimating the variables involved in a homing loop. Estimation is based on a single bearing noisy measurement. The implementation of PN was demonstrated to be feasible with a 2-states KF. The concept of shaping filters was introduced to detect target maneuvers. The rest of the chapter was dedicated to the description of a new approach to missile guidance driven by bearings-only measurements.
A major problem with this kind of application is range unobservability. The new approach embeds the analysis of the error covariance matrix from the homing loop integrated Kalman filter into a pursuit evasion differential game. The information from the filter is used to determine which missile maneuver improves range observability the most.

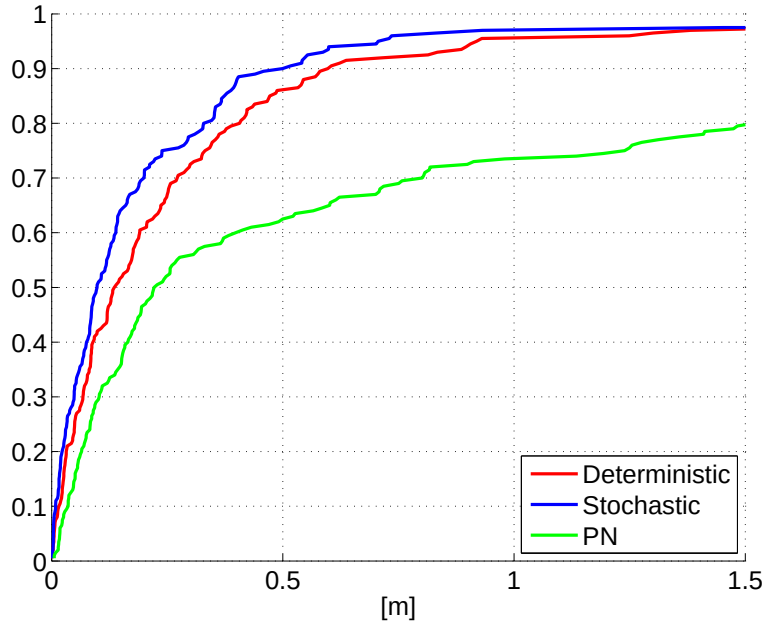

Figura 5.26. CDF - MT

Within a pursuit-evasion game the state space is divided to capture and avoidance zones. In the capture zones maneuvering does not impact the miss distance of the engagement, but it does improve the observability of the range. A new guidance strategy that makes the missile maneuver improve observability in the capture zones has been defined.

The new guidance strategy has been compared to the one resulting from the optimal solution of the deterministic pursuit-evasion differential game and to PN. Their effectiveness has been compared on a set of Monte Carlo samples in a scenario with target maneuvers and in a scenario with no target maneuvers. The results show that the new approach enhances engagement's variables estimation in both scenarios. Range estimation is particularly improved by the new strategy. The analyzed guidance laws, except PN, critically depend on the estimation of t_{go}, and hence on the estimation of range. Therefore, the overall homing performance, both in the absence and in the presence of target maneuvers, is improved.

In conclusion, the use of the pursuit-evasion game framework has allowed to reformulate the initial problem: instead of looking for the optimization of the maneuver that enhances observability, a suboptimal guidance strategy was found, that defines a maximum allowable distance from the collision triangle.

The results of the new guidance strategy will drive the requirements for the autopilot that has to be designed in the next chapters. The autopilot shall meet the requirements of the guidance system in terms of lateral maneuvering capability and response fastness.

Capitolo 6

Design of the interceptor

This chapter is dedicated to the design specifications of the interceptor. The interceptor can be a surface-to-air or an air-to-air missile. Once the boosters have burned out, the interceptor has reduced to the kill vehicle. The kill vehicle is initially given information on the target by a radar or a infrared tracker or both. Once it has entered in the terminal phase of the engagement, on board sensors take control on the steering so that the kill vehicle can operate autonomously. Kill vehicles task is to hit the target. Target destruction can be achieved through an explosive warhead or even thanks to the impact between the target and the kill vehicle. In this case the latter is called a kinetic kill vehicle. Even deviating the target from its nominal trajectory can be a goal for the kill vehicle.

The design criteria of the interceptor and, more specifically, of the kill vehicle are very demanding with regards to maneuverability, response to command, and stability. A first distinction is between exo-atmospheric and endo-atmospheric engagements. Within atmosphere, aerodynamic control can be used, while outside the atmosphere control is performed with thrusters.

The guidance laws expressed in chapter 4 can be implemented either through a set of wings or a single thruster. This was the case of the first midcourse hit-to-kill vehicle, the Homing Overlay Experiment (HOE) in 1984 [48]. A cruciform configuration of thrusters, mounted perpendicularly to the longitudinal axis of the missile, was employed in 1991 on the Exoatmospheric Reentry Intercept System (ERIS) [4], [29]. This work will focus on aerodynamic controlled kill vehicles.

The choice of the configuration heavily impacts the dynamical characteristics of the missile. Autopilots, that will be introduced in chapter 7, can improve missile response to guidance commands, but a good preliminary design of the missile will facilitate the task of the control system designer.

The chapter is organized as follows. Firstly, an introduction to aerodynamically controlled

missiles classification based on wing configuration and motor configuration will be given. Equations of attitude motion will then be derived, with particular attention to aerodynamic contributions. Linearization of the model will yield the airframe representative transfer functions. This kind of representation of the airframe is useful because it gives some insights on the dynamical properties of the missile. The parameters which describe these properties will be examined too in this chapter. Finally, two aerodynamic configurations for the missile will be compared in terms of static and dynamic properties. The best configuration will be chosen with respect to the requirements of the guidance system and will be used in chapter 7 for the design of the autopilot.

6.1 Classification of missiles

Missiles use in defense system against ballistic threats contemplates a wide range of scenarios, as described in chapter 1. Mission requirements vary with the particular engagement scenario. A variety of missile configurations exists to match the mission requirements. The most important distinctions that will be discussed here regard the aerodynamic configuration and the motor configuration.

6.1.1 Aerodynamic configuration

The missile is usually in a cruciform configuration of wings and tail. This symmetrical configuration allows lateral maneuvering in any direction without first rolling, as airplanes with fixed wings do [61]. As these missiles use direct side force to turn, they are referred to as Skid-to-turn (STT) missiles. For these missiles, inertial coupling between roll, pitch, and yaw is negligible. Bank-to-turn (BTT) missiles must roll to a banked position so that their wings are in the direction of the maneuver and then must roll back to resume straight flight. Since the maneuver must have a very short time response, BTT missiles shall have high roll rates. However, this increase the aerodynamic coupling and can raise attitude control issues [11]. Hence, BTT missiles are more difficult to control [3]. This addresses the choice of this work towards a STT missile.
Another important feature of the missile is the configuration of wings. As it is well known, tail wings are needed for stability [46]. Control surfaces are movable surfaces that allows lateral maneuvers by changing the aerodynamic forces and torques acting on the missile. There are three main configurations for control surfaces:

Wing control Wing control configuration is represented in Fig. 6.1, with the *Sea Sparrow* missile. In this configuration, wings are placed slightly forward of the center of gravity. Movable surfaces placed on them allow to perform maneuvers. Fixed surfaces on the tail

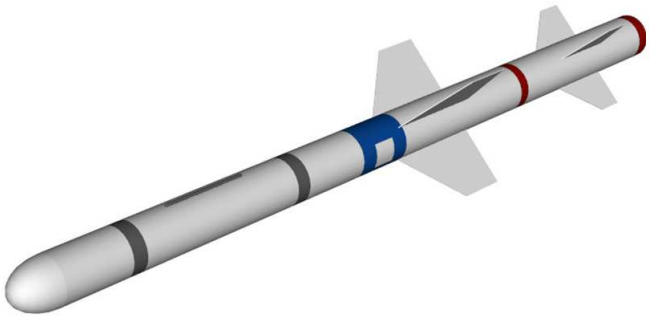

Figura 6.1. Wing control (e.g. RIM-7 Sea Sparrow)

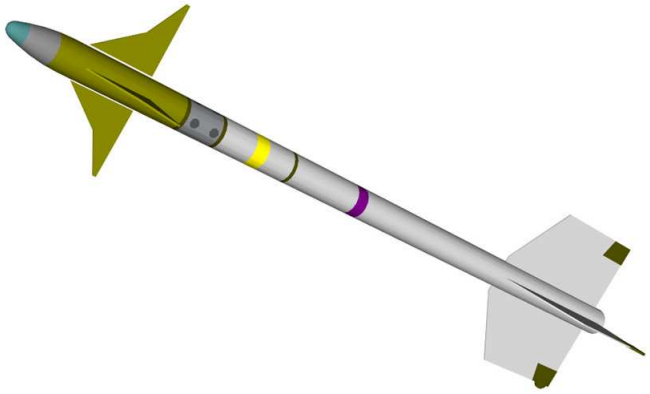

Figura 6.2. Canard (e.g. AIM-9 Sidewinder)

guarantees stability. A disadvantage with this configuration is that downwash from the control surfaces hits the tail and may cause undesired rolling moments at supersonic Mach numbers [10], [61], [16].

Canard Canard configuration is shown in Fig. 6.2 with the *Sidewinder* missile. The term canard stands in French for duck and indicates wings placed far forward from the center of gravity. Movable surfaces are on the canard wings, while the tail is fixed and usually larger than the canards for stability reasons. The same considerations on induced rolling moments from wing-control configuration generally hold for the canard configuration. However, this effect can be nullified with a properly designed (reduced) tail-span [50].

Tail control Tail control configuration is represented in Fig. 6.3 with the *Phoenix* missile. Fixed and movable aerodynamic surfaces are located on the tail. This configuration does not suffer from the induced rolling moments issue as the forward-control surfaces configurations. On the other hand, it suffers from the phenomenon known as *wrong – way* effect: the initial acceleration response of the missile is in the wrong direction with this configu-

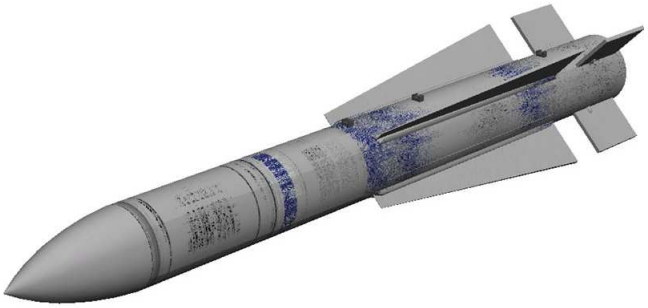

Figura 6.3. Tail control (e.g. AIM-54 Phoenix)

ration. When the movable surface is deflected, a lift force occurs on the tail. This force causes the instantaneous motion of the entire body in the direction of the lift. At the same time, it generates also a torque around the center of gravity which makes the missile rotate. After the rotation, the missile is heading towards the direction opposite to that where it was initially pointing at. The *wrong – way* effect is represented by a right-half plane zero in the transfer function from the control to the lateral acceleration. The behavior of a tail controlled missile is that of a non-minimum phase system. The wrong-way effect limits the speed of response to a lateral acceleration command, even if rolling moments are minimized [61].

Among these three configurations, the one with canards seems the most suitable for the problem of intercepting a target. Its time response to an acceleration command, indeed, is faster than with the tail wing configuration. Furthermore, they do not suffer from the wrong-way effect. The torque generated by a canard deflection has a sign opposite to that generated with the tail, because of the difference of signs in the arm of the torque. The rotation is in the same direction as the movement generated by the initial lift.
Canard configurations are known for assuring agility and maneuverability. On the other hand, the disadvantage of induced rolling moments experienced by forward-control surfaces configurations can be solved by designing a sufficiently small tail-span. In conclusion, the design of the interceptor in this study will focus on a canard configuration. The *Sidewinder* missile will then be taken as a benchmark for the design of the interceptor.

6.1.2 Motor configuration

A major consideration in the design of a missile is the propulsion system. A deep analysis of propulsion aspects is out of the scope of this work. Here only a brief description of the main missile motors categories will be given.

All-boost An all-boost motor is burning for a very short time period, reaching a high thrust peak . The missile is accelerated rapidly in the first seconds of flight. However, this causes high drag, high aerodynamic heating and short time of flight, for a given range. This motor is suitable for a tail chase engagement [61].

All-sustain An all-sustain motor has low thrust and long time of flights. The drag experienced by the missile is lower than with an all-boost motor. This kind of motor can be used in head-on engagements or in look-up engagements at high altitudes to overcome gravity.

Boost-sustain A boost-sustain motor is a compromise between the two previous categories, having a thrust peak at the beginning (lower than with an all-boost) and then maintaining a low acceleration for a the rest of the flight time (lower than with an all-sustain).

Although quite general, this classification explains the essential features of a propulsive system for guidance aspects. Propulsion modelization will not be pursued in this work. However, the best solution for the interceptor seems to have a motor of the boost-sustain type, as it can cover a wider range of missions.

6.2 Dynamical model

In chapters 4 and 5, the physics inherent to the missile was represented as a delay in the transmission of the guidance command. A first-order transfer function described the relationship between the commanded acceleration and the actual one. This approximation is commonly used in the design of guidance system. In this chapter and in the following it shall be demonstrated that the missile response to commands can meet the time constraints previously considered. The design of the autopilot is going to be based on the dynamical model derived in the following for the missile *airframe*.
There are essentially three kind of forces acting on a missile: the gravity force, the thrust and the aerodynamic. The model that is going to be hereafter developed aims at representing missile motion generated by wings deflection. For this reason gravity and thrust effects will be neglected in the analysis. The missile will be considered as it is floating at a certain altitude, thanks to the lift that balances gravity. For a tactical missile, furthermore, gravity acts on a much larger time scale than that of autopilot response and its effects are balanced at the level of the guidance system. Gravity moments are neglected due to the short dimensions of the missile
The longitudinal motion is considered balanced by the sum of thrust and drag forces. For an aerodynamically controlled missile, (i.e. without TVC) thrust is assumed to be perfectly

aligned with the longitudinal axis of the missile. Mechanical moments due to thrust are then neglected too.

The remaining forces and moments are only those generated by the interaction with the air. The missile generates lift by moving its control surfaces, which are placed on the forward wings (canards) for the considered case. Canards are deflected about their hinge line by a fin angle δ. The description of how aerodynamic forces are generated on a winged vehicle is well described in several textbooks [11], [19], [46] and will be here briefly resumed.

Since there are no changes in the forward velocity and the only variations occur in the angle of attack α and pitch angle θ, the analysis will be limited to the so called *short − period mode* [11]. The normal force F_N acts through the center of pressure of the vehicle. It can be expressed as

$$F_N = \frac{1}{2}\rho v_M^2 S_{ref} C_N = \bar{q} S_{ref} C_N(\alpha, Mach, v_M, h, \delta) \tag{6.1}$$

where ρ is the air density, S_{ref} the reference section of the missile, $\bar{q}$ the dynamic pressure and C_N the normal force coefficient. S_{ref} is taken as the cross section area of the missile. C_N depends on several aspects, such as the Mach number, the altitude h, the angle of attack α, the fin angle δ and so on.

The total moment M acting on the missile is due to the normal force multiplied by its arm and can be expressed in terms of the moment coefficient C_M as

$$M = \frac{1}{2}\rho v_M^2 S_{ref} d C_M = \bar{q} S_{ref} d C_M(\alpha, Mach, v_M, h, \delta) \tag{6.2}$$

where d is the missile diameter.

Dynamical equations can be derived from the 2^{nd} Newton's law and the Euler's law. Considering a body fixed reference system, the normal acceleration is defined as

$$n_B = \dot{w} = \frac{F_N}{m} = \frac{\bar{q} S_{ref} C_N(\alpha, Mach, v_M, h, \delta)}{m} \tag{6.3}$$

where m is the mass of the missile. The angular acceleration is

$$\ddot{\theta} = \dot{q} = \frac{M}{I_{yy}} = \frac{\bar{q} S_{ref} d C_M(\alpha, Mach, v_M, h, \delta)}{I_{yy}} \tag{6.4}$$

where I_{yy} is the missile moment of inertia. The last equations is related to α, defined as

$$\alpha = \theta - \gamma_M \tag{6.5}$$

Remembering the expression from equation 4.1 for the flight path angle and differentiating, one has

$$\dot{\alpha} = \dot{\theta} - \dot{\gamma} = \dot{\theta} - \frac{a_M}{v_M} \tag{6.6}$$

For small angles the lateral acceleration a_M can be approximated with the normal acceleration n_B:

$$\dot{\alpha} = \dot{\theta} - \frac{n_B}{v_M} \tag{6.7}$$

The short period equations for the airframe are resumed hereafter

$$\begin{cases} \dot{w} = \dfrac{\bar{q}S_{ref}C_N(\alpha, Mach, v_M, h, \delta)}{m} \\ \dot{\theta} = q \\ \dot{q} = \dfrac{\bar{q}S_{ref}dC_M(\alpha, Mach, v_M, h, \delta)}{I_{yy}} \\ \dot{\alpha} = \dot{\theta} - \dfrac{n_B}{v_M} \end{cases} \tag{6.8}$$

6.3 Linearization

In order to develop a linear control system, a linearization of equations 6.8 is needed. Assuming a flight at reference altitude h_0 and reference velocity v_{M0}, equations 6.8 can be considered linear except for the α and δ terms. Linearization can be performed assuming that the two contributions from α and δ are linear.
Thus the normal coefficient and the moment coefficient can be rewritten

$$\begin{aligned} C_N(\alpha, Mach, v_M, h, \delta) &\approx C_N(\alpha, Mach_0, v_{M0}, h_0, \delta) \approx C_{N\alpha}\alpha + C_{N\delta}\delta \\ C_M(\alpha, Mach, v_M, h, \delta) &\approx C_M(\alpha, Mach_0, v_{M0}, h_0, \delta) \approx C_{M\alpha}\alpha + C_{M\delta}\delta \end{aligned} \tag{6.9}$$

$C_{N\alpha}$, $C_{N\delta}$, $C_{M\alpha}$, $C_{M\delta}$ are the derivatives of the normal coefficient and of the moment coefficient with respect to α and δ. The expression of the flight path angle can be written

$$\dot{\gamma} \approx \frac{n_B}{v_M} = \frac{\bar{q}S_{ref}}{v_M}C_N = \frac{\bar{q}S_{ref}}{v_M}\left[C_{N\alpha}\alpha + C_{N\delta}\delta\right] = -Z_\alpha\alpha - Z_\delta\delta \tag{6.10}$$

where

$$\begin{aligned} Z_\alpha &= -\frac{\bar{q}S_{ref}C_{N\alpha}}{mv_M} \\ Z_\delta &= -\frac{\bar{q}S_{ref}C_{N\delta}}{mv_M} \end{aligned} \tag{6.11}$$

The same considerations hold for the angular acceleration

$$\dot{q} = \frac{M}{I_{yy}} = \frac{\bar{q}S_{ref}d}{I_{yy}}C_M = \frac{\bar{q}S_{ref}d}{I_{yy}}\left[C_{M\alpha}\alpha + C_{M\delta}\delta\right] = M_\alpha\alpha + M_\delta\delta \tag{6.12}$$

where

$$\begin{aligned} M_\alpha &= -\frac{\bar{q}S_{ref}dC_{M\alpha}}{I_{yy}} \\ M_\delta &= -\frac{\bar{q}S_{ref}dC_{M\delta}}{I_{yy}} \end{aligned} \tag{6.13}$$

Z_α, Z_δ, M_α, M_δ are not constants, but vary with the relative angles. They are evaluated at a trim angle. The missile is at trim when the moment acting on it is zero (C_M = 0). Substituting in the differential equation for α one gets

$$\dot{\alpha} = \dot{\theta} + Z_\alpha\alpha + Z_\delta\delta \tag{6.14}$$

The linearized system can be written in the matrix form $\dot{x} = Ax + Bu$, where the state vector is defined as $x = \begin{bmatrix} \theta & q & \alpha & \gamma \end{bmatrix}^T$ and the only control u is the fin deflection δ

$$\begin{pmatrix} \dot{\theta} \\ \dot{q} \\ \dot{\alpha} \\ \dot{\gamma} \end{pmatrix} = \begin{pmatrix} 0 & 1 & 0 & 0 \\ 0 & 0 & M_\alpha & 0 \\ 1 & 0 & 0 & -1 \\ 0 & 0 & -Z_\alpha & 0 \end{pmatrix} + \begin{pmatrix} \theta \\ q \\ \alpha \\ \gamma \end{pmatrix} + \begin{pmatrix} 0 \\ M_\delta \\ 0 \\ -Z_\delta \end{pmatrix} \delta \tag{6.15}$$

The outputs of the system are the lateral acceleration a_M and the angular rate q. For small α the lateral acceleration can be considered equal to the body acceleration n_B. The output matrices are

$$\begin{aligned} C_{acc} &= \begin{bmatrix} 0 & 0 & 0 & v_M \end{bmatrix} \\ C_{ang.rate} &= \begin{bmatrix} 0 & 1 & 0 & 0 \end{bmatrix} \end{aligned} \tag{6.16}$$

The transfer functions from the angle deflection to the lateral acceleration and to the angular rate can be derived through the well known expression $W = C(sI - A)^{-1}B$. After some algebra one obtains

$$\begin{aligned} W_{acc} = \frac{a_M}{\delta} = C_{acc}(sI - A)^{-1}B &= \frac{-v_M[M_\alpha Z_\delta - Z_\alpha M_\delta]\left[1 - \dfrac{Z_\delta}{M_\alpha Z_\delta - Z_\alpha M_\delta}s^2\right]}{M_\alpha + Z_\alpha s - s^2} \\ W_{ang.rate} = \frac{\dot{\theta}}{\delta} = C_{ang.rate}(sI - A)^{-1}B &= \frac{-[M_\alpha Z_\delta - Z_\alpha M_\delta]\left[1 + \dfrac{M_\delta}{M_\alpha Z_\delta - Z_\alpha M_\delta}s\right]}{M_\alpha + Z_\alpha s - s^2} \end{aligned} \tag{6.17}$$

By defining

$$\begin{aligned} K_1 &= \frac{-v_M[M_\alpha Z_\delta - Z_\alpha M_\delta]}{M_\alpha} \\ K_3 &= \frac{-[M_\alpha Z_\delta - Z_\alpha M_\delta]}{M_\alpha} = \frac{K_1}{v_M} \\ T_\alpha &= \frac{M_\delta}{M_\alpha Z_\delta - Z_\alpha M_\delta} \\ \omega_z &= \frac{M_\alpha Z_\delta - Z_\alpha M_\delta}{Z_\delta} \\ \omega_{AF} &= \sqrt{-M_\alpha} \\ \zeta_{AF} &= \frac{Z_\alpha \omega_{AF}}{2M_\alpha} \end{aligned} \tag{6.18}$$

the two transfer functions can be simplified to

$$\begin{aligned} W_{acc} &= \frac{K_1\left(1 - \dfrac{s^2}{\omega_z^2}\right)}{1 + \dfrac{2\zeta_{AF}}{\omega_{AF}}s + \dfrac{s^2}{\omega_{AF}^2}} \\ W_{ang.rate} &= \frac{K_3(1 + T_\alpha s)}{1 + \dfrac{2\zeta_{AF}}{\omega_{AF}}s + \dfrac{s^2}{\omega_{AF}^2}} \end{aligned} \tag{6.19}$$

ω_{AF} represents the natural frequency of the airframe; ζ_{AF} represents the damping of the airframe; ; T_α represents the missile turning rate time constant; ω_z represents the airframe zero; K_1 is called the acceleration aerodynamic gain; K_3 is called the body rate aerodynamic gain. These and other parameters will be discussed in the next section.

6.4 Considerations on the parameters of the model

Before implementing the model 6.19 in a suitable scenario, it is useful to analyze the parameters on which it is based.

Parameters 6.18 summarize some of the most important dynamical characteristics of the airframe. The airframe natural frequency it is very important because it related to the natural time constant of the airframe. The latter is, in fact, the inverse of ω_{AF}. A fast time constant means that the autopilot does not have to speed up the airframe response. Airframe time constant is a first requisite for the autopilot design and it comes from the engagement simulations performed in chapter 5, where the stochastic guidance strategy was defined and implemented. ω_{AF} decreases with increasing altitude and decreasing speed.

The airframe damping gives information on the oscillations of the airframe response to an acceleration command. A small value of ζ_{AF} means that oscillations will be slightly damped. An oscillatory actuation of the acceleration command might be unsatisfactory. To have a sufficiently damped acceleration response is another requisite for the autopilot.

The missile turning rate time constant expresses the capability of the missile to execute a maneuver. Wings or canards help reducing this value, increasing the maneuverability of the missile. T_α increases also with altitude and speed. A sufficiently small value for T_α is desirable to have an agile missile.

The airframe zero determines an important feature of the dynamical response of the missile. As mentioned earlier, in a tail-controlled missile, it usually assumes a positive value. This implies a non-minimum phase behavior of the system that drives the missile transient motion in the opposite direction with respect to the commanded one. ω_z decreases with increasing altitude and decreasing velocity. Smaller values cause more $wrong-way$ effect.

The acceleration gain returns the amplification of the steady-state acceleration for a given fin deflection. K_1 gets smaller if altitude increases or velocity decreases, because the aerodynamic force is less effective. The body rate aerodynamic gain is the equivalent for the angular rate. Also K_3 gets smaller with an increasing altitude or a decreasing speed.

Another important parameter of the model is the torque term M_α. Once that the flight conditions (e.g. missile speed, altitude, incidence, etc.) and the missile structure parameters (e.g. missile diameter, moment of inertia, etc.) are fixed, this term is a function of the aerodynamic coefficient $C_{M\alpha}$. For a flying vehicle, the longitudinal equilibrium condition is to

have a null pitching moment M, at a fixed angle of attack. If a positive (nose-up) increase in C_M causes an increase in the angle of attack from its equilibrium value, this would result in instability. The generated lift force, indeed, would feed the pitch motion and this would create a greater perturbation in α, so that this chain reaction would continue. On the other hand, if the C_M vs α relation is inversely proportional (i.e. one increases and the other decreases), this would lead to stability, because there will always be a pitching moment that tends to restore the equilibrium. This property is known as *static stability* in pitch, or *positive pitch stiffness* [19].

If $C_{M\alpha}$ is defined as the derivative of C_M with respect to α

$$C_{M\alpha} \equiv \frac{\partial C_M}{\partial \alpha} \tag{6.20}$$

then the positive pitch stiffness condition can be expressed by

$$C_{M\alpha} < 0 \tag{6.21}$$

It must be noted that condition 6.21 is neither a necessary nor a sufficient condition for stability, although it is a very useful and practical criterion for the design of the missile. $C_{M\alpha}$ can be regarded as a relative measure of static stability between two aerodynamic configurations.

Another consideration on stability involves the position of the center of gravity and the center of pressure. If the former is ahead of the latter, the missile is said to be in a stable configuration; if it is behind, the missile is said to be unstable. If the two coincide, the missile is said to be neutrally stable. The difference between the center of gravity and the center of pressure of the missile is called *static margin*. During the flight the static margin decreases because, as the propellant burns, the center of gravity moves forward. Thus, at the end of the flight, the missile is more stable than at the beginning.

The value of $C_{M\alpha}$ depends mainly on two aspects: the lifting surfaces configuration and the position of the center of gravity along the longitudinal axis of the missile. In this study the static margin will be assumed fixed at a design level, while it will be investigated the best wing configuration in order to guarantee flight stability and a satisfactory time response to command.

A statically unstable missile can be made stable through an autopilot, but at a higher cost in terms of control system design effort and provided that there is enough controllability. On the other hand, a very statically stable missile will not give a satisfactory response in terms of fastness, because it would be hard to move it from the equilibrium. A good solution to be adopted by the control system designer is to start with a stable configuration but with enough room for the autopilot design.

Tabella 6.1. Simulation scenarios

#	α	**Mach**	**Altitude**	**Mass**	I_{yy}
1	$\alpha = 0.2^\circ$	$Mach = 2.5$	$h = 1000\ m$	$86\ kg$	$60.35\ kg \cdot m^2$
2	$\alpha = 12^\circ$	$Mach = 3.5$	$h = 5000\ m$	$50\ kg$	$35.09\ kg \cdot m^2$

6.5 Wing configurations

The preliminary step for autopilot design is the design of the aerodynamic configuration of the missile. This activity will be carried out confronting the open loop responses of two models with two different wing configurations.

The benchmark missile is a *Sidewinder AIM* $-$ 9, represented in Fig. 6.4 along with its dimensions expressed in *cm*. The difference between the two configurations is the tail span b_t. In the first case b_t is 14.15 *cm*, in the second is 17.40 *cm*. The latter is represented in Fig. 6.4.

The two scenarios where the model is tested are resumed in table 6.1. They are representative for two different phases of the engagement. The first scenario is referred to the midcourse phase. Here, the relative range between the interceptor and the target is large and there is no need to perform large maneuvers in a short time. Thus, the reference angle of attack is considered small. The missile has not reached its maximum speed and altitude. The latter scenario is referred to the end-game. Here the geometry of the engagement changes very frequently and large, sudden maneuvers can be requested. The reference angle of attack is larger. The missile travels at its maximum speed and at a higher altitude than in the former case. The aerodynamic coefficients are resumed in table 6.2 for both configurations in the two scenarios. The configuration with the smaller tail span is, as expected, less stable than the other, because the tail acts against the motion generated by the canards. In the second scenario, both configurations are more statically stable than in the first one. Even though velocity is greater than in the first scenario, the aerodynamic action is less effective because of the lower air density at an higher altitude.

Static stability does not give enough information to choose the best aerodynamic configuration; the dynamical characteristics of the airframe are more useful to decide. The parameters of the airframe transfer function are resumed in table 6.3 for both configurations in the two scenarios. Fig. 6.5 shows step responses for both tail configurations in the first scenario. In order to compare the responses, they are normalized by the respective gain K_1 and by g. The same plots from the second scenario are shown in Fig. 6.6.

All the responses exhibit an intolerable oscillation that has to be damped during the design

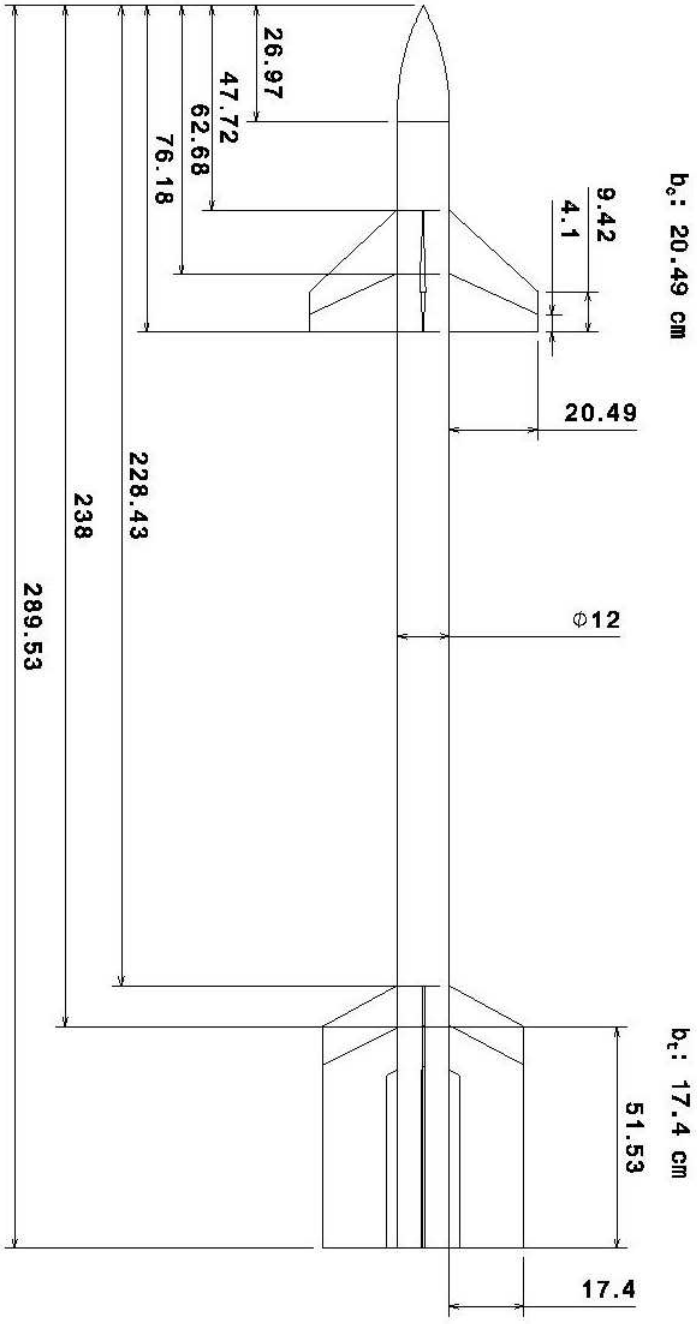

Figura 6.4. Sidewinder missile with b_t = 17.40 *cm*

Tabella 6.2. Aerodynamic coefficients

Tail span configuration	Scenario	$C_{N\alpha}$	$C_{N\delta}$	$C_{M\alpha}$	$C_{M\delta}$
b_t = 14.15 *cm*	1	40.17	0.07	-9.62	2.23
b_t = 14.15 *cm*	2	53.48	9.70	-70.62	-4.90
b_t = 17.40 *cm*	1	44.16	0.08	-47.5667	2.17
b_t = 17.40 *cm*	2	55.64	10.23	-100.16	-11.49

Tabella 6.3. Airframe parameters

Tail span	Scenario	ω_{AF}	ζ_{AF}	T_α	ω_z	K_1	K_3
b_t = 14.15 *cm*	1	10.2907	0.1431	0.3367	-12638	572.08	0.6984
b_t = 14.15 *cm*	2	50.2085	0.0922	-0.0669	-1557.1	1182.8	1.0379
b_t = 17.40 *cm*	1	22.8828	0.0707	0.2963	-12888	128.1	0.1545
b_t = 17.40 *cm*	2	59.7950	0.0805	-0.1721	-1345.4	760.0243	0.6669

of the autopilot. The largest damping comes with the smaller tail span, which also presents a smaller natural frequency. From the values in table 6.3 it can be seen that the configuration with the smaller tail span has also a larger acceleration gain, which means that the same acceleration can be produced with a smaller fin deflection. However, the response of the configuration with the larger tail span is faster than in the other case. The rising time is smaller and oscillations are damped in a shorter time with the larger tail, especially in the first scenario. Step responses in the second scenario are very similar one to each other. The main difference is in the frequency of oscillation: the configuration with a larger tail comes with a greater frequency. It is interesting to note that both configurations in both scenarios do not exhibit a zero in the right-half plane: airframe zeros ω_z are all negative. This means that the missile will not suffer from the *wrong − way* effect, as it is expected from a canard-controlled missile.

The requirement from the guidance system on the airframe response is to be able to implement the commanded acceleration in a time compatible with the constants expressed in chapter 5. Given that both tail configurations seems able to supply the required level of acceleration, the remaining principal aspect is the fastness of the response. It was shown that the configuration with a tail span b_t = 17.40 *cm* is faster than the other. Thus, it will be chosen for the final design of the missile.

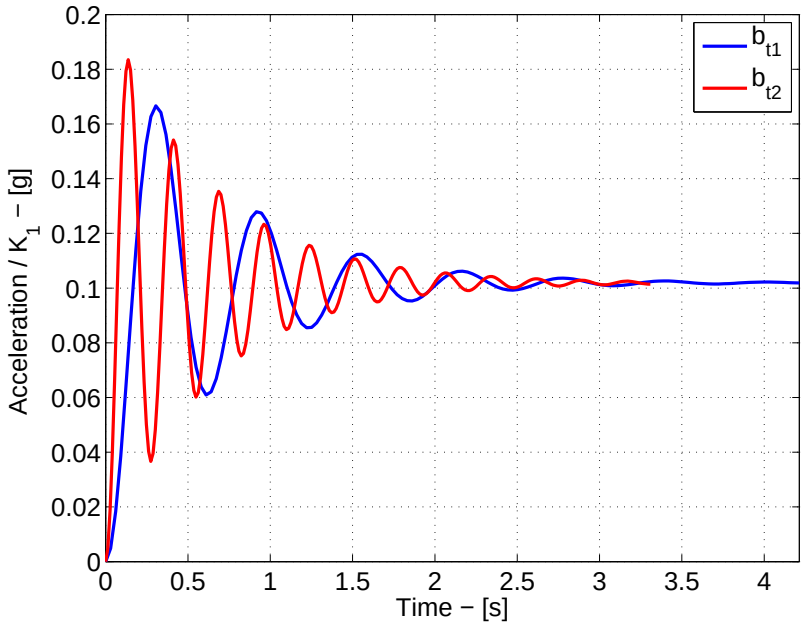

Figura 6.5. Step responses - scenario 1

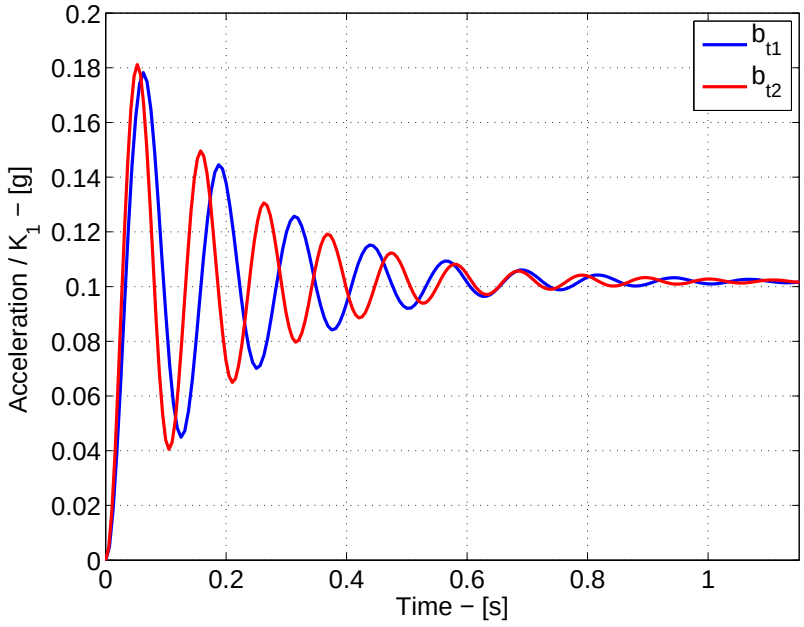

Figura 6.6. Step responses - scenario 2

6.6 Summary

This chapter has described some aspects of the design of the interceptor. The classification of missiles provided at the beginning clarified which kind of interceptor was chosen and why it was selected. The canard configuration was chosen because it presents the best maneuverability properties and does not suffer from induced rolling moments which might cause aerodynamic couplings and instability issues. The *Sidewinder* missile was taken as a benchmark for the design of the interceptor.

The dynamical model of the airframe was derived taking into account only aerodynamic effects. Gravity and thrust effects were assumed to be negligible for the considered motion of the missile. A linearization of the model has allowed to represent the airframe with two transfer functions, one between the fin deflection and the lateral acceleration and one between the fin deflection and the pitch rate of the missile.

An analysis of the aerodynamic configuration of the missile was performed at the end of the chapter. Static and dynamic properties of two tail configurations were studied in order to choose the best configuration. A tail span of 17.40 *cm* presented the fastest response to a step command and hence was chosen for the design of the missile.

Capitolo 7

Autopilot

This chapter is dedicated to the design of the autopilot of the interceptor. An autopilot is the flight control system of a missile. It has the task to stabilize the missile, if needed, and to implement the commands from the guidance system through the actuators. The guidance system forms an outer loop whose outputs are the inputs of the inner loop, the autopilot.
The first autopilots were developed for aircraft flight control systems in order to maintain the vehicles in a straight and level flight [11]. Since the transient response of the aircraft changes substantially with the flight conditions, the gains of the autopilot were chosen as a function of altitude, Mach and trim angles. Conventional autopilots can then be designed as simple, low order, control systems. In order to match stability criteria and robustness, gain scheduling techniques are used to select proper gains for the control loops [53], [51].
A major hypothesis assumed in autopilot design is that the guidance loop and the autopilot loop are spectrally separated. If this assumption holds, the two systems can be designed independently. In the last instants of interception, however, rapid changes in the geometry usually occur and the spectral separation might not be valid. In the last decades a lot of effort was put into the study of integrated design solutions [44], [54], [32], [63]. Unfortunately, the integrated design of guidance system and autopilot involves complications in the project. Moreover, the parameters of the integrated system loose their physical meanings, bringing extra difficulties in the design. In order to design a simple and practical autopilot, able to implement the new guidance strategy described in chapter 5, the integrated design will be avoided in this work.
This chapter is organized as follows. Firstly, the architecture of the flight control system will be described. Then the sensors and actuators of the autopilot will be presented. Eventually, the control loops of the autopilot will be analyzed and designed.

7.1 Autopilot architecture

The autopilot of a statically stable missile such as the one described in chapter 6 has the task to improve the time response to an acceleration command. In section 6.5, it was shown that the airframe time response presents inadequate oscillations, that must be damped by the autopilot.

Interceptor missiles usually have three distinct autopilots: one for controlling the roll motion, one for the pitch and one for the yaw. In missilry, the latter are referred to as *lateral* autopilots. Strictly speaking, the roll autopilot is not used directly in homing, but it is rather a prerequisite for the other two autopilots. A BTT missile shall have a high precision control of roll motion in order to bank in the desired position. A STT missile requires roll stabilization to directly implement pitch and yaw movement.

Missile axial symmetry allows to consider the lateral autopilots as identical. Considering a planar engagement as the one described in section 5.8.1, guidance commands can be regarded as pitch acceleration commands. Hence, in this study only the design of the pitch autopilot will be treated. Roll motion will be assumed to be already stabilized. This kind of stabilization can be performed by means of a roll rate sensor and a dedicated control system [61] or by control surfaces called *rollerons* [11].

The classical autopilot architecture is based on three control loops [67], [61]. The two inner loops are both closed on the measure from a rate gyro. The innermost has the main task to damp the airframe response. It is thus referred to as the *rate-damping loop*. The intermediate loop, sometimes named *synthetic stability loop*, is used to increase the stability margins of the airframe, moving its poles far from the origin of the complex plane. The outermost control loop is fed back by an accelerometer, commonly placed forward of the centre of gravity. This loop has the task to conveniently shape the closed loop response, in order to match the requisites from the guidance systems. It will be referred to as the *accelerometer loop*.

The autopilot architecture is represented in the block diagram of Fig. 7.1. The plant is formed by the airframe transfer functions of equation 6.19. The only input to the plant is the fin deflection δ. G_1, G_2, G_3, and G_4 are four transfer functions representing the controllers. These transfer functions will be investigated in section 7.2. The reference input is the acceleration command $a_{M_{comm}}$ from the guidance system. The architecture of the autopilot is completed by hardware components such as sensors and actuators. The described autopilot needs only an accelerometer and a rate-gyro. The actuator is the servo motor which moves the control surface around the hinge line of the canards (see Fig. 6.4). All these devices

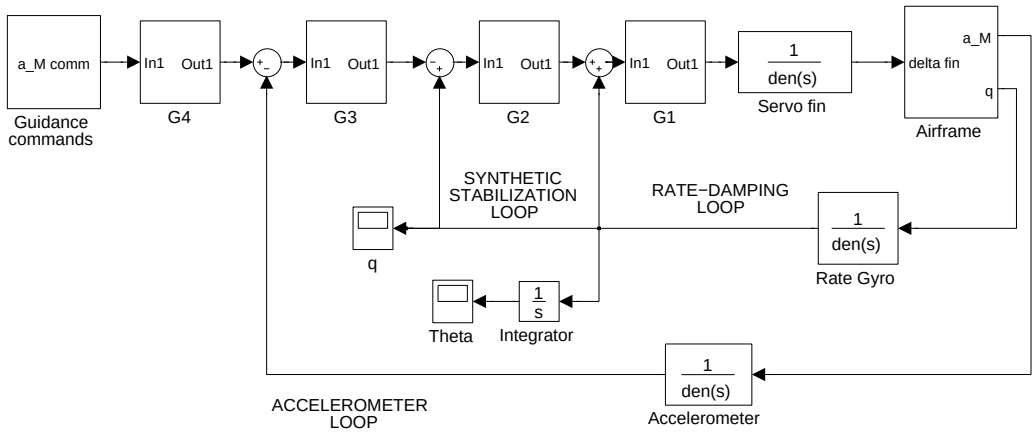

Figura 7.1. Autopilot architecture

Tabella 7.1. Autopilot components

Device	ω **(rad/s)**	ζ	**Saturation (deg)**
Accelerometer	$2\pi \cdot 50$	0.8	-
Rate-gyro	$2\pi \cdot 50$	0.8	-
Servo-fin	$2\pi \cdot 30$	0.75	25

can be represented by second order transfer functions such as

$$W = \frac{\omega^2}{\omega^2 + 2\zeta\omega + 1} \tag{7.1}$$

From the control system point of view, the effect of these devices is to transmit the signal with a certain time delay, as shown in Fig. 7.2. The fins have also a limit value of deflection, namely at 25°. This is represented by a saturation in the control loop.

7.2 Pitch autopilot design

The design of the pitch autopilot will be performed for each set of flight conditions described in section 6.5. The design starts by closing a first rate-gyro loop. Then, a second rate-gyro loop and an accelerometer loop are added.

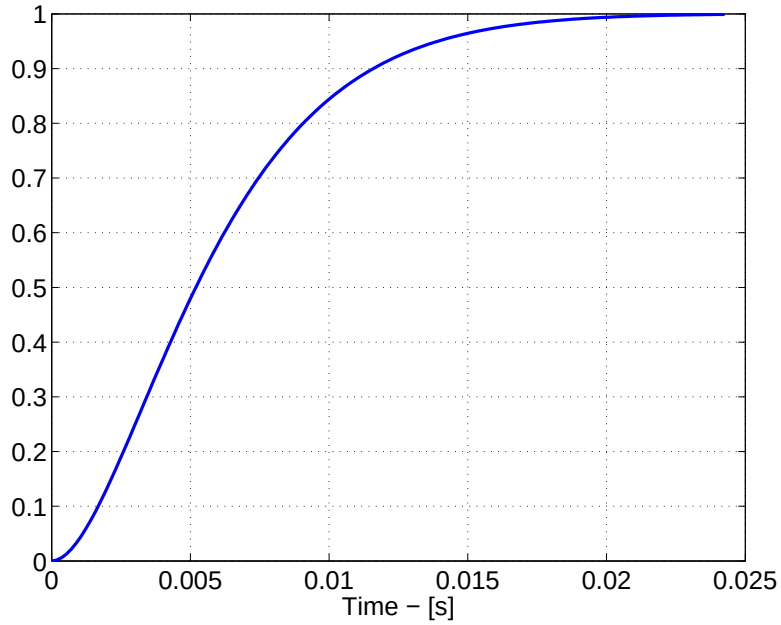

Figura 7.2. Second order system step response

7.2.1 Scenario 1

To start the control analysis, the root locus of the first rate-gyro loop is shown in Fig. 7.3. There are six complex conjugate poles. Those from the rate gyro can be recognized on the left; those from the actuator are in the middle, closer to the origin; the poles close to the imaginary axis are the typical poles of the short period [11], [22]. The latter tend to migrate towards the right half plane, causing instability.

One might think that choosing a sufficiently small gain would be a good solution to close this loop. Nevertheless, as stated earlier, the goal of this first control loop is to damp the bare airframe oscillations. These oscillations depend on the damping of the short period poles. The damping of these roots is very low (namely around 0.1, as it can be seen in Fig. 7.3). Furthermore, one can see that increasing the controller gain decrease the damping, which is not desirable at this step. This can be also seen observing the magnitude Bode plot in Fig. 7.4. The resonance peak at the airframe natural frequency must be damped. A positive gain would only shift the magnitude diagram up or down.

Even though it will produce an unstable closed loop system, a negative gain is going to damp the oscillations of the airframe response. Fig. 7.5 shows a detail of the root locus with a negative gain K_1: the roots still move towards the right half plane, but now the damping increases with an increasing gain. In order to favour the damping of the airframe,

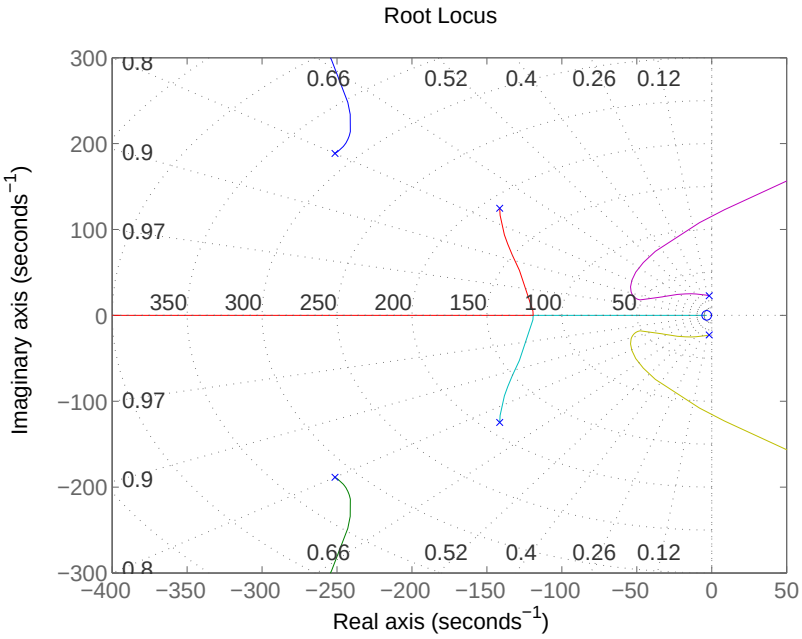

Figura 7.3. Root locus rate-damping loop - Scenario 1

a value of K_1 = -0.34 was chosen.

$$G_1 = K_1 \tag{7.2}$$

Now that the airframe oscillations have been sufficiently damped, the second rate-gyro control loop can be closed. This loop shall stabilize the system. Fig. 7.6 shows the root locus after the first closure around the pitch rate. The short period poles have a high damping, as expected. In order to grant stability, a *PI* controller can be used at this step. The controller G_2 is characterized by the transfer function

$$G_2 = K_2 \frac{1}{s} \tag{7.3}$$

A suitable value for the gain in this case is found to be K_2 = 3.7. The Bode plots of the closed loop system are shown in Fig. 7.7. The natural frequency of the airframe, around 20 rad/s is now satisfactorily damped.

The last closure left is around the acceleration. The root locus for the accelerometer loop is shown in Fig. 7.8. The short period poles are the dominant poles. Their damping is around 0.5 and they migrate to the right half plane for high gains. A small value of gain is then sufficient for the G_3 controller.

$$G_3 = K_3 = 0.0185 \tag{7.4}$$

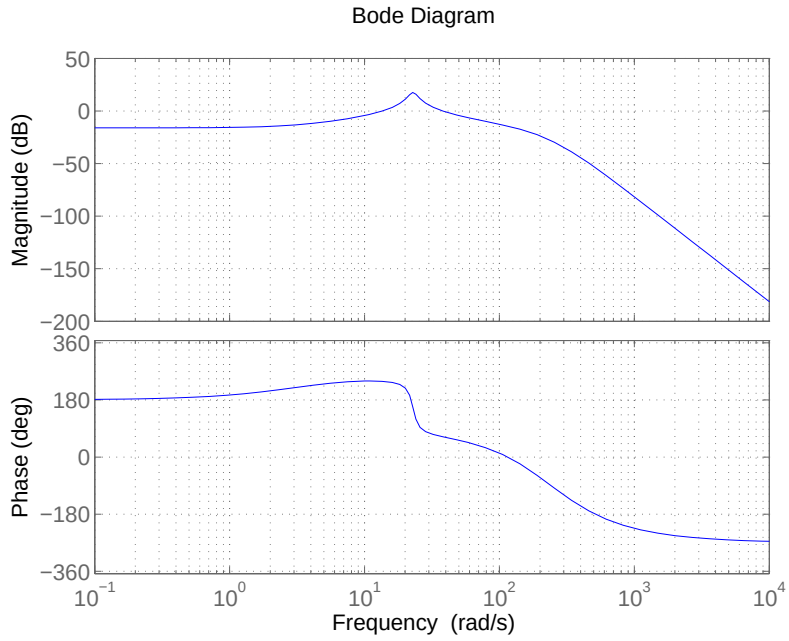

Figura 7.4. Bode plots rate-damping loop - Scenario 1

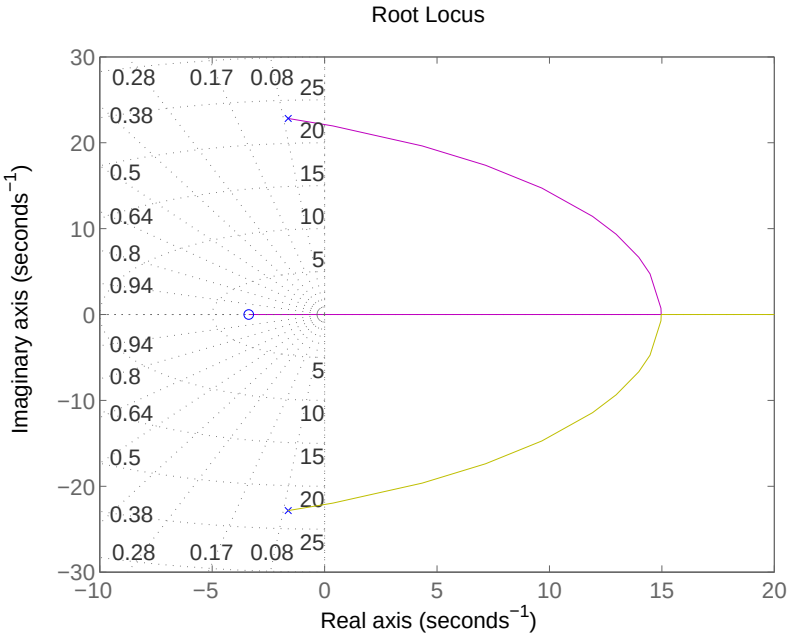

Figura 7.5. Root locus detail with negative K_1 - Scenario 1

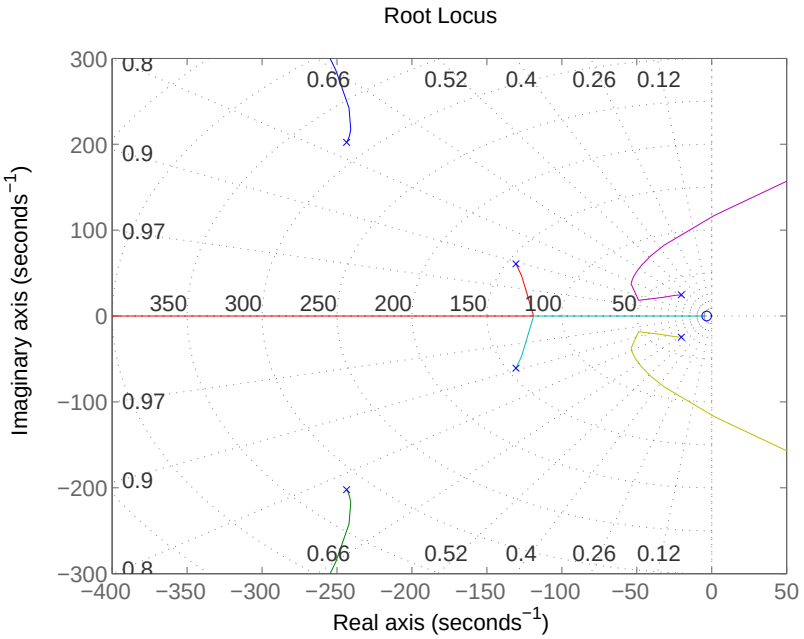

Figura 7.6. Root locus synth. stab. loop - Scenario 1

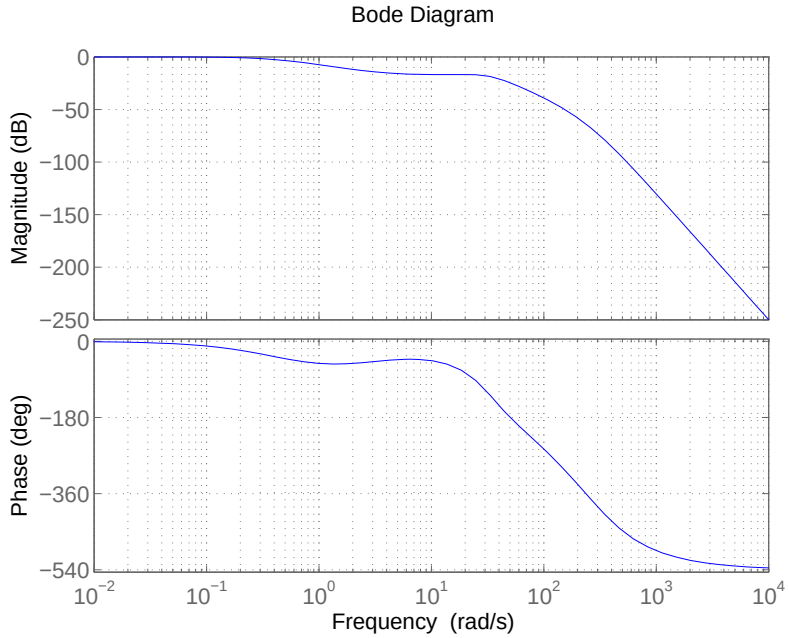

Figura 7.7. Bode plots synth. stab. loop - Scenario 1

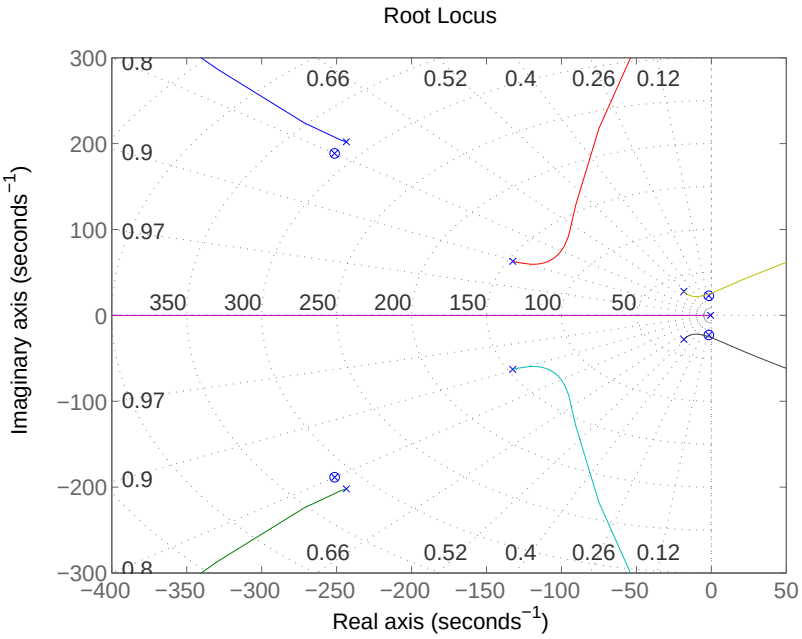

Figura 7.8. Root locus accelerometer loop - Scenario 1

At this point the time response of the closed loop system can be evaluated. Fig. 7.9 shows the response to a step acceleration command. It can be seen that the response does not reach the commanded level. Therefore, the command has to be scaled with a suitable gain. The controller G_4 is a static gain

$$G_4 = K_4 = 1.065 \tag{7.5}$$

Having defined the transfer functions of the controllers represented in Fig. 7.1, the time response of the system can now be evaluated. Fig. 7.10 shows the response of the system (blue line) to an acceleration step command. The level of commanded acceleration is $3g$ and it is represented by the black dashed line. The requirement from the guidance system was to have an autopilot represented by a first order transfer function with time constant τ = 0.1 s. This means that the output acceleration shall reach 63% of the command in 0.1 s. Since the autopilot can be approximated to a third-order system, the value for the time constant has to be corrected [67] by a term related to the damping and the natural frequency

$$\tau_{appr} = \tau + 2\frac{\zeta}{\omega} \tag{7.6}$$

Since the damping of the dominant poles (the short period poles) is now around 0.5 (see root locus in Fig. 7.8) and the natural frequency of the airframe is around 20 rad/s (see Table 6.3), the overall time constant is therefore around 0.14 s. It can be seen that the output

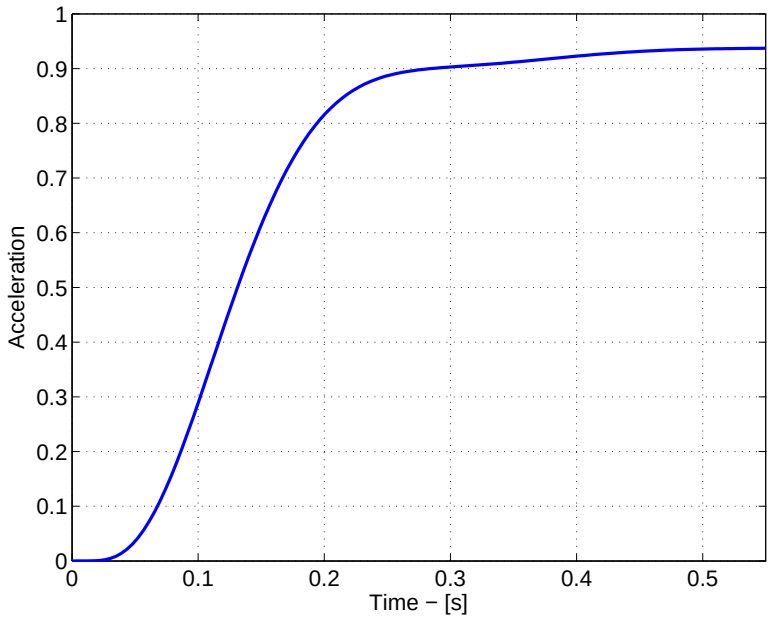

Figura 7.9. Step response accelerometer loop - Scenario 1

acceleration reaches the 63% of the commanded value (yellow dashed line) around 1.4 *s*. The requirement from the guidance system is then met.
Fig. 7.11 shows the resulting fin deflection from the same simulation. It can be seen that the requested deflection is always less than 4.5°. Therefore, the actuator never saturates.

7.2.2 Scenario 2

The autopilot analysis is now repeated for the second scenario. The root locus of the rate-damping system is shown in Fig. 7.12. The roots on the left represent the rate gyro transfer function; the roots in the middle represent the servo fin. The poles close to the imaginary axis are the short period poles. As before, they have a very low damping, resulting in a oscillatory response. In Fig. 7.13, the magnitude Bode plot of the open loop shows indeed a resonance peak at the airframe natural frequency even higher than in the first scenario.
The short period poles tend to migrate towards the unstable region. However, the damping of the short period oscillations is increasing with a positive gain. For the reasons explained in section 7.2.1, the controller G_1 is then chosen as a sufficiently small gain.

$$G_1 = K_1 = 0.0609 \tag{7.7}$$

The second closure around the rate-gyro has the goal to augment the stability of the system. This task is achieved with a *PI* controller which feeds incremental pitch angle back to the

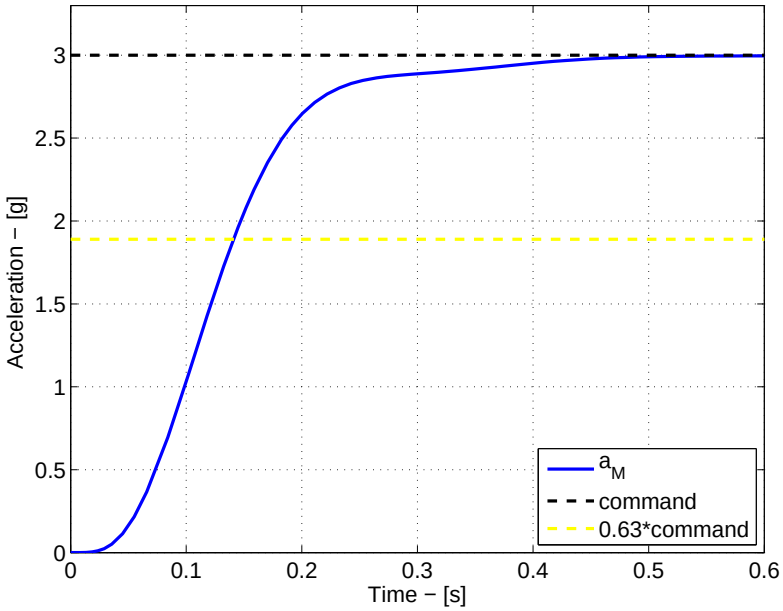

Figura 7.10. Step response - Scenario 1

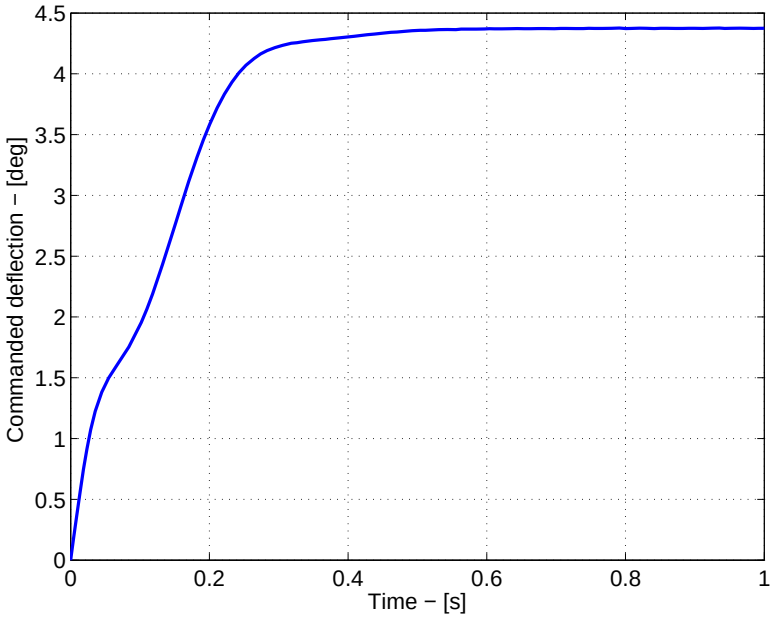

Figura 7.11. Commanded fin deflection - Scenario 1

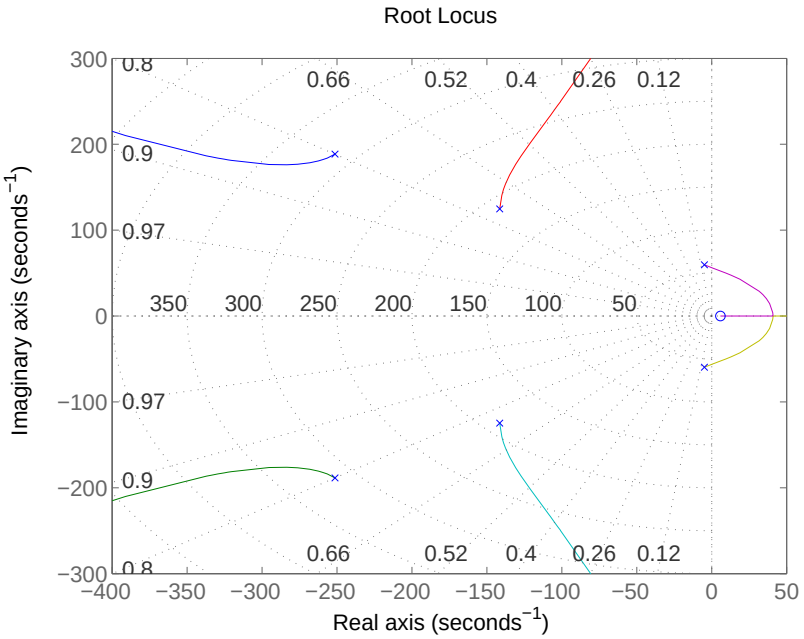

Figura 7.12. Root locus rate-damping loop - Scenario 2

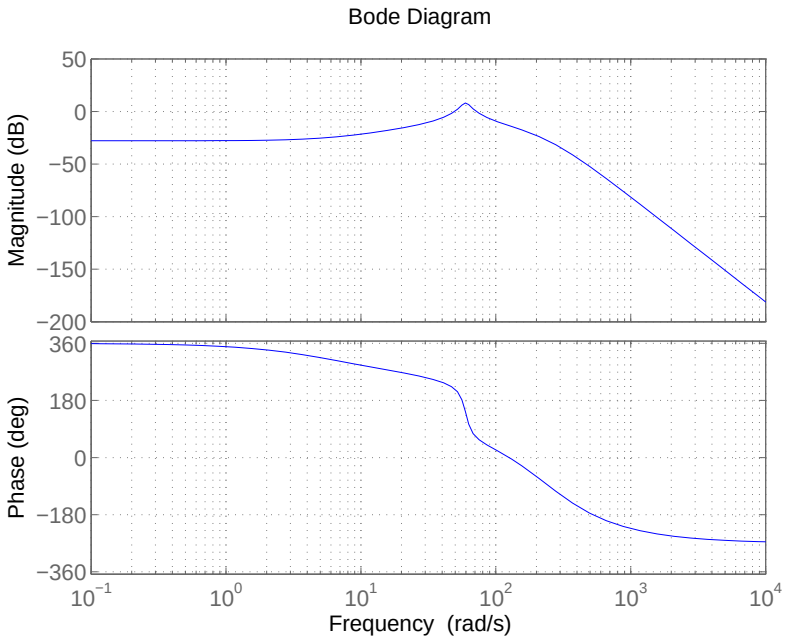

Figura 7.13. Bode plots rate-damping loop - Scenario 2

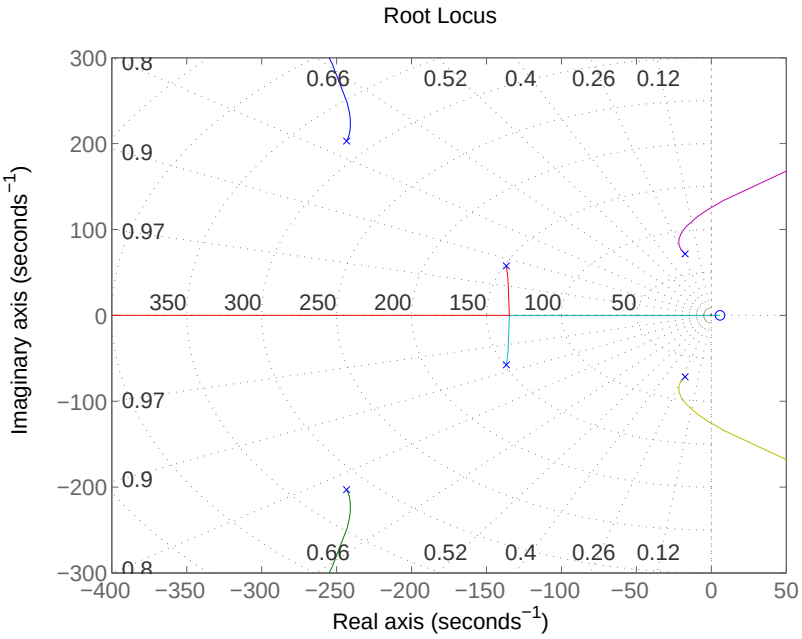

Figura 7.14. Root locus synth. stab. loop - Scenario 2

fin servos. This move the autopilot closed-loop poles away from the imaginary axis and thereby increasing the stability of the closed loop system. The G_2 controller is

$$G_2 = K_2 \frac{1}{s} = -89.4 \frac{1}{s} \tag{7.8}$$

The Bode plots in Fig. 7.15 of the closed loop system show that the initial peak resonance has been satisfactorily damped.

The third closure is designed starting from the analysis of the root locus of the open accelerometer loop represented in Fig. 7.16. The short period roots have a damping around 0.5. A sufficiently small static gain for the G_3 controller can prevent the poles from going crossing the imaginary axis. G_3 is therefore defined as

$$G_3 = K_3 = -0.000237 \tag{7.9}$$

Evaluating the step response of the accelerometer loop in Fig. 7.17 one can see that it does not reach the command level and that the response sign is inverted. Therefore, the controller G_4 shall be a negative, adequate static gain. G_4 is chosen as

$$G_4 = -2.69 \tag{7.10}$$

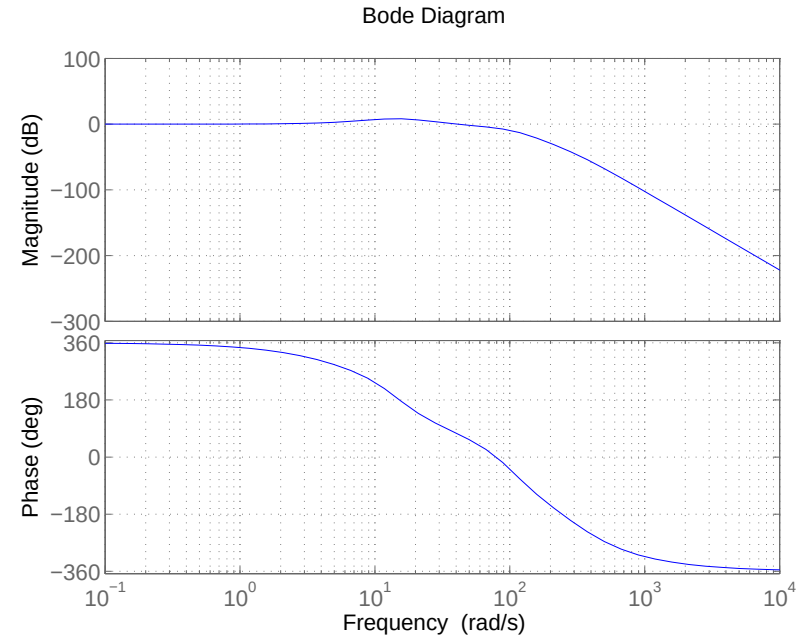

Figura 7.15. Bode plots synth. stab. loop - Scenario 2

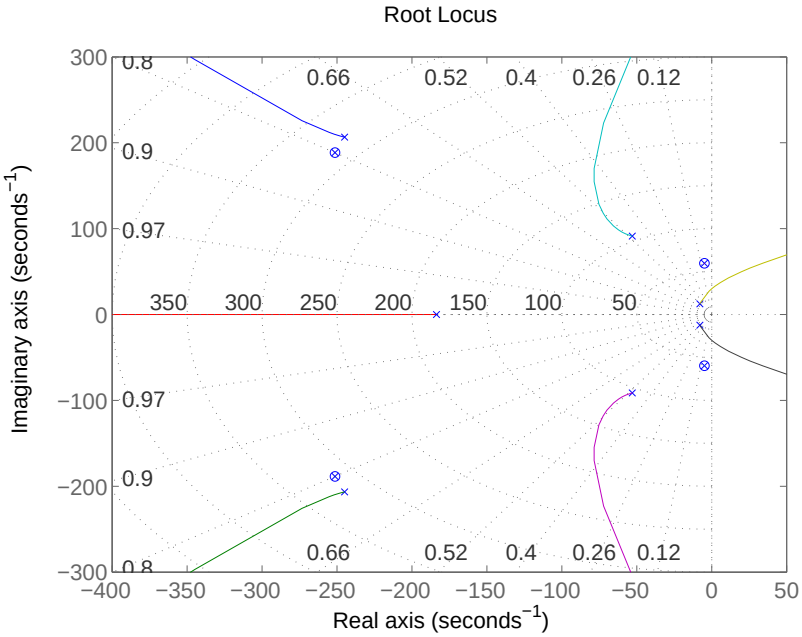

Figura 7.16. Root locus accelerometer loop - Scenario 2

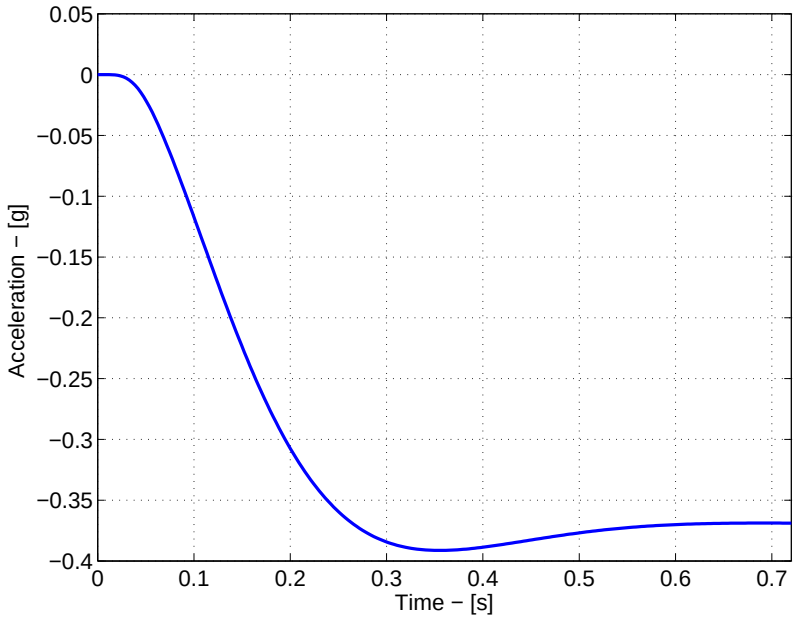

Figura 7.17. Step response accelerometer loop - Scenario 2

Now the response of the closed loop system to a 30g acceleration command can be evaluated. This is the level of acceleration used in the simulations of chapter 5, which guaranteed the success of the new guidance strategy against a maneuvering target with a 5g maximum acceleration capability. The response of the system to the 30g command (black line) is shown in Fig. 7.18 (blue line). The response presents a small overshoot (around 6% of the final value) and then converges to the desired value. It also reaches a level of 63% of the command in 0.14 s. For the reasons explained in 7.2.1 this value is consistent with the requirement from the guidance system.
The deflection requested to the fins is shown in Fig. 7.19. It reaches a steady value around 22° and a maximum value around 23°. Therefore, the saturation level is never reached.

7.3 Guidance system integration

The analysis of the control system is concluded testing the autopilot with the same commands that resulted in the simulations of section 5.8. Looking at Figs. 5.9, 5.10, 5.19, 5.20 one can see that the commanded acceleration (black line) is a bang-bang signal with variable frequency. The frequency depends on the values of the estimated ZEM and on the bounds computed from the differential game. The fast switching is due to the high sampling of measurements and to the consequent output of the Kalman filter. The highest frequency command in the simulation was found to be around 100 rad/s (17 Hz).

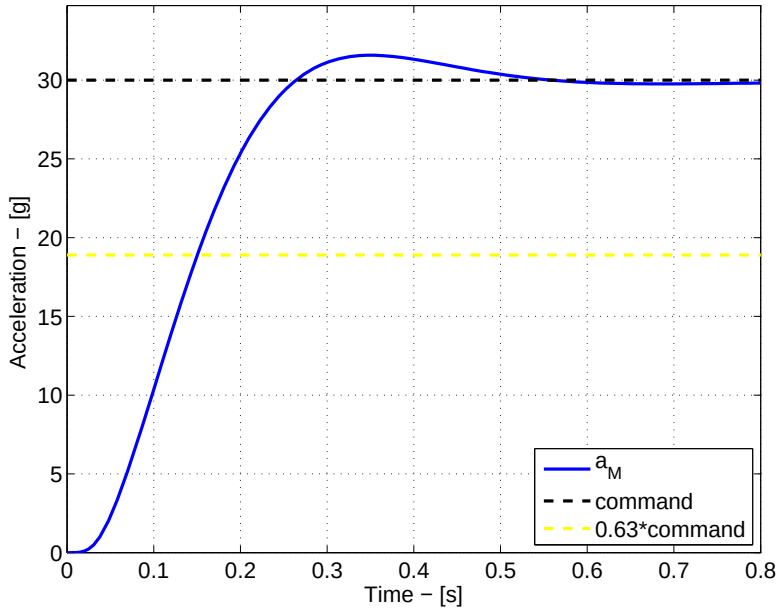

Figura 7.18. Step response - Scenario 2

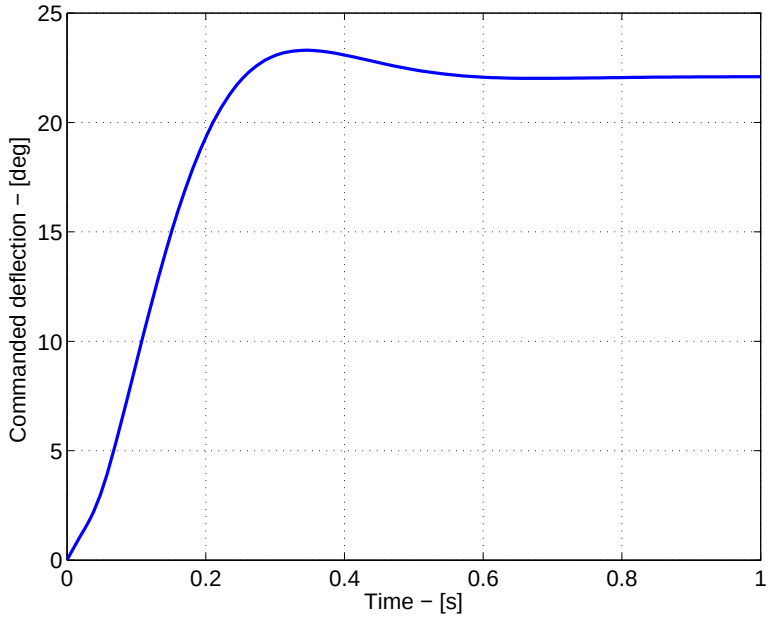

Figura 7.19. Commanded fin deflection - Scenario 2

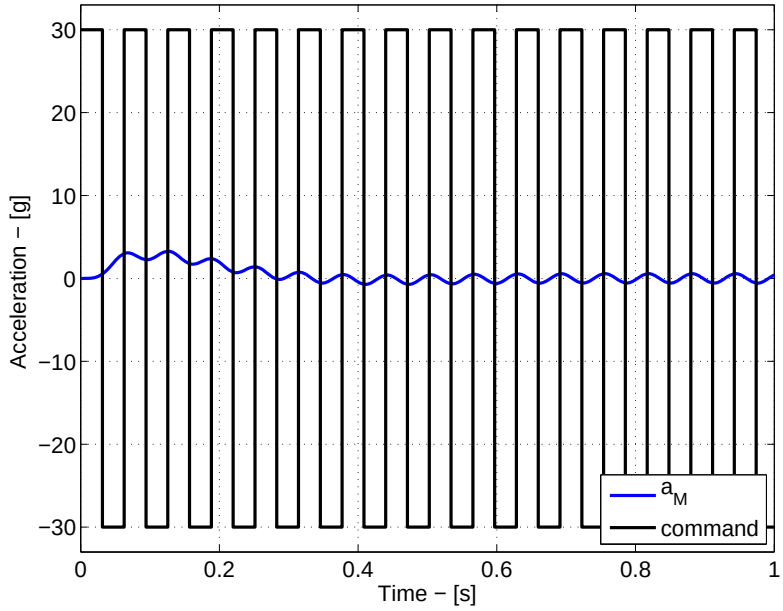

Figura 7.20. Response to a bang-bang command

Fig. 7.20 shows the response of the system to a 30 g bang-bang command with a 100 rad/s frequency. The time duration of each command is around 0.05 s, a value smaller than the requirement on the response time. Indeed, the autopilot will never have enough time to reach any of the commanded levels of acceleration. The simulations of section 5.8 resulted in a varying frequency command, where certain commands had even longer durations than 0.05 s. Therefore, this is the worst case against which testing the autopilot. Knowing that the actual acceleration will not reach the command level, it is important to verify that the autopilot does not act like a low pass filter with respect to the commands.
As it can be seen in Fig. 7.20, each time a new command is triggered, the autopilot is able to detect the new input and to consequentially change the output. This test has been performed only with the autopilot of the second scenario, since this is the only phase of flight where abrupt changes in guidance commands occur. The midcourse phase, to whom the first scenario is referred to, is characterized by smoother acceleration profiles.

7.4 Summary

This chapter has described the design of the pitch autopilot of the missile. The pitch autopilot is responsible for implementing the lateral acceleration commands from the guidance laws described in chapters 4 and 5. The autopilot is based on the linearized model derived in section 6.3 and it is tailored to the airframe characteristics and flight conditions. The-

refore, a different autopilot is designed for each of the two scenarios described in section 6.5. The two scenarios are meant to represent the two most important guided phases of flight: the midcourse, where the missile maneuver to reduce the range to the target, and the end-game, where the guidance law shall drive the missile to hit the target.

The architecture of the control system is the same for both autopilots, composed of three control loops. The two innermost loops are closed on a rate-gyro measurement. The first loop is meant to damp the oscillations of the bare airframe response; the second loop has the task to improve the stability of the missile. The outermost control loop is closed on an accelerometer measurement. This loop has the task to shape the overall response of the system, so that it meets the requirement from the guidance system. Control system gains are scheduled to take into account the differences in the two scenarios.

The evaluation of the time responses in the two scenarios has demonstrated that it is possible to implement the guidance strategies described in chapter 5, in particular the new strategy based on the evaluation of the observability of the system. The time response of the system can be compared to that of a first order transfer function with time constant of 0.1 s. The autopilot also proved to be effective in implementing bang-bang commands with switching at 100 rad/s, as those that resulted from the simulations of section 5.8.

Capitolo 8

Conclusions

In this dissertation several solutions applicable to defense systems against ballistic missiles have been presented. The wide range of aspects involved in such systems leaves room for solutions of different nature, from the employed mathematical algorithms to the adopted design configurations. As a matter of fact, each phase of the mission presents different requirements to be fulfilled.

The task of the defense system is to null the threat of an incoming missile, by destroying it or deviating it from its course. The premise to achieve this task is to have a good knowledge of the trajectory of the missile. It is well known that a suitable network of sensors can give the necessary information. Nevertheless, these measurements must be processed with a filtering algorithm to reconstruct the trajectory. It was shown that, during the acquisition phase, the estimation error can be reduced to 50 m on the position and to few m/s on the velocity. Using finer sensors for tracking yields better results: 10 m error on the position and 1 m/s on the velocity.

Defense with interceptor missiles has been studied as the solution for destroying the incoming threat. A major theme in tactical missile design concerns guidance during the terminal phase of the engagement. The so called end-game is a very critical phase, because small errors can result in large miss distance and in the failure of the engagement. State of the art guidance laws have been examined with the support of numerical simulations. Optimal Guidance Laws (OGL) have the common feature of steering the interceptor on the collision triangle. This is a particular trajectory where it sees the target under a constant line of sight.

Particular attention has been paid to issues resulting from the estimation of engagement related variables. Most missiles make use of a single bearing measurement to track their targets in the end game. The simple and practical PN guidance law can be easily implemented from this single measurement. On the other hand, more complex laws such as APN or

OGL are based on a larger number of variables. Some of them are related with the knowledge of the t_{go} to the interception and, therefore, of the relative range. Even if guidance optimality holds only under the unrealistic assumption of perfect information, OGL driven missiles tend to stay on the collision triangle with almost constant LOS angle. It is well known in literature that such a trajectory makes range estimation impossible with the only bearing measurement. Range estimation becomes possible only if the missile moves away from the collision triangle.

A difficult problem to be solved is how to optimize the maneuver in terms of observability and engagement performance, i.e. of miss distance. A guidance solution that avoids numerical optimization techniques has been proposed, based on the analysis of the eigenvalues of the error covariance matrix from the filter and on the pursuit-evasion differential game framework. The eigenvalues of the error covariance matrix, in fact, can be interpreted as a measure of the level of observability of the estimated variables. The proposed guidance strategy was indicated as *stochastic strategy*. Rather than optimizing the maneuver, the *stochastic strategy* defines a maximum allowable distance from the collision triangle. In the numerical tests carried on, it showed to give better results if compared to classical formulation of the pursuit-evasion games.

To implement the stochastic strategy on a real missile, a dedicated autopilot had to be designed. The task of the autopilot is to implement guidance commands (i.e. lateral acceleration commands) from the guidance system. Therefore, the requirements for the autopilot come from the simulated guidance. Requirements were considered on the level of lateral acceleration, on the maximum delay of command implementation and on the bandwidth of the autopilot. The selection of a suitable missile was conducted privileging the maneuvering capability, in terms of lateral acceleration and agility. The final choice was to refer to a missile with canard wings. Based on the acceleration response, an appropriate wing configuration was chosen. The design of the autopilot was carried on with linear control techniques, based on a linear model of the missile. The results showed that the autopilot was able to actuate the acceleration commands within the considered requirements.

Ringraziamenti

Roma, 10 Luglio 2013

La prima volta che varcai il cancello giallo del Centro Ricerche Progetto San Marco in Roma fu in un pomeriggio di fine Estate di quasi quattro anni fa. Sceso dall'autobus alla fermata che avrei frequentato praticamente ogni giorno nei mesi successivi, ricordo di essermi mosso attenendomi strettamente alle indicazioni che mi erano state date per giungere alla palazzina di mattoni rossi, nuova sede della Scuola. A quel tempo, ancora non sapevo come fosse difficile perdersi nell'unico viale del San Marco, nonostante la giungla di erbacce seccate dal caldo che si alzava ai lati dell'asfalto, quasi nascondendo la vista degli edifici attorno. A quel tempo, ero anche un po' rammaricato dal recente spostamento della gloriosa Scuola di Ingegneria Aerospaziale dall'ultimo piano del chiostro della facoltà di San Pietro in Vincoli al vecchio centro sulla via Salaria; ritenevo di aver perso, nel cambio, in comodità degli spostamenti e in appagamento da frequentazione continua dell'area del Colosseo.

Tra le cose rimaste immutate in questi quattro anni di studi, posso forse annoverare soltanto la vegetazione di via Salaria e gli svantaggi legati al cambio di sede avvenuto poco prima che cominciassi il mio dottorato. Questi ultimi, peraltro, sono stati nel tempo ripagati dall'esperienza di ritrovarsi immersi in un posto unico; un posto dove poter imparare qualcosa anche solo da qualche macchinario inutilizzato da vent'anni o dal racconto vivo delle persone che abitavano gli stessi laboratori nell'età dell'oro dello spazio italiano.

Tante altre cose, come dicevo, sono invece cambiate: sviluppate, trasformate, alcune probabilmente evolute in meglio. Del merito di questi miglioramenti, sento di dover dare credito a tante persone altre e a situazioni che non sono scaturite da me.

Per questo motivo voglio ringraziare il prof. Paolo Teofilatto per avermi guidato pazientemente in questi anni e per aver condiviso con me un sogno 'di coppe e di campioni' dopo il derby vinto 2 - 1 in rimonta il 18 Aprile 2010; il prof. Filippo Graziani, sempre pronto a darmi un suggerimento, una spiegazione, un incoraggiamento, nelle sempre troppe poche volte in cui a lui mi sono rivolto, sia che si trattasse di una delucidazione tecnica (come quella che mi ha consentito di rielaborare i calcoli in sezione 2.3) che di un consiglio più generale.

I ringraziamenti si estendono a tutte le persone che hanno condiviso con me l'esperienza del laboratorio GAUSS, partendo da quelli che mi hanno accolto per primi (Luigi e Fabrizio), fino a quelli che ancora ne fanno parte (Chiara, Giuseppe, Marco, Paride, Riccardo, Roberto, Stefano, in rigoroso ordine alfabetico) passando per quelli che sono andati e venuti nel frattempo (ricordo senz'altro Fabrizio e Riccardo). Tutti voi siete stati importanti,

anche solo con la presenza silenziosa, con la compagnia nei momenti di lavoro, di pausa, con una chiacchierata di pallone o con la condivisione di sogni e progetti per il futuro; senza, ovviamente, dimenticare le consulenze più strettamente tecniche nei campi più disparati! Voglio anche ringraziare il prof. Luigi Mangiacasale per avermi abbondantemente istruito nel campo del controllo dei veicoli aerospaziali e i proff. Fabio Curti e Augusto Nascetti per la loro simpatia e la cordiale collaborazione in tanti frangenti.

I am switching back to English for a while to recall a fundamental step of my PhD years (not only for the PhD itself): the period I spent in Haifa, Israel at the Technion, under the supervision of prof. Tal Shima. He taught me all I know about missile guidance and I am looking forward to work with him again in the future. I want to mention also dr. Ashwini Ratnoo for his help and dr. Joel George for being a pleasant desk mate and for sharing his Saturday trips to St Joseph's church with me.

Non voglio dimenticare l'altro lato del periodo in Israele, e quindi non posso non ricordare i quattro italiani con cui ho condiviso questa esperienza (Elisa, Maria Carla, Roberto e Stefania, ancora in ordine alfabetico): siete stati un conforto costante e un aiuto prezioso durante quei mesi e non so come avrei potuto fare senza di voi.

Un altro riferimento fisso, il più importante e non solo negli ultimi quattro anni, è quello della mia famiglia: mamma Claudia, papà Lucio, Paola e Martina. A loro devo la mia vita, la mia crescita e una mole d'affetto difficile da ricambiare.

Da ultimo, voglio annotare il cambiamento più radicale di questi anni: l'incontro con mia moglie, Chantal. In tutte le cose che accadranno nei prossimi quattro o quarant'anni - una vita all'altro capo del mondo, la famiglia che costruiremo insieme - sarai tu il mio riferimento fisso.

Bibliography

[1] V. J Aidala. Kalman filter behavior in bearings-only tracking applications. *IEEE Transactions on Aerospace and Electronic Systems*, 15(1):29–39, 1979.

[2] V. A. Andreev, V. S. Mikhailov, V. A. Solovey, and V. V. Kainov. Cluster launches of small satellites on Dnepr launch vehicle. In *Fifteenth AIAA/USU Conference on Small Satellites, Logan, UT*, 2001.

[3] A. Arrow. Status and concerns for bank-to-turn control of tactical missiles. *Journal of Guidance, Control, and Dynamics*, 8(2):267–274, 1985.

[4] D. K. Barton, R. Falcone, D. Kleppner, F. K. Lamb, M. K Lau, H. L. Lynch, D. Moncton, D. Montague, D. E. Mosher, W. Priedhorsky, et al. Report of the american physical society study group on boost-phase intercept systems for national missile defense: Scientific and technical issues. *Reviews of modern physics*, 76(3):S1–S424, 2004.

[5] R. R. Bate, D. D. Mueller, and J. E. White. *Fundamentals of astrodynamics*. Courier Dover Publications, 1971.

[6] R. H. Battin. *An introduction to the mathematics and methods of astrodynamics*. AIAA, 1999.

[7] J. Z. Ben-Asher and I. Yaesh. Optimal guidance with reduced sensitivity to time-to-go estimation errors. *Journal of Guidance, Control, and Dynamics*, 20(1):158–163, 1997.

[8] J. Z. Ben-Asher and I. Yaesh. *Advances in Missile Guidance Theory*. AIAA (American Institute of Aeronautics & Astronautics), 1998.

[9] S. M. Bezick, A. J. Pue, and C. M. Patzelt. Inertial navigation for guided missile systems. *Johns Hopkins APL technical digest*, 28(4):331–342, 2010.

[10] A.B. Blair, J.M. Allen, G. Hernandez, United States. National Aeronautics, Space Administration. Scientific, and Technical Information Branch. *Effect on tail-fin span*

on stability and control characteristics of a canard-controlled missile at supersonic Mach numbers. NASA technical paper. National Aeronautics and Space Administration, Scientific and Technical Information Branch, 1983.

[11] J. H. Blakelock. *Automatic control of aircraft and missiles*, volume 6. Wiley New York, 1991.

[12] A. M. Bruckstein. Why the ant trails look so straight and nice. *Mathematical Intelligencer*, 15:59–62, 1993.

[13] A. E. Bryson. Linear feedback solutions for minimum effort interception, rendezvous, and soft landing. *AIAA Journal*, 3(8), 1965.

[14] A. E. Bryson. Applications of optimal control theory in aerospace engineering. *Journal of Spacecraft and Rockets*, 4:545–553, 1967.

[15] A. E. Bryson and Y. Ho. *Applied optimal control: optimization, estimation, and control*. Blaisdell Pub. Co., 1969.

[16] J. R. Burt Jr. The effectiveness of canards for roll control. Technical report, DTIC Document, 1976.

[17] B. A. Conway and M. Pontani. Optimal interception of evasive missile warheads: numerical solution of the differential game. *Journal of Guidance, Control, and Dynamics*, 31(4):1111–1122, 2008.

[18] G. J. Culler and B. D. Fried. Universal gravity turn trajectories. *Journal of Applied Physics*, 28(6):672–676, 1957.

[19] B. Etkin. *Dynamics of atmospheric flight*. John Wiley & Sons Inc, 1972.

[20] J. A. Fawcett. Effect of course maneuvers on bearings-only range estimation. *IEEE Transactions on Acoustics, Speech and Signal Processing*, 36(8):1193–1199, August 2002.

[21] R. J. Fitzgerald. Shaping filters for disturbances with random starting times. *Journal of Guidance, Control, and Dynamics*, 2(2):152–154, 1979.

[22] A.L. Greensite. *Analysis and design of space vehicle flight control systems*. 1969.

[23] S. Gutman. On optimal guidance for homing missiles. *Journal of Guidance and Control, vol. 2, July-Aug. 1979, p. 296-300.*, 2:296–300, 1979.

[24] S. Gutman and G. Leitmann. Optimal strategies in the neighborhood of a collision course. *AIAA Journal*, 14(9):1210–1212, 1976.

[25] F. M. Ham and R. G. Brown. Observability, Eigenvalues, and Kalman Filtering. *IEEE Transactions on Aerospace and Electronic Systems*, AES-19, 1983.

[26] S. E. Hammel, P. T. Liu, E. J. Hilliard, and K. F. Gong. Optimal observer motion for localization with bearing measurements. *Computers & Mathematics With Applications*, 18:171–180, 1989.

[27] S. A. R. Hepner and H. P. Geering. Observability analysis for target maneuver estimation via bearing-only and bearing-rate-only measurements. *Journal of Guidance, Control, and Dynamics*, 13(6):977–983, 1990.

[28] G. Hexner and H. Weiss. Stochastic approach to optimal guidance with uncertain intercept time. *IEEE Transactions on Aerospace and Electronic Systems*, 46(4):1804–1820, 2010.

[29] S. A. Hildreth. Kinetic energy kill for ballistic missile defense: A status overview. DTIC Document, 2007.

[30] Y. Ho, A. E. Bryson, and S. Baron. Differential games and optimal pursuit-evasion strategies. *IEEE Transactions on Automatic Control*, 10(4):385–389, 1965.

[31] D. G. Hull, J. L. Speyer, and C. Y. Tseng. Maximum-information guidance for homing missiles. *Journal of Guidance, Control, and Dynamics*, 8(4):494–497, 1985.

[32] M. Idan, T. Shima, and O. M. Golan. Integrated sliding mode autopilot-guidance for dual-control missiles. *Journal of Guidance, Control, and Dynamics*, 30(4):1081–1089, 2007.

[33] R. Isaacs. *Differential Games: A Mathematical Theory with Applications to Welfare and Pursuit, Control and Optimization*. John Wiley and Sons, 1965.

[34] S. J. Julier and J. K. Uhlmann. New extension of the Kalman filter to nonlinear systems. In *AeroSense'97*, pages 182–193. International Society for Optics and Photonics, 1997.

[35] S. J. Julier and J. K. Uhlmann. Unscented filtering and nonlinear estimation. *Proceedings of the IEEE*, 92(3):401–422, 2004.

[36] S. J. Julier, J. K. Uhlmann, and H. F. Durrant-Whyte. A new approach for filtering nonlinear systems. In *Proceedings of the American Control Conference, 1995*, volume 3, pages 1628–1632. IEEE, 1995.

[37] R. E. Kalman et al. A new approach to linear filtering and prediction problems. *Journal of basic Engineering*, 82(1):35–45, 1960.

[38] J. Kidd and H. Caldwell. Defense support program - support to a changing world. In *1992 AIAA Space Programs and Technologies Conference*, 1992.

[39] F.H. Kishi and T.S. Bettwy. *Optimal and Sub-optimal Designs of Proportional Navigation Systems.*, volume Recent Advances in Optimization Techniques, pages 519–540. John Wiley, 1965.

[40] I. Kliger. A simple derivation of certain optimal control laws. Memo SAD 1230, Raytheon, Nov. 1970.

[41] F. L. Lewis, L. Xie, and D. Popa. *Optimal and robust estimation: with an introduction to stochastic control theory*, volume 26. CRC, 2008.

[42] G. N. Lewis and T. A. Postol. Future challenges to ballistic missile defense. *IEEE Spectrum*, 34(9):60–68, 1997.

[43] X. R. Li and V. P. Jilkov. Survey of maneuvering target tracking: *iii*. measurement models. In *International Symposium on Optical Science and Technology*, pages 423–446. International Society for Optics and Photonics, 2001.

[44] CF. Lin, Q. Wang, J. L. Spayer, J. H. Evers, and J. R. Cloutier. Integrated estimation, guidance, and control system design using game theoretic approach. In *American Control Conference, 1992*, pages 3220–3224. IEEE, 1992.

[45] D. J. Murphy. *Noisy bearings-only target motion analysis*. PhD thesis, Dept. Elec. Eng., Northeastern Univ., 1969.

[46] R. C. Nelson. *Flight stability and automatic control*. McGraw-Hill New York, 1989.

[47] S. L. Nelson and P. Zarchan. Alternative approach to the solution of lambert's problem. *Journal of Guidance, Control, and Dynamics*, 15(4):1003–1009, 1992.

[48] United States. General Accounting Office, United States. Congress. Senate. Committee on Governmental Affairs. Subcommittee on Federal Services, Post Office, and Civil Service. *Ballistic missile defense: records indicate deception program did not affect 1984 test results: report to the Chairman, Subcommittee on Federal Services, Post Office, and Civil Service, Committee on Governmental Affairs, US Senate*. The Office, 1994.

[49] Y. Oshman and P. Davidson. Optimization of observer trajectories for bearings-only target localization. *IEEE Transactions on Aerospace and Electronic Systems*, 35(3):892 – 902, 1999.

[50] G.H. Rapp. *Peformance improvements with Sidewinder missile airframe variants*. American Institute of Aeronautics and Astronautics, 1979.

[51] R. T. Reichert. Dynamic scheduling of modern-robust-control autopilot designs for missiles. *IEEE Control Systems*, 12(5):35–42, 1992.

[52] R. D. Robinett, G. G. Parker, H. Schaub, J. L. Junkins, J.F. Bellantoni, and K.W. Dodge. A square root formulation of the Kalman-Schmidt filter. *AIAA journal*, 5(7):1309–1314, 1967.

[53] J. S. Shamma and J. R. Cloutier. Gain-scheduled missile autopilot design using linear parameter varying transformations. *Journal of Guidance, Control, and Dynamics*, 16(2):256–263, 1993.

[54] T. Shima, M. Idan, and O. M. Golan. Sliding-mode control for integrated missile autopilot guidance. *Journal of Guidance, Control, and Dynamics*, 29(2):250–260, 2006.

[55] T. Shima and J. Shinar. Time varying linear pursuit evasion game models with bounded controls. *Journal of Guidance, Control, and Dynamics*, 25(3), 2002.

[56] J. Shinar. Solution techniques for realistic pursuit-evasion games. *Control Dyn. Syst., Adv. Theory Appl.*, 17:63–124, 1981.

[57] J. Shinar and T. Shima. Nonorthodox guidance law development approach for intercepting maneuvering targets. *Journal of Guidance, Control, and Dynamics*, 25(4):658–666, 2002.

[58] N.A. Shneydor. *Missile Guidance and Pursuit: Kinematics, Dynamics and Control*. Woodhead Publishing, 1998.

[59] F. S. Simmons. *Rocket exhaust plume phenomenology*. Aerospace Corp, 2000.

[60] D. Simon. *Optimal state estimation: Kalman, H infinity, and nonlinear approaches*. Wiley-Interscience, 2006.

[61] G. M. Siouris. *Missile guidance and control systems*. Springer, 2004.

[62] T.L. Song and T.Y. Um. Practical guidance for homing missiles with bearings-only measurements. *IEEE Transactions on Aerospace and Electronic Systems*, 32(1):434 – 443, 1996.

[63] F. Tan, M. Hou, and H. Zhao. Autopilot design for homing missiles considering guidance loop dynamics. In *Intelligent Control and Information Processing (ICICIP), 2011 2nd International Conference on*, volume 1, pages 1–5. IEEE, 2011.

[64] J. K. Uhlmann. *Dynamic map building and localization: New theoretical foundations*. PhD thesis, University of Oxford, 1995.

[65] D. A. Wilkening. Airborne boost-phase ballistic missile defense. *Science and Global Security*, 12:1–67, 2004.

[66] P. Zarchan. Representation of realistic evasive maneuvers by the use of shaping filters. *Journal of Guidance, Control, and Dynamics*, 2(4), 1979.

[67] P. Zarchan. Tactical and strategic missile guidance. *Washington, DC: American Institute of Aeronautics and Astronautics, Inc, 1994.*, 1994.

[68] P. Zarchan. Boost-phase filtering options: Is simpler better? *Journal of Guidance, Control, and Dynamics*, 33(6):1724–1731, 2010.